



HAL
open science

Advanced Numerical Simulations for Conventional and Non-Conventional Welding Processes: A Model Order Reduction Approach

Diego Canales Aguilera

► **To cite this version:**

Diego Canales Aguilera. Advanced Numerical Simulations for Conventional and Non-Conventional Welding Processes: A Model Order Reduction Approach. Mechanics of materials [physics.class-ph]. École centrale de Nantes; Universidad de Zaragoza (Espagne), 2017. English. NNT : 2017ECDN0012 . tel-02145905

HAL Id: tel-02145905

<https://theses.hal.science/tel-02145905>

Submitted on 3 Jun 2019

HAL is a multi-disciplinary open access archive for the deposit and dissemination of scientific research documents, whether they are published or not. The documents may come from teaching and research institutions in France or abroad, or from public or private research centers.

L'archive ouverte pluridisciplinaire **HAL**, est destinée au dépôt et à la diffusion de documents scientifiques de niveau recherche, publiés ou non, émanant des établissements d'enseignement et de recherche français ou étrangers, des laboratoires publics ou privés.

Thèse de Doctorat

Diego CANALES AGUILERA

*Mémoire présenté en vue de l'obtention
du grade de Docteur de l'École Centrale de Nantes
Docteur de l'Université de Saragosse
Sous le label de l'UNIVERSITÉ BRETAGNE LOIRE*

École doctorale : Sciences Pour l'Ingénieur, Géosciences, Architecture

Discipline : Mécanique des solides, des matériaux, des structures et des surfaces

Unité de recherche : Institute de Calcul Intensif, École Centrale de Nantes

Soutenu le 31 mai 2017

Stratégies numériques avancées pour la simulation efficace de procédés de soudage conventionnels et non conventionnels : Une approche de réduction de modèles.

JURY

Président :	Jean-Michel BERGHEAU , Professeur des Universités, École nationale d'ingénieurs de Saint-Étienne
Rapporteurs :	Pierre LADEVEZE , Professeur émérite, Ecole Normale Supérieure Paris-Saclay Khemaïs SAANOÛNI , Professeur des Universités, Université de technologie de Troyes
Examineurs:	José Vicente AGUADO , Docteur, Ecole Centrale de Nantes Jean-Michel BERGHEAU , Professeur des Universités, École nationale d'ingénieurs de Saint-Étienne Frédéric BOITOUT , Docteur, Chef de projet, ESI Group, Lyon
Invité:	Antonio HUERTA , Professeur des Universités, ICREA, Espagne
Directeur de thèse :	Francisco CHINESTA , Professeur des Universités, École Centrale de Nantes
Co-directeur de thèse :	Elías CUETO , Professeur des Universités, Université de Saragosse, Espagne
Co-encadrant de thèse :	Éric FEULVARCH , Maître de conférences HDR, École nationale d'ingénieurs de Saint-Étienne

Abstract

Numerical simulations represent a fundamental tool for the design and optimization of industrial manufacturing processes such as welding. Despite the impressive development of the numerical methods and the means of calculation, the complexity of these processes and the new demands of the more advanced industries make it necessary to rethink the available methods, strategies and simulation algorithms.

In this thesis, we propose new numerical methods with a Model Order Reduction approach, a consolidated discipline that has provided surprising solutions in different applications, such as advanced manufacturing processes.

First, different strategies for the efficient simulation of conventional welding processes are proposed. To this end, the use of Computational Vademecums is introduced for the improvement of methods such as the Generalized Finite Element for thermal calculation, the local-global approach for the mechanical calculation or the direct construction of vademecums useful for pre-design phases. Then, an efficient PGD solver for thermo-mechanical simulations for friction stir welding is presented.

This thesis shows how Model Order Reduction, apart from being an end, can be an excellent ingredient to improve the efficiency of traditional numerical methods, with great interest for the industry.

Résumé

Les simulations numériques représentent un outil fondamental pour la conception et l'optimisation de procédés industriels de fabrication tels que le soudage. Malgré le développement impressionnant des méthodes numériques et des moyens de calcul utilisables, la complexité des procédés de fabrication et les nouvelles exigences des industries les plus avancées obligent à repenser les méthodes, les stratégies et les algorithmes de simulation disponibles.

Dans cette thèse, de nouvelles méthodes numériques avec une approche de Réduction des Modèles sont proposées, une discipline consolidée qui a fourni des solutions étonnantes dans différentes applications, comme les procédés de fabrication avancés.

Tout d'abord, différentes stratégies sont proposées pour la simulation efficace des procédés de soudage conventionnel, à cet effet, l'utilisation de Computational Vademecums est introduite. En second lieu, un solveur PGD efficace est présenté pour les simulations thermo-mécaniques de soudage par friction-malaxage.

L'introduction de ces abaques numériques améliorent des méthodes telles que : les éléments finis généralisés pour le calcul thermique, l'approche locale-globale pour le calcul mécanique et enfin, la construction directe des abaques utiles pour la phase de pré-design.

Cette thèse montre comment la réduction des modèles, en plus d'être une fin en soi, peut être un excellent ingrédient pour améliorer l'efficacité des méthodes numériques traditionnelles. Cela représente un grand intérêt pour l'industrie.

Resumen, conclusiones y aportaciones científicas

Resumen

Las simulaciones numéricas representan hoy en día una herramienta fundamental para la concepción y optimización de procesos de fabricación industrial tales como la soldadura. A pesar del impresionante desarrollo de los métodos numéricos y de los medios de cálculo disponibles, la complejidad de estos procesos y las nuevas exigencias de las industrias más avanzadas, obligan a repensar los métodos, las estrategias y los algoritmos de simulación actuales.

En esta tesis, se proponen nuevos métodos numéricos con un enfoque de reducción de modelos, una disciplina consolidada que ha proporcionado resultados excepcionales en diferentes aplicaciones como la de los procesos avanzados de fabricación.

En primer lugar, se presentan diferentes estrategias para la simulación eficaz termo-mecánica de la soldadura convencional. Para ello, se introducen los denominados *Computational Vademecums*. Estos ábacos permiten mejorar métodos como el de los Elementos Finitos Generalizados o el enfoque *local-global* para el análisis de la soldadura. Además, se muestra cómo estos ábacos constituyen una extraordinaria herramienta para fases de prediseño.

En segundo lugar, se presenta un solver avanzado para la simulación termo-mecánica de procesos de fabricación con aplicación directa al *friction stir welding*,

un proceso de soldadura no convencional.

Esta tesis muestra como la Reducción de Modelos, lejos de representar un fin último, puede ser un ingrediente formidable para mejorar la eficacia de métodos numéricos y estrategias tradicionales. Además, esto se puede realizar de forma mínimamente intrusiva lo que despierta un gran interés en la industria.

Conclusiones

En esta tesis se han presentado diferentes herramientas para la simulación de procesos de soldadura convencional y no convencional. La originalidad de este trabajo reside en el uso de técnicas de reducción de modelos con enfoques distintos a los tradicionales buscando su mayor aplicabilidad industrial. Esto ha significado la propuesta de mejora de estrategias numéricas robustas y de fácil integración en plataformas de cálculo preexistentes.

La V-GFEM es un método para la simulación eficaz de modelos térmicos transitorios. Su principal ventaja consiste en adaptar el espacio de aproximación de la solución en función de los parámetros de la simulación en tiempo real. Esto se logra mediante la introducción de un ingrediente clave: un *computational vademecum* que se puede calcular *offline*. La V-GFEM no sólo hereda las buenas propiedades de la GFEM (aproximabilidad, conformidad y carácter *meshless*) sino que además tiene una importante ventaja: tan solo necesita una función de enriquecimiento que será la adecuada para esa simulación en ese preciso instante. El costo computacional de la V-GFEM es el mismo que cualquier método GFEM donde se emplee una sola función de enriquecimiento. En los ejemplos presentados se ha obtenido aproximadamente una diferencia de un orden magnitud entre el cálculo de una solución con V-GFEM y una solución FEM h-adaptada a una misma precisión.

El método Metalocal-global presentado es una estrategia eficaz para estimar distorsiones y tensiones residuales en grandes estructuras donde se realizan una gran cantidad de soldaduras. Esta estrategia se basa en el enfoque local-global solucionando una de sus limitaciones: la consideración de la influencia de la estructura global sobre la región local de una forma eficiente. El método Metalocal-global

sustituye la simulación local por un *computational vademecum* que proporciona la solución plástica local para cualquier influencia elástica global sobre la región de soldadura. Es un método sistemático para construir una base de datos de *computational vademecums* que puede ser utilizada para diferentes geometrías y condiciones de contorno de grandes estructuras.

La simulación completa de la soldadura tradicional ha sido estudiada en un escenario simplificado: el estado estacionario. No obstante, se ha mostrado como la posibilidad de construir *computational vademecums* de estos procesos abre la puerta a nuevos escenarios de gran interés para la industria en preproceso, optimización y ajuste de datos experimentales para la simulación de procesos de soldadura. Se ha hecho especial hincapié en la baja intrusividad del método, permitiendo utilizar códigos industriales para su elaboración.

Finalmente, se ha presentado un solver basado en la PGD para la simulación eficaz de modelos termo-mecánicos y en particular para *friction stir welding*, un proceso de soldadura no convencional. Este solver permite resolver un problema 3D mediante un conjunto de problemas 2D, disminuyendo dramáticamente el coste computacional asociado.

Aportaciones científicas

En esta tesis se han realizado las siguientes aportaciones científicas originales:

- Elaboración del método V-GFEM para la simulación eficaz de modelos térmicos transitorios y en particular para el análisis de térmico de la soldadura convencional.
- Introducción del método Metalocal-global para la mejora de la simulación mecánica de procesos de soldadura convencional bajo la hipótesis de separación local-global.
- Creación de *computational vademecums* no intrusivos para el análisis completo de la soldadura en régimen estacionario (térmico, metalúrgico y mecánico) empleando plataformas de simulación préxistentes.

- Proposición de un solver eficiente basado en la PGD para la simulación de procesos de termo-mecánicos de fabricación como *friction stir welding*.

Publications

Some of this work was previously published in the following papers:

- Canales, D., Leygue, A., Chinesta, F., González, D., Cueto, E., Feulvarch, E., ... & Huerta, A. (2016). Vademecum-based GFEM (V-GFEM): optimal enrichment for transient problems. *International Journal for Numerical Methods in Engineering*.
- Canales, D., Leygue, A., Chinesta, F., Alfaro, I., González, D., Cueto, E., ... & Bergheau, J. M. (2016). In-plane/out-of-plane separated representations of updated Lagrangian descriptions of viscoplastic flow models in plate domains. *Comptes Rendus Mécanique*, 344(4), 225-235.

And in the following conference procedures:

- Canales, D., Cueto, E., Feulvarch, E., & Chinesta, F. (2014). First steps towards parametric modeling of FSW processes by using advanced separated representations: Numerical techniques. In *Key Engineering Materials* (Vol. 611, pp. 513-520). Trans Tech Publications.
- Canales, D., Leygue, A., Chinesta, F., Cueto, E., Feulvarch, E., Bergheau, J. M., ... & Boitout, F. (2015). Efficient Updated-Lagrangian Simulations in Forming Processes. In *Key Engineering Materials* (Vol. 651, pp. 1294-1300). Trans Tech Publications.

Remerciements

Cette thèse est le résultat du travail et de la générosité de nombreuses personnes à qui j'exprime tout ma reconnaissance. Je souhaiterais tout d'abord remercier mes directeurs, Paco Chinesta, Elías Cueto et Eric Feulvarch, qui m'ont constamment encadré avec optimisme et de grandes idées. Plus particulièrement, je remercie Paco Chinesta de m'avoir donné l'opportunité de vivre cette expérience et le respect qu'il sait avoir à l'encontre de ses élèves quant à leur personnalité et qui m'a permis de grandir et d'évoluer scientifiquement.

Je tiens également à remercier les membres du jury et rapporteurs pour leur participation et leur disponibilité. J'adresse aussi mes remerciements à ESI Group, pour le financement et pour leurs propositions de grand défis scientifiques et d'ingénierie, sans lesquelles cette thèse n'aurait jamais pu exister. Merci en particulier à Frédéric Boitout et Mickael Fontaine pour nos innombrables discussions scientifiques et l'accueil chaleureux qu'ils m'ont réservé à Lyon. Et encore je voudrais remercier Jean-Michel Berghau pour son aide sur la compréhension de la simulation de soudage, pour sa participation à des réunions, nos discussions par visioconférence et pour ses cours particuliers pendant les congrès.

Je remercie aussi de leur soutien Elías Cueto, David González et Icíar Alfaro à Saragosse, l'accueil enthousiaste qu'ils m'ont réservé a été fondamental à diverses étapes de cette thèse.

Je remercie tout spécialement Antonio Huerta, un scientifique exceptionnel, une référence pour moi et surtout pour ses idées intervenues toujours au moment propice.

Merci beaucoup à Adrien Leygue et Felipe Bordeu, mes grands maîtres dans

la première partie de la thèse, pour leurs outils sans lesquels ces travaux auraient été très difficiles à réaliser et surtout pour avoir guidé mes premiers pas dans mes fonctions de chercheur. À Michel Coret et à Erwan Verron, merci de m'avoir fait confiance comme enseignant... en français !

Merci beaucoup à ceux qui m'ont fait connaître Valencia et sa province sans jamais y être allé. Un grand merci à José Vicente Aguado et Doménico Borzacchiello, mes guides de thèse et aussi ma deuxième famille à Nantes, sans vous tout cela n'aurait simplement pas été possible.

Finalmente agradecer a mi familia que han vivido este periplo desde la distancia, a Paca, Encarna, Antonio y Ernesto, que han estado más lejos de sus hijos y nietas de lo que les hubiese gustado. Y por supuesto a Elisa, por vivir generosamente conmigo esta aventura.

Contents

Introduction	1
1 Introduction to MOR methods.	5
1.1 Introduction to MOR methods	7
1.1.1 General classification of MOR methods	10
1.1.2 Reduced Basis	12
1.1.2.1 The Proper Orthogonal Decomposition	14
1.1.3 The Proper Generalized Decomposition	15
1.1.3.1 The PGD as a <i>computational vademecum</i> constructor	19
1.1.3.2 The PGD as an efficient solver	23
1.1.4 The Sparse Subspace Learning method	26
1.2 MOR applications to manufacturing processes	30
2 V-GFEM for transient problems	33
2.1 Introduction	35
2.2 Generalized Finite Element Method	36
2.2.1 The functional enrichment issue	40
2.3 <i>Vademecum</i> -GFEM	41
2.3.1 Introducing a precomputed adaptive enrichment using the PGD	41

2.3.2	General scheme and implementation	45
2.4	Numerical Examples	51
2.4.1	Statement of the problem	52
2.4.2	V-GFEM VS FEM	55
2.4.3	Accounting for variable technological parameters	57
2.4.4	Timing	59
3	Metalocal-global method for the analysis of large welded structures	63
3.1	Introduction	65
3.2	Metalocal-Global Method	69
3.2.1	Identification of the equivalent stiffness coefficients	69
3.2.2	General Algorithm of the Metalocal-global method	73
3.3	Numerical examples	75
3.3.1	Linear thermo-elastic benchmark	75
3.3.2	Thermo elasto-plastic example and computational vademecum	78
4	Computational Vademecums for steady-state welding simulations	85
4.1	Introduction	87
4.2	Steady-state formulations	90
4.2.1	Thermal and metallurgical formulation	90
4.2.2	Mechanical formulation	91
4.3	Numerical example	94
5	PGD solver for thermomechanical models	103
5.1	Introduction	105
5.2	Proposed strategy	107

5.2.1	The in-plane/out-of-plane decomposition in an updated Lagrangian framework	109
5.2.2	FE-SCNI	112
5.3	Validation of the strategy	114
5.3.1	Revisiting PGD through a Poisson's problem	114
5.3.2	Unsteady convection-diffusion equation	115
5.4	FSW-like kinematics	120
	Conclusion	125
	Bibliography	129

Table of figures

1.1	Scheme of the manifold and its approximation	13
1.2	Lagrangian polynomials of the first four levels	28
1.3	Full grid vs Sparse grid	29
2.1	V-GFEM stages	46
2.2	V-GFEM online stage	48
2.3	Enrichment function vademecum	50
2.4	Residual vademecum	51
2.5	Another particularization of residual vademecum	52
2.6	Scheme of the problem	53
2.7	Computational Vademecum	54
2.8	V-GFEM solution vs FEM solution	55
2.9	Adaptivity of the enrichment function	56
2.10	V-GFEM solution vs FEM solution with change in BCs	57
2.11	Enrichment functions at different advance velocities	58
2.12	Relative errors with and without adapting the enrichment function	58
2.13	Enrichment functions in different areas of incidence of the heat source	59

2.14	Difference between solution with and without updating the enrichment function	60
2.15	Thermal history of a material point	61
3.1	Large welded structure	65
3.2	Scheme of CMW methods.	68
3.3	General local-global problem.	70
3.4	Auxiliary local problem.	72
3.5	Scheme of a large structure welded at different regions.	74
3.6	Linear thermo-elastic example.	76
3.7	Linear thermo-elastic reference solutions.	76
3.8	Linear thermo-elastic local solutions with equivalent stiffness coefficients.	77
3.9	Relative errors for fixed Γ_G	77
3.10	Relative errors for traction-free Γ_G	78
3.11	Equivalent stiffness approach in a circular plate.	78
3.12	Equivalent stiffness approach with fixed Γ_G	80
3.13	Equivalent stiffness approach with traction-free condition.	81
3.14	Absolute errors of fixed local domain and equivalent stiffness approach for Γ_G fixed.	81
3.15	The first four spatial modes of the computational vademecum.	82
3.16	The first four modes of parameter α_1 of the computational vademecum.	83
3.17	The first four modes of parameter α_2 of the computational vademecum.	83
3.18	Screenshot of the ParaView interface to visualize computational vademecums.	84
4.1	Eulerian framework and Goldak ellipsoid	87

4.2	Experimental measure for source fitting	89
4.3	Relationship between material and integration points	91
4.4	Fixed displacements in the T beam	95
4.5	First two modes of spatial dimension	96
4.6	First two modes of each parametric dimension	97
4.7	Thermal vademecum	98
4.8	Parametric sliders	98
4.9	Orthogonal cut of thermal vademecum for source fitting	99
4.10	Sensitivity of temperature with respect A	99
4.11	Equivalent plastic strains vademecum	100
4.12	Proportion of phase II (Bainite) vademecum	101
5.1	General scheme of the proposed strategy	108
5.2	Voronoi tessellation to perform the SCNI	113
5.3	PDE absolute error.	116
5.4	Reference solution (continuous) versus PGD solution (spheres)	117
5.5	Relative errors in L^2 norm	119
5.6	FEM solution versus PGD solution in a convection-dominated problem	120
5.7	FSW kinematics model	121
5.8	Viscosity of a material particle with respect to the distance to the entrance	122
5.9	Material viscosity along some material pathlines	123
5.10	Direct visualization of material mixing	124

Para Eli, Lucía y Paula.

Introduction

The emergence and development of computer simulations have constituted a real revolution in science and engineering, thus having a great impact on our society. Simulations have expanded theoretical science based on mathematical models to arrive at new physical predictions, to build new scientific theories and to validate existing theories. A good example to understand that simulations *do science* today, is the gravitational waves: computational simulations predicted with amazing accuracy (and many years in advance! (Novak and Ibáñez, 2000)) recent experimental observations (Abbott et al., 2016). But in addition, numerical simulations are a formidable tool for the simulation of engineered systems. Like in fundamental science, computational simulations have taken the physical and mathematical foundations of engineering enriching them with their own disciplines such as computer science or applied mathematics, to create a new paradigm for understanding current engineering: Simulation-Based Engineering Science (SBES) (Oden et al., 2006).

If we see engineering as an interface between science and society, we can appreciate the impact that computer simulation has on our lives for their fundamental contributions in civil engineering, automotive, aeronautics, energy industries, defense, meteorology or the environment to name just a few examples. It can be said, without any doubt, that in all the above fields the incorporation of numerical simulations has been a real breakthrough in its development.

Numerical simulations in engineering began more than 60 years ago, although it is perhaps from the '90s onwards when they have revolutionized all its application fields, thanks to the important development of algorithms and the great capacity of calculation that was becoming available. Nowadays the enormous advantages of

numerical simulations are clear, among others, *in silico* experimentation without the limitations of the real world, time and economical savings, apart from no human or environmental risks.

However, there is some consensus in the scientific community (Oden et al., 2011, 2003) about the fact that the next scientific and technical challenges in our society far exceed the capabilities of the current SBES paradigm. More ambitious applications, more competitive industries, new manufacturing processes and the need of reducing environmental impact, will require rethinking calculation methods and algorithms, the management of massive data and even the role of numerical simulations in future engineers' academic training.

In this context, this thesis focuses on proposing new computational algorithms and enriching existing methods in computational mechanics to respond to some of these new requirements. In particular those concerned with advanced industries for efficient simulation of conventional and non-conventional welding processes.

The simulation of manufacturing processes involves many challenges for which traditional methods find many difficulties. Some of these are:

- Complex multiphysical and coupled models that are more and more used.
- Increasing demand for *virtual simulation platforms* that cover all stages of the design taking into account the manufacturing process itself or even products' service life.
- High-dimensional design spaces that are impossible to explore using conventional techniques.
- Need to introduce real-time simulations in deployed devices for augmented reality environments and control of data-driven manufacturing processes.

The common denominator of the different contributions included in this work to obtain simulations that can respond to these scenarios is the *Model Order Reduction* (MOR). This computational mechanic discipline has proven to be an appealing option to address the challenges of this new paradigm of computation. One of the

fundamental goal of this thesis is to show how MOR techniques not only can solve problems by themselves, but also be integrated in other traditional methods to enhance them increasing their efficiency.

After this very brief introduction, the thesis is structured as follows. In Chapter 1, a state-of-the-art of different techniques of model order reduction is elaborated, emphasizing those that have been used throughout this work. Additionally, at the end of this first chapter, different contributions of MOR for different industrial manufacturing processes are presented. In Chapter 2, a Generalized Finite Element method enriched with a *Computational Vademecum* is presented for the thermal analysis of conventional welding and thermal treatments. In Chapter 3, the mechanical analysis of conventional welding is stated. In this same chapter, computational vademecum as a library of pre-calculated knowledge are used. This allows us to greatly decrease the computational cost of certain types of welding simulations, *local-global* approach, very useful in practice. In Chapter 4, the thermal and mechanical steady-state analysis for conventional welding are elaborated and the construction of computational vademecums for them is proposed. Chapter 5 proposes an advanced high-efficiency solver for thermomechanical problems involving large deformations in plate-like geometries. This solver is based on the Proper Generalized Decomposition, one of the reduction techniques of models introduced in Chapter 1. Friction Stir Welding, a non-conventional welding process, is proposed as an application of this technique. Finally, the general conclusions of this thesis and the future lines of research that remain open are drafted.

The work introduced here has been encouraged by the scientific and industrial challenges transmitted by our industrial partner ESI Group. Without relinquishing to make scientific contributions of interest, this thesis reflects a new trend: the integration of MOR methods in a less intrusive way, taking advantage of the available tools and also for problems of industrial interest. If this has been accomplished, it has been thanks to the continued collaborative work between ESI Group and our research team.

Chapter 1

Introduction to Model Order Reduction and applications to manufacturing processes.

Model Order Reduction (MOR) is an appealing scientific discipline to address the above mentioned new challenges. In a nutshell, a MOR method is any numerical approach that aims to replace a high-fidelity simulation by another one with a much lower computational cost. A high-fidelity simulation is one carried out using traditional numerical methods such as Finite Elements, Finite Volumes or Spectral Methods, where generic approximation spaces and resolution techniques are applied. In contrast, MOR techniques pursue great computational savings through the introduction of more suitable approximation spaces for the problem in hand and more efficient solvers. The price to pay is an additional error coming from *reduction*.

MOR methods are the key ingredient of each one of the techniques presented in this thesis. Thus, it is pertinent to present a brief classification of the different families of MOR methods and to introduce the most relevant methods for this work. Namely, the Reduced Basis method (RB), the Proper Generalized Decomposition (PGD) and the Sparse Subspace Learning method (SSL) will be elaborated.

Contents

1.1	Introduction to MOR methods	7
1.1.1	General classification of MOR methods	10
1.1.2	Reduced Basis	12
1.1.3	The Proper Generalized Decomposition	15
1.1.4	The Sparse Subspace Learning method	26
1.2	MOR applications to manufacturing processes	30

1.1 Introduction to MOR methods

Model Order Reduction is a discipline of Computational Mechanics that date back to the '80s and the early '90s with the application of POD in fluid mechanics Deane et al. (1991); Gatski and Glauser (1992), following the developments in POD by Lumley Lumley (1967) in the late '60s. After these first applications in flow simulations, a large number of MOR methods and strategies has emerged for a plethora of different applications. Even with the expansion of High Performance Computing (HPC) occurring at the same time, MOR methods have been increasingly used in many fields in response to highly challenging scenarios such as:

- Optimization problems with lot of parameters where performing only one simulation can take days.
- Stochastics PDEs.
- Simulations that must be performed in real time. Such as Dynamic Data Driven Application Systems (DDDAS) applications (Darema, 2004).
- Problems defined in high dimensional spaces, such as the kinetic theory model presented in the PGD foundation paper (Ammar et al., 2006).
- The integration of numerical simulations in new contexts such as surgery (Quarteroni and Formaggia, 2004).

MOR methods do not simplify the physical model but construct new numerical strategies to compute compact and inexpensive approximations of multidimensional solutions. They exploit the correlations that naturally exist between the degrees of freedom of a numerical model, and reduces the problem's computational complexity by giving a lower dimensional representation of the solution.

The ways to classify MOR methods have been diverse according to their different features. In this section we will present a classic classification, which can be found in (Benner et al., 2013) seasoned with more current contributions from (Aguado, 2016) and (Cohen and DeVore, 2015). Due to its generality and interest, we will use a notation similar to (Cohen and DeVore, 2015).

In Computational Mechanics the modeling of a system is generally performed through Partial Differential Equations (PDEs) defined in a physical domain where certain parameters are fixed. These parameters are of different nature (geometric, material or technological parameters) and they can be formulated typically by the definition of some coefficients, flows or boundary conditions in the PDE. We speak of parametric PDEs when any of these parameters can vary within a range of interest. In general we write:

$$\mathcal{P}(u, \boldsymbol{\mu}) = 0, \quad (1.1)$$

where u is the unknown, $\boldsymbol{\mu}$ represents the parameters and $\mathcal{P} : V \times X \rightarrow W$ is a linear or nonlinear differential operator where (X, V, W) is a triplet of Banach spaces. Supposing that $\boldsymbol{\mu}$ is defined over a compact set $\mathcal{A} \subset X$ and for each value $\boldsymbol{\mu}$ a unique solution $u = u(\boldsymbol{\mu})$ exists, then the solution map,

$$u : \boldsymbol{\mu} \mapsto u(\boldsymbol{\mu}),$$

and the solution manifold,

$$\mathcal{M} = u(\mathcal{A}) = \{u(\boldsymbol{\mu}) : \boldsymbol{\mu} \in \mathcal{A}\},$$

can be defined.

It is important to note that the fact that the operator \mathcal{P} could be linear does not imply the linearity of the solution map. The calculation of this manifold may be impracticable in many of the scenarios mentioned above: high dimensionality of the parametric space X or the need to perform calculations in real time.

The solution map may also be viewed as a function

$$(x, \boldsymbol{\mu}) \mapsto u(x, \boldsymbol{\mu}),$$

and MOR methods, by exploiting certain properties of the solution map, such as holomorphy and anisotropy, (see (Cohen and DeVore, 2015) for more details), try to

approach it as follows:

$$(x, \boldsymbol{\mu}) \mapsto u_n(x, \boldsymbol{\mu}) := \sum_{i=1}^n v_i(x) \phi_i(\boldsymbol{\mu}) \quad (1.2)$$

where $\{v_1, \dots, v_n\}$ are functions of x living in the solution space V and $\{\phi_1, \dots, \phi_n\}$ are functions of $\boldsymbol{\mu}$ with values in \mathbb{R} or \mathbb{C} . This approximation is analogous to low-rank approximation of matrices and, although it is out of the scope of this work, the interested reader can find in (Aguado, 2016) a more thorough exposition of this idea.

The optimal separability of the solution map given by Eq. (1.2) leads to the concept of Kolmogorov's *n-width*, which in general, because of its computational cost, is not practical for MOR methods. Thus, we will seek separate sub-optimal approaches, which will conform the different families of MOR methods.

A fundamental idea in MOR techniques, making them very convenient to address with the challenging scenarios presented above, is the offline-online approach. These methods structure the workload in two phases:

- Offline phase. In this first stage, the approximate solution map representation (Eq. (1.2)) is constructed in a complete or partial way. It is computationally expensive but typically it is performed only once and using important computational resources (HPC).
- Online phase. In this phase, the problem in question is solved in a very economical or even trivial way, depending on whether the separated form has been calculated partially or completely.

At this point, the reader might wonder how the offline-online structure, with a costly offline stage, could lead to computational savings in comparison with traditional simulation where the workload is performed in just one stage. On the one hand, there is a gain from the fact that the offline phase is done in an “intelligent” way, working with an approximation of the solution manifolds that provides good results with a much lower computational cost. On the other hand, this structure allows to perform simulations online in light computer platforms and deployed de-

VICES, which is in itself a fundamental competitive advantage for many applications already mentioned. The workload distribution between both stages varies significantly between the different MOR methods.

1.1.1 General classification of MOR methods

We can classify the different MOR methods according to different characteristics, which are not mutually exclusive:

- *A priori / A posteriori*. Those methods that inspect the mapping of the solution, typically solving the full problem for different values of μ (snapshots), are called *a posteriori*. Those who do not perform this inspection of the solution are considered *a priori*. Reduced Basis and methods based on the POD can be considered *a posteriori*. The PGD and other low-rank approximation techniques can be considered *a priori*.
- *Adaptivity*: A non-adaptive method is one that, for a given n , selects the basis of functions $\{v_1, \dots, v_n\}$ and even $\{\phi_1, \dots, \phi_n\}$ of Eq. (1.2) *a priori* (up to a multiplicative set of coefficients), typically through some knowledge of the solution. On the contrary, an adaptive method is the one that, typically in a greedy way, adds a function n which depends on the $n - 1$ previously obtained to enrich them. This classification might seem equivalent to the former one, since it is commonly thought that any non-adaptive method is *a priori* and any adaptive method is *a posteriori*. However, in the opinion of the author, these features are not correlated. This is the case, for example, of the PGD, where without requiring snapshots (it is an *a priori* method) follows a greedy strategy to construct, in an adaptive way, the separated form. In general adaptive techniques provide better results. In this thesis, all the techniques used (whether the calculation of snapshots is needed or not) are adaptive.
- *Projective / Interpolant*. In MOR, a simplified form of the mapping of the solution is sought. However, this can be done in different ways and with different workload distribution between the offline-online phases. Projective

methods only compute $\{v_1, \dots, v_n\}$ in the offline phase, constructing a basis. On this basis, the original PDE is projected, being expressed in a much smaller dimension. Then, the reduced PDE is solved to calculate the coefficients $\{\phi_1(\boldsymbol{\mu}), \dots, \phi_n(\boldsymbol{\mu})\}$ in the online phase. On the contrary, the interpolating methods calculate the entire separated form during the offline stage, leaving for the online one the trivial task of substituting the values of the parameter in the previous expression. These methods are able to calculate a numerical handbook of the solution, also known as *computational vademecum* (Chinesta et al., 2013b), since the solution is precomputed offline with an explicit dependence of the parameters.

- **Intrusiveness.** It is said that a method is non-intrusive if it is possible to implement it without substantially modifying the high-fidelity simulation solver and without knowing the exact form of the PDE. An ideal non-intrusive MOR method uses the high-fidelity solver as a black-box and without needing to know the original PDE that is being solved. In contrast, an intrusive method makes use of the PDE structure itself and modifies the resolution method. *A priori* methods, such as PGD, are clear examples of intrusive methods, whereas those based on POD, Reduced Basis or polynomial interpolation approaches are non-intrusive (or very slightly intrusive). Sometimes intrusiveness is not a problem but a goal. It is the case of the reformulation of a solver using a MOR technique to gain efficiency. An example is the in-plane-out-of-plane PGD decomposition that is used in Chapter 5. However, and generally speaking, intrusiveness is an impediment to the incorporation of MOR solutions into preexisting simulation platforms. This problem is very present today, and intrusive methods such as the PGD are being reformulated in much less intrusive (Borzacchiello et al., 2017, 2016) versions. This thesis is also an example of this tendency and the MOR methods that appear in Chapters 2, 3 and 4 are non-intrusive.

After this brief classification we will elaborate the two MOR methods that are used in the following chapters of this thesis: the PGD and the SSL. Also, for a better understanding of these methods, the Reduced Basis method is introduced first.

1.1.2 Reduced Basis

Although this family of MOR methods is not used in this thesis, for the sake of completeness, in this section we will briefly describe the generalities of Reduced Basis methods (Maday et al., 2002; Patera and Rozza, 2007; Quarteroni et al., 2015). Moreover, the POD which is not a MOR method itself, but the main ingredient to construct reduced spaces, is also introduced. We will focus on the Galerkin Reduced Basis (G-RB), which will enable us to understand the principles of the majority of projective MOR methods.

Let us consider a parametric PDE with a set of parameters $\boldsymbol{\mu}$ expressed in Eq. (1.1). The set of solutions $u(\boldsymbol{\mu})$ generated as $\boldsymbol{\mu}$ varies in its domain \mathcal{A} producing a manifold \mathcal{M} (see Fig. 1.1). The fundamental hypothesis of RB is that this manifold can be approximated by the linear combination of a few elements of \mathcal{M} . The underlying idea is to generate an approximated solution that belongs to a subspace $V_N \in V$ of dimension $N \ll \dim(V)$ and, in that way, much less expensive computational-wise. The following are the steps involved:

- I The high-fidelity problem is solved for a given set $S = \{\boldsymbol{\mu}_1, \dots, \boldsymbol{\mu}_p\}$ of values of the parameters. These solutions are called snapshots:

$$\{u(\boldsymbol{\mu}_1), \dots, u(\boldsymbol{\mu}_p)\}.$$

- II From these snapshots, using the POD (see section 1.1.2.1), a basis of N functions is constructed,

$$\{v_1, \dots, v_N\},$$

which generates the reduced basis space:

$$V_N = \text{span}\{v_1, \dots, v_N\}.$$

It is important to note that none of the functions v_i are solution of the high-fidelity problem.

- III Once the basis is obtained, the reduced problem is generated by projection of the

discretized PDE, generating a system of N independent equations. This implies the orthogonalization of the residual of the high-fidelity problem calculated in the reduced solution with respect to a subspace $W_N \in V$ of dimension N . If $W_N = V_N$, then it is the particular case of a Galerkin Reduced Basis method that can be formulated as follows. Find $u_N(\boldsymbol{\mu}) \in V_N$ such that

$$a(u_N(\boldsymbol{\mu}), w_N; \boldsymbol{\mu}) = f(w_N; \boldsymbol{\mu}) \quad \forall w_N \in V_N. \quad (1.3)$$

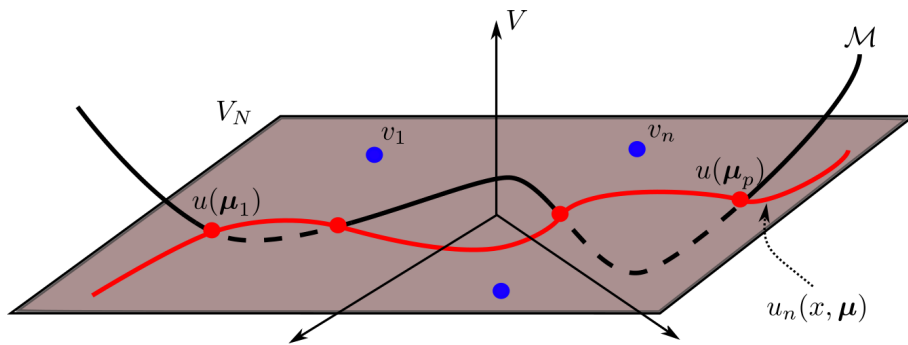


Figure 1.1: Scheme of the manifold and its approximation

Taking into account the offline-online division, previous scheme's phases I and II are performed offline while III is carried out online. It is clear how, unlike other MOR methods, the use of Reduced Basis methods also implies a resolution of a PDE (with reduced dimensionality size) in the online phase (Eq. (1.3)).

It is important to note that resolution complexity scales with the reduced dimension N provided the PDE is linear. In the case of having a nonlinear PDE, the resolution of the reduced PDE will continue to imply a computational cost that depends on the dimensionality of the high-fidelity problem. This is because nonlinear terms must be reconstructed in the original space V to be evaluated. This problem is today one of today's most actively researched topics in the MOR community and there are several widely accepted methods such as the Empirical Interpolation Method (EIM) (Barrault et al., 2004), its discrete counterpart DEIM (Chaturantabut and Sorensen, 2010) and the Hyper-reduction methods (Farhat et al., 2015; Hernández et al., 2017).

1.1.2.1 The Proper Orthogonal Decomposition

The POD is not a MOR method in itself but a key algorithm for important methods such as Reduced Basis and projected MOR methods in general. The POD is a technique for reducing the dimensionality of a dataset by its representation on an orthonormal basis that is optimal in a least-square sense. The original variables are transformed into a new set of uncorrelated variables (called modes). Ideally, considering only a few of these modes, most of the energy present with the original variables is retained.

If we consider the set of snapshots $S = \{\boldsymbol{\mu}_1, \dots, \boldsymbol{\mu}_p\}$, we define the snapshot matrix $\mathbf{S} \in \mathbb{R}^{d \times p}$, with $d = \dim(V)$, as

$$\mathbf{S} = [\mathbf{u}_1 \mid \dots \mid \mathbf{u}_p],$$

where u_i is the resolution of the high-fidelity problem for the set of parameter values $\boldsymbol{\mu}_p$. Making a Singular Value Decomposition (Golub and Van Loan, 2012) of \mathbf{S} we obtain

$$\mathbf{S} = \mathbf{U}\boldsymbol{\Sigma}\mathbf{Z}^T,$$

where $\mathbf{U} = [\boldsymbol{\varphi}_1 \mid \dots \mid \boldsymbol{\varphi}_d] \in \mathbb{R}^{d \times p}$ and $\mathbf{Z} = [\boldsymbol{\chi}_1 \mid \dots \mid \boldsymbol{\chi}_d] \in \mathbb{R}^{p \times p}$ are orthogonal arrays and $\boldsymbol{\Sigma} = \text{diag}(\sigma_1, \dots, \sigma_r) \in \mathbb{R}^{d \times p}$ with $\sigma_1 \geq \sigma_2 \geq \dots \geq \sigma_r$. Since

$$\mathbf{S}^T \boldsymbol{\varphi}_i = \sigma_i^2 \boldsymbol{\chi}_i, \quad i = 1, \dots, r$$

or equivalently,

$$\mathbf{S}\mathbf{S}^T \boldsymbol{\varphi}_i = \sigma_i^2 \boldsymbol{\varphi}_i, \quad i = 1, \dots, r,$$

then $\sigma_i^2, i = 1, \dots, r$, are the nonzero eigenvalues of the matrix $\mathbf{S}^T \mathbf{S}$ (the so-called correlation matrix), listed in nondecreasing order.

For any $N < n_p$, the POD basis $V \in \mathbb{R}^{d \times N}$ of dimension N (step II of the algorithm of the Reduced Basis) is defined as the set of the first N left singular vectors $\boldsymbol{\varphi}_1, \dots, \boldsymbol{\varphi}_N$ of \mathbf{U} .

It can be proved that the error in the POD basis is equal to the sum of the

squares of the singular values corresponding to the neglected POD modes (Benner and Sokolov, 2006). Therefore, to select the dimension $N < r$ such that the projection error is less than a desired ϵ_{POD} tolerance it is sufficient to choose N as the smallest integer such that

$$I(N) = \frac{\sum_{i=1}^N \sigma_i^2}{\sum_{i=1}^r \sigma_i^2} \geq 1 - \epsilon_{POD}^2.$$

1.1.3 The Proper Generalized Decomposition

In the previous section we have described the basic principles of Reduced Basis, *a posteriori* projective MOR method. These techniques present certain limitations, mainly the difficulty to apply them to problems involving a large number of parameters (*the curse of dimensionality* (Bellman, 1956)) and the criterion of choosing the appropriate snapshots to build the reduced basis. These limitations motivated the emergence of other techniques that could circumvent these problems, as is the case of the PGD.

The PGD, proposed in 2006 by Chinesta et al (Ammar et al., 2006), generalizes the radial decomposition previously introduced by Ladeveze (Ladeveze, 1985) as an ingredient of the LATIN method, considering parameters of any nature with surprising results. It is an *a priori* MOR method (it does not need snapshots), and thanks to its incremental algorithm of construction that uses alternated directions, it efficiently amends the curse of dimensionality.

In the first place we are going to introduce the PGD with a general formalism, following the presentation of (Aguado, 2016). This approach allows us to appreciate the elegance of the PGD by extracting it from particular discretization methods or a specific algorithm of construction.

Let us consider the variational form of the parametric PDE given in Eq. (1.1), for the particular case of having only one parameter μ . The problem can be formulated as finding $u \in V_s$, where V_s is an appropriate approximation space, such that

$$a(u, w; \mu) = l(w), \tag{1.4}$$

for every $w \in V_s$ and some $\mu \in I_\mu$. Bilinear and linear forms are denoted by $a(\cdot, \cdot) : V_s \times V_s \rightarrow \mathbb{K}$ and $l(\cdot) : V_s \rightarrow \mathbb{K}$, respectively, where \mathbb{K} is \mathbb{R} or \mathbb{C} . The former model is the so-called high-fidelity problem, even when u is an approximated solution.

For a proper understanding of the PGD principles it is necessary to first introduce the notion of tensor product spaces. Let us construct an approximation of the solution in the parametric domain, so the high-fidelity problem must be reformulated: find $u \in V := V_s \otimes V_\mu$, a tensor product space (Kolda and Bader, 2009), such that

$$a(u, w) = l(w),$$

for every $w \in V$. It is important to note that the parametric dependence is omitted since the approximation space covers the parametric domain. This means that the parameter is a new coordinate just as space and time.

If $V_s := \text{span}\{v_s^{1 \leq i \leq N}\}$ and $V_\mu := \text{span}\{v_\mu^{1 \leq i \leq M}\}$, an element of the tensor product space, V , of these spaces reads:

$$u = \sum_{i=1}^N \sum_{j=1}^M \alpha_{ij} v_s^i v_\mu^j, \quad (1.5)$$

where v_s and v_μ are elements of V_s and V_μ respectively. α_{ij} defines the entries of a two-dimensional tensor, $\alpha \in \mathbb{K}^{N \times M}$.

The construction of a solution in the form given by Eq.(1.5), in general, entails a prohibitive computational cost, since its complexity scales exponentially with the number of dimensions of the problem. Instead, other separate solutions are sought that imply a much lower cost, such as the PGD.

Let us consider the high-fidelity problem and the functional spaces \mathcal{V}_s and \mathcal{V}_μ , the spatial and parametric functional spaces respectively. Let us define the tensor product space $\mathcal{V} := \mathcal{V}_s \otimes \mathcal{V}_\mu$ that can be built from them. Consider now the R pairs of functions $(u_s^r, u_\mu^r) \in \mathcal{V}_s \times \mathcal{V}_\mu$ such that the solution of Eq.(1.4) can be well approximated as follows:

$$u \approx \sum_{r=1}^R u_s^r u_\mu^r. \quad (1.6)$$

Eq. (1.6) is called a separated representation of order R , because it is a sum of function products of space and parameter. The objective of PGD is to compute the function pairs (u_s^r, u_μ^r) , also called space and parameter *modes*, respectively.

Let us consider the following finite dimensional approximation spaces defined from the modes:

$$V_s := \text{span} \left\{ v_s^r = \frac{u_s^r}{\|u_s^r\|}, 1 \leq r \leq R \right\} \quad \text{and} \quad V_\mu := \text{span} \left\{ v_\mu^r = \frac{u_\mu^r}{\|u_\mu^r\|}, 1 \leq r \leq R \right\},$$

both of dimension R . A tensor product space can be built from these spaces as $V := V_s \otimes V_\mu \subset \mathcal{V}$. Let us introduce a subset of that tensor product space:

$$S_R := \left\{ v \in V : v = \sum_{r=1}^R u_r v_s^r v_\mu^r, \text{ with } v_s^r \in V_s, v_\mu^r \in V_\mu \text{ and } u_r \in \mathbb{K} \right\}.$$

We denote by u^R an element of S_R , also called a rank- R separated representation. From Eq. (1.6), the approximation $u \approx u^R$ belongs to that subset.

PGD allows building S_R progressively: S_1, S_2, \dots , each one of them defined from $S_R = S_{R-1} + S_1$, for $R \geq 2$. Therefore, the successive approximation spaces are nested, i.e. $S_{R-1} \subset S_R$. This is made by seeking a pair $(u_s, u_\mu) \in \mathcal{V}_s \times \mathcal{V}_\mu$. When it is available, V_s and V_μ are updated by normalizing u_s and u_μ , respectively. The new approximation will be defined from

$$u^{(R+1)} = u^R + u_s u_\mu \quad \Leftrightarrow \quad u^{(R+1)} = \sum_{r=1}^{R+1} u_r v_s^r v_\mu^r.$$

In order to introduce the PGD algorithm, let us assume that we have already built S_R , i.e. u^R is known, and we want to compute a couple $(u_s, u_\mu) \in \mathcal{V}_s \times \mathcal{V}_\mu$ such that:

$$a(u_s u_\mu, w) = r(u^R, w), \tag{1.7}$$

for every $w \in \mathcal{V}$. We denote by $r(\cdot, \cdot)$ the residual, defined as

$$r(u^R, w) := l(w) - a(u^R, w).$$

Observe that computing both u_s and u_μ is a nonlinear problem. Let us assume that the problem to be solved is elliptic. Then, Eq. (1.7) can be turned into an equivalent nonlinear optimization problem:

$$\min_{u_s, u_\mu} \mathcal{J}(u_s, u_\mu) := \frac{1}{2}a(u_s u_\mu, u_s u_\mu) - r(u^R, u_s u_\mu).$$

The stationarity conditions of the functional can be found by means of calculus of variations. Consider the following arbitrary variations: $u_s + \xi w_s$ and $u_\mu + \eta w_\mu$. Substituting and taking derivatives with respect to ξ and η :

$$a(u_s u_\mu, w_s u_\mu) = r(u^R, w_s u_\mu), \quad \forall w_s \in \mathcal{V}_s, \quad (1.8a)$$

$$a(u_s u_\mu, u_s w_\mu) = r(u^R, u_s w_\mu), \quad \forall w_\mu \in \mathcal{V}_\mu. \quad (1.8b)$$

The stationarity conditions can be expressed in a single equation as follows: find $(u_s, u_\mu) \in \mathcal{V}_s \times \mathcal{V}_\mu$ such that

$$a(u_s u_\mu, w_s u_\mu + u_s w_\mu) = r(u^R, w_s u_\mu + u_s w_\mu), \quad \forall (w_s, w_\mu) \in \mathcal{V}_s \times \mathcal{V}_\mu. \quad (1.9)$$

Eq. (1.9) can be interpreted as a Galerkin formulation which imposes the cancellation (i.e. orthogonality) of the residual simultaneously with respect to $\mathcal{V}_s \otimes \{u_\mu\}$ and $\{u_s\} \otimes \mathcal{V}_\mu$ (Nouy, 2010).

Eq. (1.8) suggests applying a fixed-point algorithm to solve the nonlinear optimization problem. The fixed-point is as follows:

- I Assume u_μ is known, then update u_s from Eq. (1.8a).
- II From u_s just computed, update u_μ by solving Eq. (1.8b).
- III Go back to the first step.

Once presented this general formulation, we will particularize the PGD with two worked examples that will serve to understand two of the most important applications of PGD that have been used in this thesis: the PGD as a computational vademecum constructor (Chinesta et al., 2013b; Courard et al., 2016) and the PGD

as a particularly efficient differential solver. The reader thus engaged can find in (Chinesta et al., 2013a) more details about PGD and even in (Cueto et al., 2016) Matlab codes to solve similar examples to those presented here.

1.1.3.1 The PGD as a *computational vademecum* constructor

Let us consider the following parametric heat transfer equation:

$$\frac{\partial u}{\partial t} - k \cdot \Delta u = f$$

with homogeneous initial and boundary conditions. PGD opens the possibility of introducing general parameters of the problem as extra coordinates in order to construct a *computational vademecum*. It means that, for example, the material properties or the applied forces are no longer parameters but coordinates of the problem. Thus, the solution can be particularized later for any particular value of each parameter (coordinate) inside their domains of definition. Instead of tackling the original problem, an offline more complex problem is constructed. Once the latter is solved, we can get the original problem's solution for any particular case. In order to do so, we just have to run online evaluations with a negligible cost.

The price to pay is an increase of the problem dimensionality and the resulting nonlinear formulation. The first drawback is overcome by the fact that the PGD formulation scales linearly with the dimensions so it is not a major issue. The second one is circumvented using an appropriate iterative solver, in practice, the alternate direction fixed-point algorithm.

The weighted residual form of the problem reads:

$$\int_{\Omega \times \mathcal{I}_t \times \mathcal{I}_k} u^* \cdot \left(\frac{\partial u}{\partial t} - k \cdot \Delta u - f \right) d\mathbf{x} \cdot dt \cdot dk = 0$$

for every test function u^* in its appropriate functional space.

In this example we introduce the time and the conductivity of the material as extra coordinates of the computational vademecum. This implies that the desired

solution will have the next form:

$$u(\mathbf{x}, t, k) \approx \sum_{i=1}^N X_i(\mathbf{x}) \cdot T_i(t) \cdot K_i(k).$$

Assuming that we are in the enrichment step n , the following approximation is already known,

$$u^{n-1}(\mathbf{x}, t, k) \approx \sum_{i=1}^{n-1} X_i(\mathbf{x}) \cdot T_i(t) \cdot K_i(k).$$

and one desires to compute a new functional product $X_n(\mathbf{x}) \cdot T_n(t) \cdot K_n(k)$, which we write as $R_n(\mathbf{x}) \cdot S_n(t) \cdot W_n(k)$ for notational simplicity. Thus, the solution in this step n reads:

$$u^n = u^{n-1} + R_n(\mathbf{x}) \cdot S_n(t) \cdot W_n(k). \quad (1.10)$$

In order to compute the new enrichment functional we consider the next test function:

$$u^* = R_n^*(\mathbf{x}) \cdot S_n(t) \cdot W_n(k) + R_n(\mathbf{x}) \cdot S_n^*(t) \cdot W_n(k) + R_n(\mathbf{x}) \cdot S_n(t) \cdot W_n^*(k). \quad (1.11)$$

Hence, trial and test functions are given by the equations (1.10) and (1.11) respectively. Introducing them in the variational form, the next nonlinear problem is obtained:

$$\begin{aligned} \int_{\Omega \times \mathcal{I}_t \times \mathcal{I}_k} u^* \cdot \left(R \cdot W \frac{dS}{dt} - k \cdot S \cdot W \Delta R \right) d\mathbf{x} \cdot dt \cdot dk = \\ \int_{\Omega \times \mathcal{I}_t \times \mathcal{I}_k} u^* \cdot f - \sum_{i=1}^{n-1} \int_{\Omega \times \mathcal{I}_t \times \mathcal{I}_k} u^* \cdot \left(X_i \cdot K_i \frac{dT_i}{dt} - k \cdot K_i \cdot T_i \Delta X_i \right) d\mathbf{x} \cdot dt \cdot dk \end{aligned}$$

where the coordinate dependencies have been removed to alleviate the notation. Additionally, we will consider that the source function can be expressed in a separated form:

$$f \approx \sum_{j=1}^m f_j^x(\mathbf{x}) \times f_j^t(t) \times f_j^k(k),$$

which can be obtained using a HOSVD or applying a PGD approximation, as we will study in the first example of this chapter.

As we have indicate before, this problem is solved with the alternated direction fixed-point algorithm which works as follows:

I Assuming $S(t)$ and $W(k)$ known, $R(x)$ is computed:

$$\begin{aligned}
 -\alpha^x \beta^x \int_{\Omega} R^* R d\mathbf{x} - \gamma^x \delta^x \int_{\Omega} R^* \Delta R d\mathbf{x} &= \sum_{j=1}^m \chi_j^x \pi_j^x \int_{\Omega} R^* f_j^x d\mathbf{x} - \\
 &- \sum_{i=1}^{n-1} \left(\alpha_i^x \beta_i^x \int_{\Omega} R^* X_i d\mathbf{x} - \gamma_i^x \delta_i^x \int_{\Omega} R^* \Delta X_i d\mathbf{x} \right), \quad (1.12)
 \end{aligned}$$

where the the integrals have been split and the next scalar values are known at this point:

$$\begin{aligned}
 \alpha^x &= \int_{\mathcal{I}_k} W^2 dk & \alpha_i^x &= \int_{\mathcal{I}_k} kW K_i dk \\
 \beta^x &= \int_{\mathcal{I}_t} S \frac{dS}{dt} dt & \beta_i^x &= \int_{\mathcal{I}_t} S \frac{dT_i}{dt} dt \\
 \gamma^x &= \int_{\mathcal{I}_k} kW^2 dk & \gamma_i^x &= \int_{\mathcal{I}_k} kW K_i dk \\
 \delta^x &= \int_{\mathcal{I}_t} S^2 dt & \delta_i^x &= \int_{\mathcal{I}_t} S T_i dt \\
 \chi_j^x &= \int_{\mathcal{I}_k} W f_j^k dk & \pi_j^x &= \int_{\mathcal{I}_t} S f_j^t dt.
 \end{aligned}$$

II With the assumed $W(k)$ and the previously computed $R(x)$, $S(t)$ is obtained solving:

$$\begin{aligned}
 \alpha^t \beta^t \int_{\mathcal{I}_t} S^* \frac{dS}{dt} dt - \gamma^t \delta^t \int_{\mathcal{I}_t} S^* S dt &= \sum_{j=1}^m \chi_j^t \pi_j^t \int_{\mathcal{I}_t} S^* f_j^t dt - \\
 &- \sum_{i=1}^{n-1} \left(\alpha_i^t \beta_i^t \int_{\mathcal{I}_t} S^* \frac{dT_i}{dt} dt - \gamma_i^t \delta_i^t \int_{\mathcal{I}_t} S^* T_i dt \right), \quad (1.13)
 \end{aligned}$$

where the scalar values read:

$$\begin{aligned}
 \alpha^t &= \int_{\Omega} R^2 d\mathbf{x} & \alpha_i^t &= \int_{\Omega} R X_i d\mathbf{x} \\
 \beta^t &= \int_{\mathcal{I}_k} W^2 dk & \beta_i^t &= \int_{\mathcal{I}_k} W K_i dk \\
 \gamma^t &= \int_{\Omega} R \Delta R d\mathbf{x} & \gamma_i^t &= \int_{\Omega} R \Delta X_i d\mathbf{x} \\
 \delta^t &= \int_{\mathcal{I}_k} k W^2 dk & \delta_i^t &= \int_{\mathcal{I}_k} k W K_i dk \\
 \chi_j^t &= \int_{\Omega} R f_j^x d\mathbf{x} & \pi_j^t &= \int_{\mathcal{I}_k} W f_j^k dk.
 \end{aligned}$$

III Finally, using $R(x)$ and $S(t)$ from previous steps $W(k)$ is computed:

$$\begin{aligned}
 \alpha^k \beta^k \int_{\mathcal{I}_k} W^* W dk - \gamma^k \delta^k \int_{\mathcal{I}_k} k W^* W dk &= \sum_{j=1}^m \chi_j^k \pi_j^k \int_{\mathcal{I}_k} W^* f_j^k dk - \\
 &- \sum_{i=1}^{n-1} \left(\alpha_i^k \beta_i^k \int_{\mathcal{I}_k} W^* K_i dk - \gamma_i^k \delta_i^k \int_{\mathcal{I}_k} k W^* K_i dk \right), \quad (1.14)
 \end{aligned}$$

where

$$\begin{aligned}
 \alpha^k &= \int_{\Omega} R^2 d\mathbf{x} & \alpha_i^k &= \int_{\Omega} R X_i d\mathbf{x} \\
 \beta^k &= \int_{\mathcal{I}_t} S \frac{dS}{dt} dt & \beta_i^k &= \int_{\mathcal{I}_t} S \frac{dT_i}{dt} dt \\
 \gamma^k &= \int_{\Omega} R \Delta R d\mathbf{x} & \gamma_i^k &= \int_{\Omega} R \Delta X_i d\mathbf{x} \\
 \delta^k &= \int_{\mathcal{I}_t} S^2 dk & \delta_i^k &= \int_{\mathcal{I}_t} S T_i dt \\
 \chi_j^k &= \int_{\Omega} R f_j^x d\mathbf{x} & \pi_j^k &= \int_{\mathcal{I}_t} S f_j^t dt.
 \end{aligned}$$

This three steps are repeated in a loop until the convergence of the new functional product is achieved. It is important to remark that Eq. (1.12) is a regular second order PDE which can be solved for any method. In practice, the integration by parts is applied and then linear interpolations can be used. If the strong form is recovered, Eq. (1.13) is a first order ODE that can be solved with any temporal integrator. Eq. (1.14) does not involve any derivatives, it is a linear system of equations.

1.1.3.2 The PGD as an efficient solver

One of the most prolific PGD applications, because of the quality of the results and its diverse applicability, is the so-called in-plane-out-of-plane decomposition. The first applications in linear elasticity were published in (Bognet et al., 2012a,b). More recently it has been used in no-Newtonian squeeze flows with porous media (Ghnatios et al., 2015).

Many of the models of material forming and composites manufacturing processes are defined in degenerated three-dimensional domains. It is called degenerated domain such domain in which one or two of the dimensions are much smaller than the others, as in plate-type geometries. Mesh-based solution of models defined in such domains is a challenging issue because they involve meshes with too many degrees of freedom. Often, the physics of the problem is very rich in the direction of the degenerated coordinate (typically the thickness) and a very fine mesh is required. This could lead to unaffordable computational costs.

Traditionally in engineering, this problem has been solved using simplified models defined in domains with less dimensions. This is the case of the classical theories of strength of materials, where three-dimensional solids are approximated by 1D or 2D models (beams, plates and shells) (Timoshenko et al., 1956). These approximations involve some kinematical and mechanical hypotheses on the evolution of the solution through the degenerated dimension. Then, the solution is only valid in those points in which the Saint-Venant principle is satisfied.

The PGD has the advantage of the separation of the variables to decrease the dimensionality of the operators to compute. As we have previously seen, it is possible to find the solution in the form

$$u(\mathbf{x}) \approx \sum_{i=1}^N X_i(x) \cdot Y_i(y) \cdot Z_i(z),$$

but also using a plate-type decomposition,

$$u(\mathbf{x}) \approx \sum_{i=1}^N X_i(x, y) \cdot Z_i(z).$$

In the first case, a complete separation is carried out. This means that we also need a fully-separated geometry, which is complicated to find in practice. However, the plate-type decomposition or the in-plane-out-of-plane decomposition is much more versatile: many geometries involved in practical problems can be generated using the extrusion of a generic 2D section. This technique is used throughout this work and it will be explained in detail.

It has to be remarked that the in-plane-out-of-plane PGD solution is not a simplified mode such as the beams or plates theories. It is a fully 3D solution which is able to represent the 3D effects that the simplified theories cannot do. Thus, comparisons should be made with real 3D FEM models. This fact does not mean that no relationships could be established between the PGD separated solution and some simplified models. The first PGD modes usually capture the solution of the simplified models, enriching the solution with the following modes.

Let us illustrate the technique with a simple problem, a linear elastic problem in a plate-shape $\Xi = \Omega \times \mathcal{I}$ domain. Assuming the next separated form of the displacement field

$$\mathbf{u}(x, y, z) = \begin{pmatrix} u(x, y, z) \\ v(x, y, z) \\ w(x, y, z) \end{pmatrix} \approx \sum_{i=1}^N \begin{pmatrix} u_{xy}^i(x, y) \cdot u_z^i(z) \\ v_{xy}^i(x, y) \cdot v_z^i(z) \\ w_{xy}^i(x, y) \cdot w_z^i(z) \end{pmatrix}.$$

where $u_{xy}(x, y)$, $v_{xy}(x, y)$ and $w_{xy}(x, y)$ are function of the in-plane coordinates, whereas $u_z(z)$, $v_z^i(z)$ and $w_z(z)$ are functions involving the thickness coordinate. The weak formulation of this problem reads:

$$\int_{\Xi} \boldsymbol{\varepsilon}(\mathbf{u}^*) \cdot \mathbf{K} \cdot \boldsymbol{\varepsilon}(\mathbf{u}) d\Xi = \int_{\Xi} \mathbf{u}^* \cdot \mathbf{f}_d d\Xi + \int_{\Gamma_N} \mathbf{u}^* \cdot \mathbf{F}_d d\Gamma,$$

where \mathbf{K} is the Hooke tensor, \mathbf{f}_d represents the body forces and \mathbf{F}_d the forces

applied on the boundary Γ_N . The strains have the next separated expression:

$$\boldsymbol{\varepsilon}(\mathbf{u}(x, y, z)) \approx \sum_{i=1}^N \begin{pmatrix} u_{xy,x}^i \cdot u_z^i \\ v_{xy,y}^i \cdot v_z^i \\ w_{xy}^i \cdot w_{z,z}^i \\ u_{xy,y}^i \cdot u_z^i + v_{xy,x}^i \cdot v_z^i \\ u_{xy}^i \cdot u_{z,z}^i + w_{xy,x}^i \cdot w_z^i \\ v_{xy}^i \cdot v_{z,z}^i + w_{xy,y}^i \cdot w_z^i \end{pmatrix}.$$

Assuming that the first n modes have been computed, we want enrich the solution adding another functional product:

$$\mathbf{u}^{n+1}(x, y, z) = \mathbf{u}^n(x, y, z) + \begin{pmatrix} R_u(x, y) \cdot S_u(z) \\ R_v(x, y) \cdot S_v(z) \\ R_w(x, y) \cdot S_w(z) \end{pmatrix}.$$

The last expression conforms the trial function. As we have seen in the previous section, the test function has the next form:

$$\mathbf{u}^*(x, y, z) = \begin{pmatrix} R_u^*(x, y) \cdot S_u(z) + R_u(x, y) \cdot S_u^*(z) \\ R_v^*(x, y) \cdot S_v(z) + R_v(x, y) \cdot S_v^*(z) \\ R_w^*(x, y) \cdot S_w(z) + R_w(x, y) \cdot S_w^*(z) \end{pmatrix}.$$

The weak form, after introducing the trial and test function, reads:

$$\begin{aligned} & \int_{xy} \int_z \boldsymbol{\varepsilon}(\mathbf{u}^*(x, y, z)) \cdot \mathbf{K} \cdot \boldsymbol{\varepsilon}(\mathbf{u}^{n+1}(x, y, z)) \, dx \, dy \, dz \\ &= \int_{xy} \int_z \mathbf{u}^*(\mathbf{x}, \mathbf{y}, z) \cdot \mathbf{f}_d \, dx \, dy \, dz + \int_{\Gamma_N} \mathbf{u}^*(\mathbf{x}, \mathbf{y}, z) \cdot \mathbf{F}_d \, d\Gamma. \end{aligned} \quad (1.15)$$

It is easy to check that, due to the product of unknown functions, the problem has become nonlinear. To solve it, the alternated direction fixed-point algorithm previously described is employed.

Given an initial value $\mathbf{S}^{(0)}(z)$ of $\mathbf{S}(z)$ arbitrarily chosen, all z dependent functions are known. Eq. (1.15) therefore is reduced to a 2D problem where the three

components of $\mathbf{R}(x, y)$ are the unknown fields. Its solution yields $\mathbf{R}^{(1)}(x, y)$, a first approximation of $\mathbf{R}(x, y)$. Then using the just computed $\mathbf{R}^{(1)}(x, y)$ in (1.15), we similarly obtain a 1D problem which allows computing the three components of $\mathbf{S}^{(1)}(z)$ that constitutes the next approximation of $\mathbf{S}(z)$. This fixed point loop keeps running until reaching convergence, i.e:

$$\int_{\Xi} \sum_{i=1}^{i=3} \left(\mathbf{R}^{(j)}(x, y) \cdot \mathbf{S}^{(j)}(z) - \mathbf{R}^{(j-1)}(x, y) \cdot \mathbf{S}^{(j-1)}(z) \right)^2 dx dy dz \leq \epsilon,$$

where ϵ is a small enough tolerance.

One continues adding new PGD modes until certain approximation grade is reached. In general this is achieved by imposing a minimum bound to the residual of the PDE after the new mode is added. In practice the residual is not computed after each new incorporation because it is computationally expensive. Depending on the application, the residual is computed after 5, 10 or more PGD modes.

1.1.4 The Sparse Subspace Learning method

This is an adaptive and *a posteriori* MOR method which does not produce a reduced system of equations but the parametric solution itself (interpolant method).

The SSL can be coupled, in principle, to any third-party simulation software in a non-intrusive way. The nonlinear problems become completely transparent to the user and the intrinsic parallelism of the parametric collocation approach results in a very competitive method (Borzacchiello et al., 2017).

The SSL method introduces a collocation approach in the parametric domain and a hierarchical interpolation basis with an incremental strategy in order to control the rank of the approximation. Let us assume that $\boldsymbol{\mu}$ is the vector of the parameters of the problem and $u(\boldsymbol{\mu})$ the computational vademecum sought. With the SSL method, the exact solution u is computed in a given set of defined points $\boldsymbol{\mu}_j$ called collocation points and then the solution is interpolated over the parametric space by interpolation,

$$u(\mathbf{x}, \boldsymbol{\mu}) = \sum_m \psi_s^m(\mathbf{x}) \psi_p^m(\boldsymbol{\mu}),$$

where $\psi_p^m(\boldsymbol{\mu})$ are given *a priori*, while the $\psi_s^m(\boldsymbol{x})$ are to be determined through the solution of full problem in collocation points. The *a priori* functions and the optimal collocation points must be defined consistently.

The solutions corresponding to the different sampling parameters can be computed separately using a standard deterministic solver to which the parameters are fed as input. In this sense, the parametric solution is approximated based only on the output of a black-box solver, provided that the representation basis is chosen in a suitable manner. Once the functions $\psi_p^m(\boldsymbol{\mu})$ are selected, optimal collocation points can be defined accordingly. Among different available options, an hierarchical approach involving Gauss-Chebyshev-Lobatto points and Lagrangian polynomials is very convenient for its efficiency and straightforward implementation.

For the sake of simplicity, let us consider first the case in which only one parameter μ is introduced. The collocation points are naturally chosen as the GCL points,

$$\mathcal{P}_n = \{p_0, p_1, \dots, p_n\},$$

comprising extrema of the n -th order Chebyshev polynomial of the first kind, $T_n(\mu)$, defined in $\Omega_\mu \equiv [\mu_{min}, \mu_{max}]$, plus the ending points $p_0 = \mu_{min}$ and $p_n = \mu_{max}$.

GCL points have the important property of being “nested”, as in:

$$\dots \subset \mathcal{P}_{2(k-1)} \subset \mathcal{P}_{2k} \subset \mathcal{P}_{2(k+1)} \subset \dots \quad \text{for } k \in \mathbb{N}.$$

The 0-th level of the grid hierarchy only includes the ending points of the parametric space allowing for a linear approximation. Therefore:

$$\begin{aligned} \psi_s^1(\boldsymbol{x}) &\equiv u(\boldsymbol{x}; \mu_{min}), & \psi_p^1(\mu) &= \frac{\mu_{min} - \mu}{\mu_{max} - \mu_{min}}, \\ \psi_s^2(\boldsymbol{x}) &\equiv u(\boldsymbol{x}; \mu_{max}), & \psi_p^2(\mu) &= \frac{\mu_{max} - \mu}{\mu_{max} - \mu_{min}}. \end{aligned}$$

Each subsequent level k of the hierarchy is constructed using the following procedure:

- The parametric functions $\psi_p^m(\mu)$ are identified with the Lagrangian polynomials

als (see Fig. 1.2):

$$\mathcal{L}_i^k(\mu) = \frac{\prod_{j \neq i} (\mu - p_j)}{\prod_{j \neq i} p_i - p_j},$$

with

$$p_i \in \mathcal{P}_{2k} \setminus \mathcal{P}_{2(k-1)} \quad \text{and} \quad p_j \in \mathcal{P}_{2k}.$$

- The corresponding surplus functions are determined as the difference between the solution computed for the new collocation points, p_i , and the approximation given by the interpolation from the previous hierarchical level, u^{k-1} . Hence:

$$\psi_s^m(x) = u(\mathbf{x}; p_i) - u^{k-1}(\mathbf{x}, p_i).$$

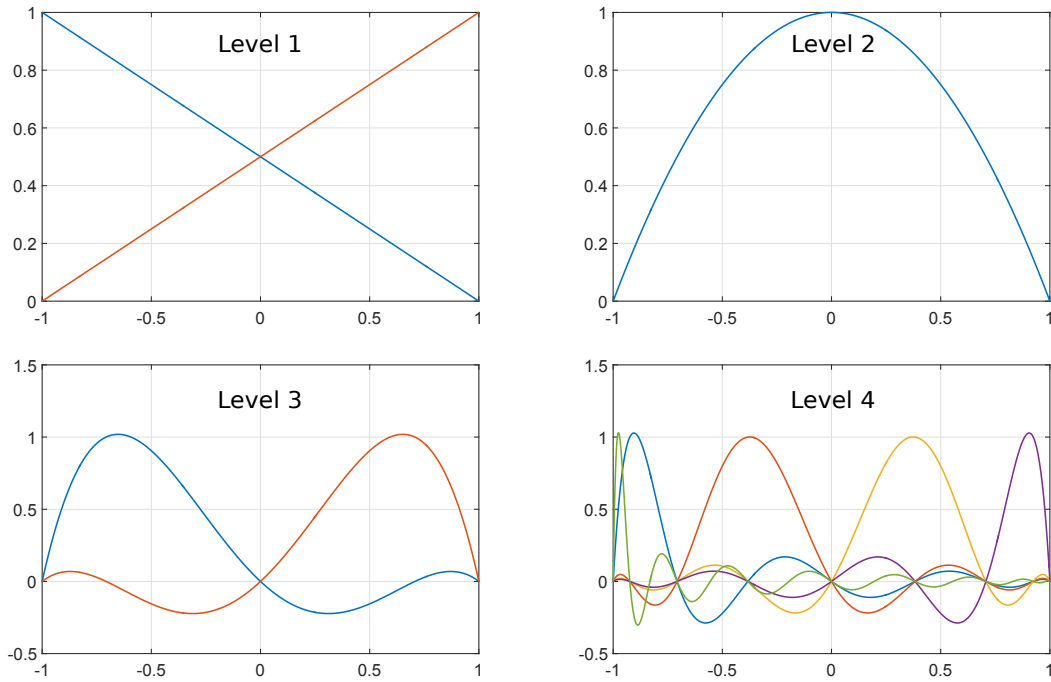


Figure 1.2: Lagrangian polynomials of the first four levels

This implies that the functions $\psi_s^m(\mathbf{x})$ are not simply the high-fidelity solution in the collocation points, but represents the difference between two consecutive hierarchical levels. These hierarchical surplus functions also offer a natural way to assess the convergence of the hierarchical enrichment procedure, which is stopped

when the norm of all the newly added $\psi_s^m(\mathbf{x})$ functions in a level is smaller than a desired tolerance.

Once the separated solution is computed, a PGD in approximation can be performed, obtaining a separated solution with considerably less modes. This allows a high data compression providing a more compact computational vademecum. Moreover, this approximation can be computed after the calculation of each hierarchical level. This compression is key to having a performance method when many parameters are considered.

For several parameters, the same strategy can be paired with Smolyak's technique to generate Sparse Grids (SG) from the tensor product of one dimensional grids without incurring in the curse of dimensionality. This method retains the same convergence rate up to a logarithmic factor provided that the function has smooth high order mixed derivatives (Smolyak, 1963). An example of a three-dimensional sparse grid is shown in Fig. 1.3, where the important diminishing of collocation points with respect to a regular grid can be observed.

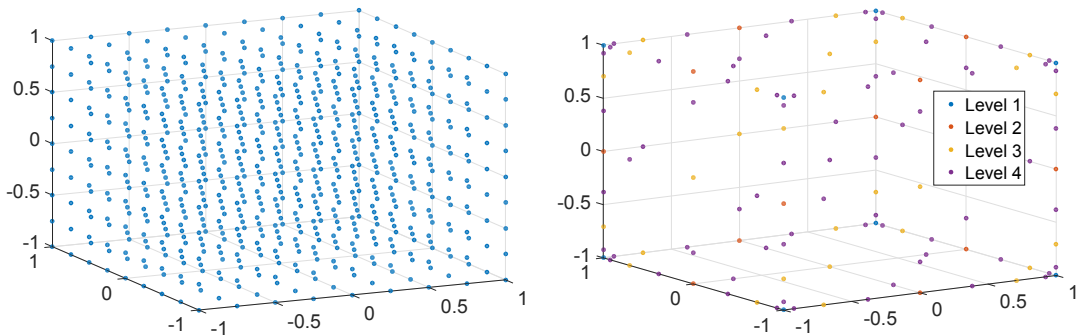


Figure 1.3: Full grid vs Sparse grid

Each level is constructed considering the tensor products of the one dimensional grids and neglecting the high order terms. Thus, the collocation points corresponding to the level N reads,

$$\mathcal{P}_N = \bigcup_{i=1}^N \bigcup_{j=1}^{N+1-i} \mathcal{Q}_{ij},$$

where \mathcal{Q}_{ij} is the set of collocations points given by the tensor product of the one di-

mensional i -th and j -th grid levels of the hierarchical discretization of the dimensions α_x and α_y respectively.

1.2 MOR applications to manufacturing processes

To conclude the chapter, some applications of the mentioned MOR families for manufacturing simulation that can be found in literature are introduced.

Historically, the first reduced simulations were carried out using *a posteriori* projective methods. We find POD-based methods for Casting (Hibbeler et al., 2016), forming (Radermacher et al., 2013), cold rolling (Seidel and Ernst, 2014), sheet forming (Rigopoulos et al., 1997) or welding (Sikström et al., 2012). In all these examples, the mapping of the solution is explored generating snapshots and, by means of the POD, a reduced basis is built. Then, the PDE associated to the original model is projected on this basis. Nevertheless, it can be observed that there is not a very extensive literature on projective MOR methods for manufacturing processes. This is fundamentally due to:

- The complexity of these processes, which makes finding a good enough basis to represent the problem solution an expensive problem-dependent task.
- The presence of nonlinearities that leads to reconstruct the complete solution in the original approximation space at each iteration to evaluate the nonlinear terms.

Both difficulties are currently being addressed through the introduction of hyper-reduced projective MOR techniques (Cosimo et al., 2014) with more general formulations. Thus, we can find several references for the hyper-reduction of elastoplastic processes involving internal variables (Ryckelynck, 2009) and general elastoplastic problems (Hernández et al., 2017), which are of applicability for almost any manufacturing simulation.

More recently, the construction of computational vademecums has been proposed for manufacturing processes simulation. The primary importance of the choice and

control of technological and material parameters in these processes and the appealing idea of performing real time simulations constitute a very favorable scenario for this technique. In this way, we can find its application for the real-time prediction and correction of tool trajectories in milling processes (Poulhaon et al., 2013), for real-time simulation of composites manufacturing by automated tape placement (Chinesta et al., 2014), microwaves (Barasinski et al., 2016) or thermo-forming (Prulière et al., 2010).

Finally, new hybrid MOR techniques are emerging which combine different *a priori* and *a posteriori* reduction techniques for complex manufacturing simulations. This is the case of (Aguado et al., 2017), where a *simulation app* for the manufacture of outlet guide vanes by resin injection is elaborated. This *simulation apps*, ideally, can execute multiphysical reduced models in a few seconds and in a light-computer platform and deployed devices.

Chapter 2

Vademecum-based GFEM (V-GFEM): Optimal Enrichment for transient problems

In this chapter, a generalized finite element method based on the use of parametric solutions as enrichment functions is proposed. These parametric solutions are precomputed offline and stored in memory in the form of a computational vademecum so that they can be used online with negligible cost. This renders a more efficient computational method than traditional finite element methods at performing simulations of processes. One key issue of the proposed method is the efficient computation of the parametric enrichments. These are computed and efficiently stored in memory by employing proper generalized decompositions. Although the presented method can be broadly applied, it is particularly well suited in manufacturing processes involving localized physics that depend on many parameters, such as welding.

Contents

2.1	Introduction	35
2.2	Generalized Finite Element Method	36
2.2.1	The functional enrichment issue	40
2.3	<i>Vademecum</i>-GFEM	41
2.3.1	Introducing a precomputed adaptive enrichment using the PGD	41
2.3.2	General scheme and implementation	45
2.4	Numerical Examples	51
2.4.1	Statement of the problem	52
2.4.2	V-GFEM VS FEM	55
2.4.3	Accounting for variable technological parameters	57
2.4.4	Timing	59

2.1 Introduction

The detailed transient analysis of welding processes is a high time-consuming task even with the current computational means available. It usually involves very fine meshes around the weld line and frequent remeshing processes must be carried out. This chapter is devoted to the development of a general methodology for the efficient simulation of transient thermal problems that can be of applicability for the thermal welding analysis.

One could think of an ideal simulation method that uses very crude meshes, providing results at very high feedback rates, and is also capable of capturing complex physics. The Generalized Finite Element Method (GFEM) (Melenk, 1995; Melenk and Babuška, 1996; Babuška et al., 1994; Duarte and Oden, 1996) is one candidate that fits this description well. By using *enrichment* functions, GFEM is able to provide solutions that capture subgrid features of the physics underneath. The main difficulty associated with GFEM methods is the development of an efficient and accurate strategy to compute these enrichment functions.

GFEM methods and the XFEM method (Dolbow and Belytschko, 1999; Belytschko et al., 2001; Moës and Belytschko, 2002) were developed simultaneously. Even if the XFEM is more focused in the representation of cracks and discontinuities, it has provided fundamental advances in the understanding and application of partition of unity methods. The interested reader can find in (Belytschko et al., 2009) a didactic introduction and comparison of both methods.

Ideally, this enrichment should be composed of one single function, so as to minimize the computational cost of the resulting method. But, as can easily be imagined, one single function can hardly serve for the enrichment of every element in the mesh, regardless of the physics in that particular region.

For this reason, the main objective of this chapter is the development of a method which is able to capture sharp features of the solution, in a variety of different scenarios, with minimal extra degrees of freedom. To obtain such an ideal enrichment function, one can imagine a sort of parametric function dependent on boundary conditions, material characteristics, load values and other parameters that could be

particularized to fit the approximation space in every region of the model.

Obtaining such a solution is of course not an easy task. However, computational techniques exist which are capable of obtaining such *response surfaces* efficiently. Among these techniques, PGD is particularly appealing, due to its ability to efficiently construct the aforementioned parametric functions.

The resulting method, which we have called *Vademecum*-GFEM (V-GFEM), is no more than a finite element method that introduces, transparently to the user, an enrichment consisting of just one single function.

V-GFEM is a general-purpose method. However, it is particularly well adapted to transient problems involving localized physics dependent on several technological parameters. This is the case, for example, of welding and surface heat treatments. In this chapter, the V-GFEM formulation and some numerical examples related to the mentioned processes are presented.

After this introduction, the chapter is organized as follows. In Section 2.2, GFEM is presented as well as the major approaches that exist in literature to introduce the enrichment functions, a crucial issue in this method. In Section 2.3, the V-GFEM is presented, the adaptative enrichment using the *Computational Vademecum à la* PGD is explained, exposing the main ideas underpinning its construction. In this section, details about its implementation are also included. Finally, in Section 2.4, the suitability of the V-GFEM for transient problems is presented through several numerical examples.

2.2 Generalized Finite Element Method

The accuracy obtained with a numerical method, and in particular with FEM, largely depends on how suitably the method has been adapted to the specific problem. In practice, we can follow different strategies to adapt our FEM formulation to the problem at hand. Some traditional strategies are *h*-adaptivity, *p*-adaptivity or *hp*-adaptivity (Fish and Belytschko, 2007). These classical strategies are implemented in most commercial simulation tools. The GFEM can be seen as a general-

ization of the classical h , p and hp adaptivity techniques.

For the sake of completeness, it is interesting to revisit one of the first attempts in creating advanced adaptive strategies. In 1992, J. Fish et al. proposed the S-FEM (Fish, 1992), in which a fine discretized patch is superimposed on a coarse discretized domain in the region of interest. In this way, the approximation of the variables reads:

$$u^h = \sum_i N_i^c(\mathbf{x})U_i^c + \sum_j N_j^f(\mathbf{x})U_j^f,$$

where one can see two different kinds of shape functions: the set of $N^c(\mathbf{x})$ functions associated to the coarse mesh (global domain) and the set of $N^f(\mathbf{x})$ functions associated to the fine one (patch). The continuity between the patch and the global domain can be ensured imposing $U^f = 0$ on the boundary of the patch. In this manner, S-FEM tries to avoid remeshing, a real bottleneck in 3D simulations. However, some precautions should be taken to handle two computational meshes (Fish and Yuan, 2005):

- Numerical quadratures are in general difficult to perform. A special mesh (intersection of the coarse and the fine one) should be created to achieve accurate results.
- Rank deficiency must be prevented.

We have applied this technique in (Ammar et al., 2009), (Ammar et al., 2011) and (Niroomandi et al., 2012) for locally-enriching solutions expressed in a reduced basis.

Some years later, the Generalized Finite Element Method (GFEM) was proposed by Melenk and Babuška (Melenk, 1995). The main idea of this method is to introduce in the trial space the available information about the solution.

There are many other techniques based on the same idea such as PUM, PUFEM, XFEM or Special FEM (Melenk, 1995; Melenk and Babuška, 1996; Babuška et al., 1994; Duarte and Oden, 1996; Dolbow and Belytschko, 1999; Oden et al., 1998; Strouboulis et al., 2000). The GFEM is based in two properties:

- Local approximability. GFEM is able to construct space of functions which can approximate the solution even better than the FE space of piece-wise polynomials.
- Conformity. The method is able to preserve the inter-element continuity without losing approximation properties.

The first property will depend on the suitability of the so-called enrichment functions for a given problem. This question will be discussed in detail in subsection 2.2.1 because it is a key aspect of this work. With respect to the second one, the inter-element continuity is guaranteed if the enrichment is introduced in a space which satisfies the partition of unity. The formal definition of partition of unity can be found in (Melenk, 1995), and it can be used to construct these spaces in a general manner, even without a mesh. In our context it is enough to say that in any traditional finite element discretization of a domain Ω , the trial space satisfies the partition of unity if and only if:

$$\sum_i N_i(\mathbf{x}) = 1, \forall \mathbf{x} \in \Omega,$$

where $N_i(\mathbf{x})$ are the shape functions.

When this property is satisfied, the GFEM approximation u^h of our solution u reads,

$$u^h = \sum_{i \in I} N_i(\mathbf{x}) U_i + \sum_{e \in I_{enr} \subset I} N_e(\mathbf{x}) \sum_j \phi^j b_e^j, \quad (2.1)$$

where the first term is a traditional FEM approximation and the second one is the enrichment added. The set of nodes is represented in I and I_{enr} is the subset of enriched nodes. The functions ϕ^j are responsible for introducing prior information we have of the solution, and therefore depend on the problem being solved.

Eq. (2.1) shows that the traditional shape functions are also present in the enrichment term, multiplying each of the ϕ^j functions. This means that, regardless of whether ϕ^j were local or global functions, each of the new shape functions $N_e \phi^j$ are local. In other words, the new shape functions also have compact support. This property is vital for an easy and efficient implementation of the method (Zienkiewicz

and Taylor, 2005).

The enriched nodes, the subset I_{enr} in Eq. (2.1), are just located in areas of interest where a greater accuracy is desired. These zones may be those where strong gradients occur or there are certain localized phenomena, for example cracks or damage. Thus, we can expect that the number of enriched nodes is relatively small compared to the total number of nodes of the discretization.

Moreover, GFEM has a very interesting meshless character which extends its applicability. Since the local features of a solution can be described in terms of nodal values at the nodes of the original mesh, neither remeshing nor structured meshes are needed. This is the case of welding processes. With a traditional h -adaptive strategy, the computational mesh is refined in the welding locations. However, due to the deformations induced in the process or in the assembly with other pieces, these locations could change. Thus, the reference configuration is not useful anymore and the mesh should be recomputed. Using GFEM this issue is circumvented, since the enrichment can be added to the original mesh where necessary and no refinement is needed.

As a counterpart, the degrees of freedom (DOFs) of the problem will be those attached to the nodes of the discretization, U_i , plus those attached to each enriched node and each of the enrichment functions b_e^j . Moreover, GFEM will typically require the use of a large number of integration points (O'Hara, 2010). This is a consequence of using enriched shape functions which are in general non-polynomial and require accurate enough quadrature rules.

Thus, from the point of view of computational efficiency, for any given accuracy, it is desirable to use a coarse mesh using the fewest enriched nodes and enrichment functions possible. In the limit, the best GFEM method will use only one enrichment function with the best possible local approximation properties of the solution. This is, as we will see, the fundamental advantage of the V-GFEM.

2.2.1 The functional enrichment issue

The main difficulty of the construction of a GFEM solution is the selection of the enrichment functions set. The superiority of the GFEM compared with a conventional FEM depends directly on the efficacy of the enrichment functions chosen for a given application. In literature, the following approaches can be found:

- Analytical constructions (Dolbow and Belytschko, 1999; Merle and Dolbow, 2002). They exploit the structure of the differential equation or use some fundamental solution of it.
- Global-Local technique (GFEM^{gl}) (O'Hara, 2010; O'Hara et al., 2009, 2011; Duarte and Kim, 2008). The enrichment function is the solution of a fine online-local problem with essential boundary conditions which come from an online-coarse global one.
- Proper Orthogonal Decomposition (POD) (Aquino et al., 2009). The enrichment functions are the principal POD modes of a set of snapshots of the problem.

Analytical enrichment functions are problematic since they are hardly available for most applications of practical interest. Because of this, the construction of enriched functions by computational methods (Global-Local and POD) has become more relevant in recent years. The Global-Local implies solving iteratively both an online-global problem (coarse) and a online-local one (fine problem). Lastly, construction by POD has two drawbacks: firstly, the reduced basis indeed cannot in general capture all the details related to the solutions of models different from the one from which the reduced basis has been extracted (Chinesta et al., 2013a) and secondly, the number of relevant modes could be very large causing GFEM to be too expensive.

When the problem is time dependent, the issue of selecting shape functions is further complicated. In literature, one can find analytical time-dependent enrichment functions, but they are for very specific applications (O'Hara, 2010). With a Global-Local approach it is possible to build time dependent enrichment functions,

but the iterative process must be repeated in each time step. Lastly, with a POD approach the time-dependent enrichment functions could be potentially numerous.

The strategy introduced in this chapter aims at overcoming these difficulties by proposing the use of a *Computational Vademecum* (also known as *Computational Handbook*) à la PGD for generating an improved approximation space. We believe that this approach has noteworthy advantages over existing methods.

2.3 *Vademecum*-GFEM

The method proposed in this chapter, the V-GFEM, is composed of two main elements: the GFEM as the framework, described in the previous section, and the vademecum as the key ingredient for constructing offline the optimal enrichment function.

It is important to note that, in the V-GFEM, the computational vademecum is used to construct a better approximation space, not the solution in any subdomain. The GFEM framework provides many advantages since neither remeshing nor conformal meshes are needed, as it is usually the case for Domain Decomposition techniques. Moreover, during the construction of the vademecum some phenomena can be neglected, such as transient effects, since they are accounted for in the global problem. This fact is in accordance with the results presented in (O'Hara et al., 2011).

In this section we elaborate the construction of the latter, which constitutes a true precomputed adaptive enrichment. Moreover, a general scheme of the V-GFEM is presented, providing further details of its implementation.

2.3.1 Introducing a precomputed adaptive enrichment using the PGD

As has been explained in Section 1.1.3, PGD constitutes an efficient multidimensional solver that allows introducing model parameters (such as boundary conditions,

initial conditions, geometrical parameters or material and process parameters) as extra-coordinates. Then by solving only once and offline the resulting multidimensional model we have access to the parametric solution that can be viewed as a sort of handbook or computational vademecum that can be then used online.

Its use allows us to perform efficient inverse analysis, data-driven applications and optimal design in large parametrical spaces (Chinesta et al., 2013b). Unlike other MOR approaches, PGD does not assume the form of the basis functions of the model. Consequently, it emerges from the physics of the problem itself on the fly.

In the V-GFEM, the computational vademecum is used to generate the proper enrichment function that depends on technological and material parameters of the process which are treated as extra-coordinates.

Let us assume the mathematical model related to a certain physics. In general, this model will be expressed in terms of a system of partial differential equations (PDEs), defined in a spatial domain under given boundary conditions. The variational formulation of one PDE of this generic problem reads,

$$a(u, v; p_1, p_2, \dots, p_n) = l(v; q_1, q_2, \dots, q_m), \quad (2.2)$$

where \mathbf{u} and \mathbf{v} are the trial and test functions respectively and p_i and q_j , with $i = 1, \dots, n$ and $j = 1, \dots, m$ are parameters on which the problem depends. The functions \mathbf{u} and \mathbf{v} are defined in the appropriate functional spaces (Johnson, 2012).

Using traditional numerical methods (FEM, finite differences, spectral methods...), the solution \mathbf{u} of the variational form (2.2) is an approximation

$$u^h(\mathbf{x}; \hat{p}_1, \hat{p}_2, \dots, \hat{p}_n, \hat{q}_1, \hat{q}_2, \dots, \hat{q}_m)$$

for each particularization \hat{p}_i, \hat{p}_j of the parameters p_i and q_j . Then, if one wants to explore the parametrical space to obtain optimal solutions, the solution process must be repeated for any possible combination of particularizations of the parameters.

Surrogate models consider the problem solution for some choices of the parameters and then use appropriate interpolation (e.g. Kriging). POD or RB-based

techniques circumvent this difficulty by generating a reduced approximation basis from some solution snapshots after extracting the relevant information.

The PGD, on the other hand, constructs the approximated solution as follows,

$$u^h = \sum_{k=1}^N F^k(\mathbf{x}) \prod_i P_i^k(p_i) \prod_j Q_j^k(q_j),$$

where the parameters appear explicitly in the solution as extra-coordinates. Even if the problem becomes highly multidimensional in most cases, the use of separated representations allows circumventing the aforementioned “curse of dimensionality”. Thus, once the parametric solution is computed, the PGD solution provides all the possible solutions to the problem within the parametric domain $p_i \in [p_i^{min}, p_i^{max}]$, $q_j \in [q_j^{min}, q_j^{max}]$. It is worth highlighting that the construction of the vademecum does not rely on the linearity of the problem. It can be also obtained in cases involving nonlinear materials with state variables. However, the number of required modes, N , may depend on the complexity of the problem. For many applications of interest, tens of them are often enough.

The most successful implementation of the PGD involves a simple fixed-point alternated direction algorithm, that computes alternatively the problem involving the functions of a coordinate, assuming all the functions related to the remaining coordinates known (calculated at the previous iteration). This implementation has proved to be very robust and computationally efficient, circumventing the curse of dimensionality, since it only needs to solve one low-dimensional problem at a time, as it has been elaborated in Section 1.1.3.1.

In the V-GFEM, the computational vademecum is introduced in a GFEM framework, which provides a performance that goes beyond the proposals made so far. This method is able to generate real-time customized approximation spaces, which not only accounts for material and technological parameters, but also for the value of the variable on the boundaries of the enriched region. This means that the enrichment region can “see” the changes that may occur in the global problem and adapt accordingly. All these parameters can vary during the simulation without loss of applicability and without compromising the solver efficiency.

The V-GFEM formulation can be expressed in the following compact form:

$$u^h = \sum_{i \in I} N_i(\mathbf{x}) U_i + \sum_{e \in I_{enr} \subset I} N_e(\mathbf{x}) \phi(\mathbf{x}, p_1, \dots, p_n, q_1, \dots, q_m) b_e, \quad (2.3)$$

where the enrichment function ϕ is nothing but a parametric general solution computed *à la* PGD. One can observe that the trial space now depends explicitly on the parameters introduced in the vademecum.

The selection of these parameters should be done wisely, and should not be limited to technological parameters. Others, such as the values of the main variable on the border of the enriched region u_{Γ_e} are of great interest in order to build a good enrichment function (O'Hara, 2010). In this case, u_{Γ_e} should be represented on a global basis with respect to the domain of the vademecum. This basis can be, for example, a polynomial one. In 2D, for each side of the domain, u_{Γ_e} reads,

$$u_{\Gamma_e}^i = a_1 + a_2 s_i + a_3 s_i^2 + \dots + a_n s_i^{n-1}, \quad (2.4)$$

where s^i is the local coordinate and $u_{\Gamma_e}^i$ the value of u_{Γ_e} on the i -side. The uniqueness of u_{Γ_e} must be enforced at the corners of the domain.

The set of enriched nodes I_{enr} is a subset of the nodal set of the discretized problem. This set is determined by a geometric region (the so-called enrichment region) which is generally much smaller than the global domain. In the following examples, the enrichment region is attached to the movement of a heat source, where the thermal gradients are important and the solution cannot be found accurately using a coarse mesh.

2.3.2 General scheme and implementation

For the sake of clarity, let us assume a thermal transient problem with a moving heat source $s(\mathbf{x}, t)$ in a domain Ω and in the temporal interval $\mathcal{T} \in (0, T)$,

$$\begin{cases} u_t - \nabla \cdot (k \nabla u) = s(\mathbf{x}, t) & \text{in } \Omega \times \mathcal{T} & (2.5a) \\ u = u_D & \text{on } \Gamma_D \times \mathcal{T} & (2.5b) \\ \frac{\partial u}{\partial \mathbf{n}} = u_N & \text{on } \Gamma_N \times \mathcal{T} & (2.5c) \\ u(\mathbf{x}, 0) = u_0(\mathbf{x}) & \text{at } t = 0 & (2.5d) \end{cases}$$

where the main variable u is the temperature, k the thermal diffusivity, the essential and natural boundary conditions u_D and u_N are imposed on Γ_D and Γ_N respectively, and the initial temperature is u_0 .

Attached to the source, an enrichment region, say Ω_e , is set. Its size must be determined for each particular case, taking into account that it should be large enough to capture the finer features of the solution. The geometry of this moving region is fixed and, at each time step, the nodes located inside are affected with the optimal enrichment function that simply consist in particularizing the parametric solution (computational vademecum) precomputed offline. In short, the trial space in this region is more suitable to approximate the solution than the traditional FEM.

The V-GFEM can be divided into two stages: offline and online, as is presented in Fig. 2.1.

In the offline stage, the vademecum is computed introducing the technological parameters of the process, $\mathbf{p} = [p_1, p_2, \dots, p_n]^T$, and the essential boundary conditions, u_{Γ_e} , as extra-coordinates. The size of the domain of the computational vademecum is equivalent to the enriched region, and a very fine discretization can be used because it is computed offline. The model to solve is the same as in the original problem, but considering a moving reference frame, say Ω_l . Thus, in this case, the movement of the heat source is considered from a convective operator and

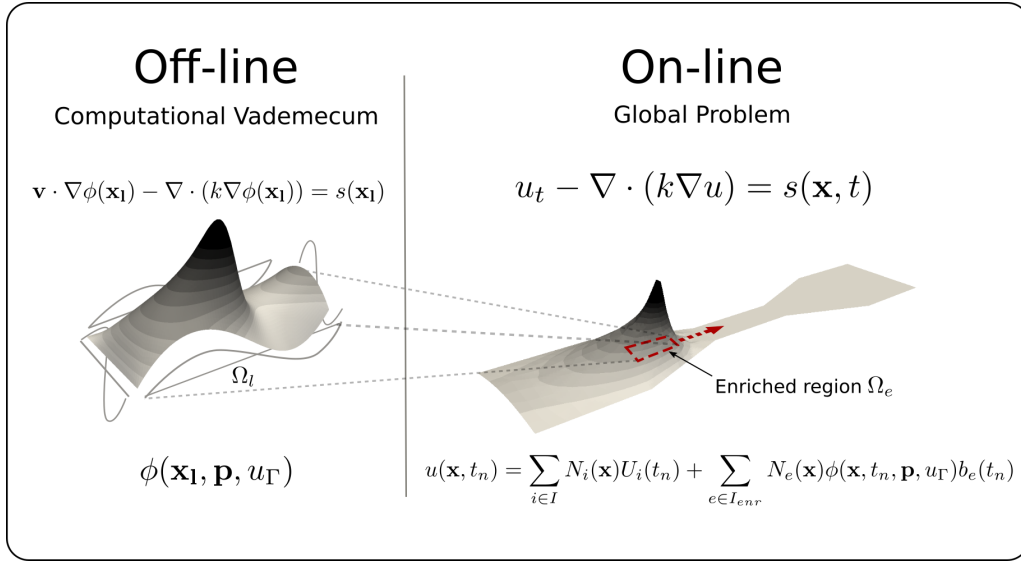


Figure 2.1: V-GFEM stages

the problem reads

$$\mathbf{v} \cdot \nabla \phi(x_l) - \nabla \cdot (k \nabla \phi(x_l)) = s(\mathbf{x}_l) \quad \text{in } \Omega_l, \quad (2.6)$$

where the main variable $\phi(x_l)$ is the enrichment function of the global problem.

Supposing a rectilinear motion, in each time t , Ω_e can be defined as $\Omega_e = \{\mathbf{x} | \mathbf{x} - \mathbf{v}t - \mathbf{r}_0 \in \Omega_l\}$, where \mathbf{r}_0 is the position vector between the vademecum reference system and Ω_e at initial time.

The essential boundary conditions in this problem u_{Γ_e} are not imposed since they are extra-coordinates of the solution, like other technological parameters. In this way, using the PGD, the Eq. (2.6) can be solved in an extended domain $\Omega_l \times \mathcal{I}_{p_1} \times \cdots \times \mathcal{I}_{p_n} \times \mathcal{I}_{a_1} \times \cdots \times \mathcal{I}_{a_m}$ to obtain,

$$\phi(\mathbf{x}_l, \mathbf{p}, \mathbf{a}) = \sum_{k=1}^N F^k(\mathbf{x}_l) \prod_{i=1}^n P_i^k(p_i) \prod_{j=1}^m A_j^k(a_j),$$

where $\mathbf{p} = [p_1, \dots, p_n] \in \mathcal{I}_{p_1} \times \cdots \times \mathcal{I}_{p_n}$ are the technological parameters of the problem (thermal source velocity, power and shape of the heat source...) and $\mathbf{a} = [a_1, \dots, a_m] \in \mathcal{I}_{a_1} \times \cdots \times \mathcal{I}_{a_m}$ are the coefficients of the polynomial basis of u_{Γ_e} in

Eq. (2.4).

It is important to note that the computational vademecum generates steady enrichment functions, suitable when a stationary regime in the global problem is reached. Being rigorous, that means that to introduce the best approximation space in the pure transient phases of the simulation, the acceleration of the source should also be included as an extra-coordinate.

In the online phase, at the time step t , the global problem is solved within the GFEM framework with the enrichment function obtained from particularizing the parametric local problem. This can be carried out in two ways:

- Explicitly: The particularization is carried out according to the technological parameters in the current time step, but the solution on the enrichment domain boundary in the previous time step, i.e. $\phi^t(\mathbf{p}^t, u_{\Gamma_e}^{t-1})$. This explicit scheme works well if the time step is not very large and the solution evolves smoothly as it is the case, for example, in welding simulation.
- Implicitly: Using a point-fixed strategy, the global problem is solved iteratively updating u_{Γ_e} until the enrichment function ϕ^t converges. This scheme is presented in Fig. 2.2, where $\hat{\phi}$ is an auxiliary function to check this convergence and the upper index $t - 1$ represents a value in the previous time step of the current one.

It should be noted that the explicit strategy is a particularization of the implicit one where $\hat{\phi}$ is not computed, omitting the decision block. For the examples presented here, the explicit scheme provides excellent results.

At each time step, a good initial guess is the enrichment function from the boundary conditions in the parametric solution coming from the previous time step. For stationary problems, a simple and effective idea is to introduce the particularization of the vademecum with $u_{\Gamma_e} = 0$, a sort of “fundamental solution” of the problem, performing the fixed-point iterations if necessary. Note that this point-fixed iteration does not imply a great computational effort, since the updating of the enrichment function is performed at negligible cost. In addition, to solve the

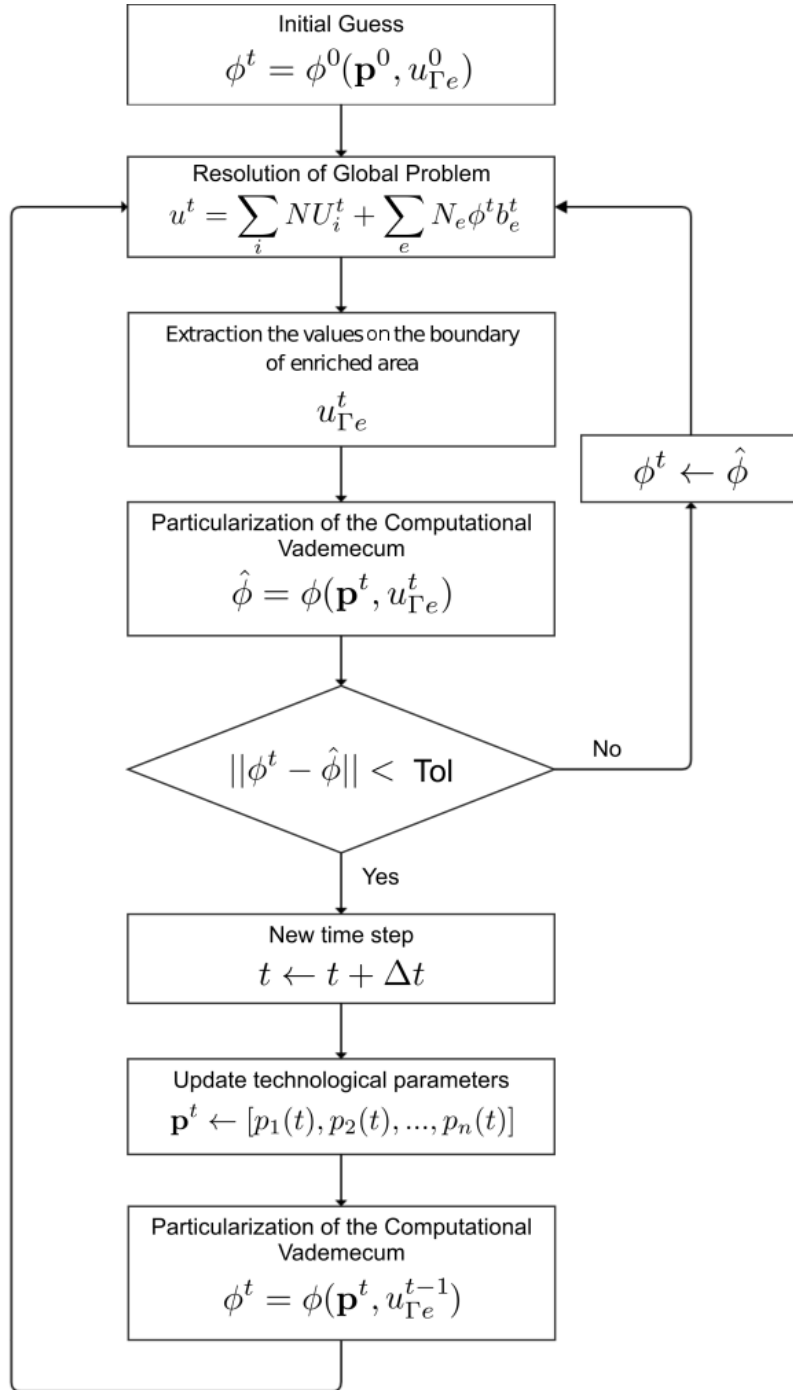


Figure 2.2: V-GFEM online stage

global problem, because the domain remains fixed, several reanalysis techniques can be used, alleviating the computational cost of the solution (O'Hara, 2010).

This strategy is analogous to the iterative strategy concerned with improving the local boundary conditions in the GFEM^{gl} presented in (O'Hara et al., 2009, 2011) and analyzed in (Gupta et al., 2012). In these references an alternative strategy is proposed, the introduction of a *buffer zone*. This zone enlarges the local domain using layers of coarse elements in order to introduce smoother boundary conditions to the local problem. In the context of the V-GFEM, this implies changing the domain of the computational vademecum with no other alterations to the general scheme.

In order to extract $u_{\Gamma_e}^t$ in each time step, the global solution u^t has to be projected on the borders of the enriched area on the basis given by Eq. (2.4). In this work a simple L_2 projection is carried out.

For certain parameter values, the parametric solution in some regions of its domain of definition could be accurately represented by the subjacent FE coarse approximation, leading to rank deficiency. This fact indicates that as soon as the enriched solution in a particular region of the domain in which the enrichment is performed can be accurately described by the coarse approximation, the associated nodes should be removed from the enrichment nodal list I_e . For this purpose we can generate a second vademecum, by projecting, again offline, the parametric solution, $\phi(\mathbf{x}_l, \mathbf{p}, \mathbf{a})$, from which the enrichment function is extracted, on different coarse FE element approximations associated with different mesh size $h \in [h_1, \dots, h_M]$. This projection writes

$$\int_{\Omega} u^{h_i^*} u^{h_i} d\omega = \int_{\Omega} u^{h_i^*} \phi d\omega, \quad (2.7)$$

being $u^{h_i}(\mathbf{x}_l, \mathbf{p}, \mathbf{a})$ the projected solution on a mesh of size h_i , and then the projection must be performed for each considered mesh characterized by its size h_i , even if the mesh size could be introduced as an extra-coordinate within the PGD framework. Then, once the projected parametric solutions u^{h_i} are available, the parametric residual,

$$r^{h_i}(\mathbf{x}_l, \mathbf{p}, \mathbf{a}) = \phi - u^{h_i}, \quad (2.8)$$

could be computed and compared to a threshold value ϵ according to

$$r^{hi2} < \epsilon^2. \quad (2.9)$$

As soon as for the given parameters the parametric solution constituting the GFEM enrichment is particularized, at each node in the enrichment region (domain in which the enrichment solution is defined) we particularize the residual (2.8), and if the inequality (2.9) holds, we remove from the enrichment nodal list that node. This procedure ensures an optimal enrichment while avoiding rank deficiency.

The solution of the Eq. 2.7 can be very expensive computational-wise if the PGD method is used to construct the enrichment vademecum, since the projection cannot be only performed over the spatial modes but over the whole reconstructed solution. However, if the SSL method introduced in Section 1.1.4 is used, the projection can be performed over the spatial modes exclusively (before recomputing with the PGD). To illustrate this idea, let us consider an enrichment function vademecum constructed using the SSL with Sysweld depicted in Fig. 2.3. Without loss of generality, only technological parameters associated to the heat source have been considered (see the numerical example of Chapter 4 for further details).

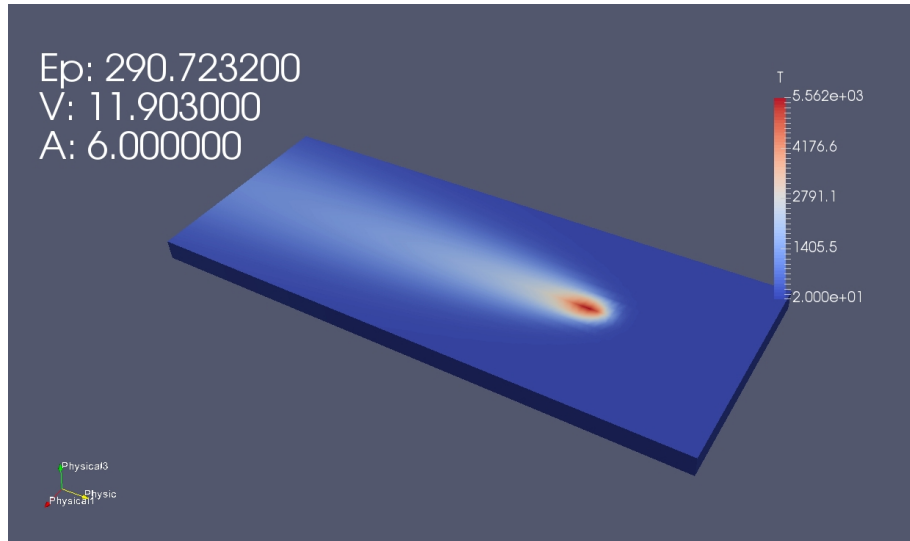


Figure 2.3: Enrichment function vademecum

For a certain coarse mesh a residual vademecum $r^{hi}(\mathbf{x}_l, \mathbf{p}, \mathbf{a})$ can be constructed, as shown in Fig. 2.4 and Fig. 2.5. For different parameter values, one can decide what region must be enriched according to a certain tolerance ϵ . Fig. 2.4 and Fig. 2.5 indicate that dark blue regions must not be enriched to prevent rank deficiency.

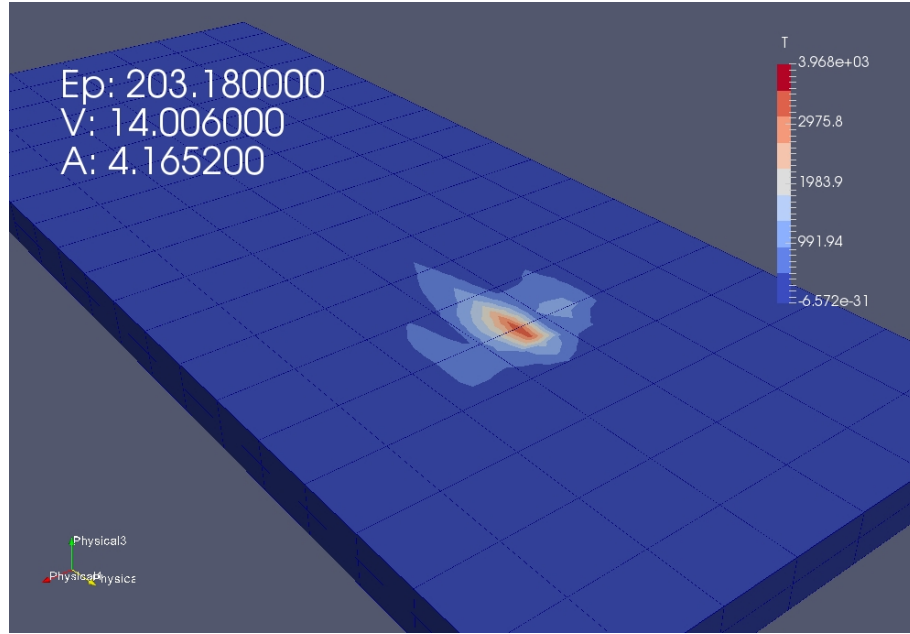


Figure 2.4: Residual vademecum

2.4 Numerical Examples

As it was said in the introduction, the V-GFEM is particularly well suited for the simulation of processes involving moving heat sources, such as welding or surface heat treatments. This is because there is a small region where physical changes are much more pronounced (Heat Affected Zone, HAZ) and the process strategy should be optimized in large parametric spaces.

In this section, several numerical examples using the V-GFEM for an unsteady heat equation are shown. This equation is encountered in the thermal analysis of the mentioned processes (Bergheau and Fortunier, 2013). The examples presented in this section are relatively simple with the purpose of illustrating the potential of the

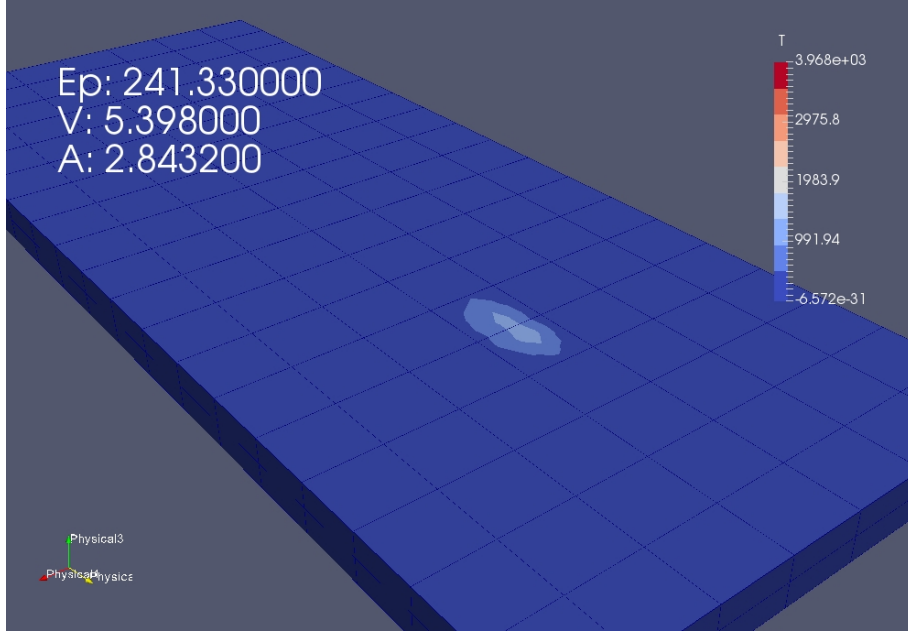


Figure 2.5: Another particularization of residual vademecum

V-GFEM for this kind of simulations: the domain is 2D and the technological and material parameters do not correspond to any real process. However, the method can be applied to the 3D simulation of real industrial processes.

2.4.1 Statement of the problem

Let us consider the transient PDE (2.5) in the domain Ω depicted in Fig. 2.6, where $s(\mathbf{x}, t)$ reads

$$s(\mathbf{x}, t) = \frac{Q}{\sigma\sqrt{2\pi}} \exp\left(\frac{1}{2}\left(\frac{x - (x_c + Vt)}{\sigma}\right)^2 - \frac{1}{2}\left(\frac{y - y_c}{\sigma}\right)^2\right),$$

where $\mathbf{x} = (x, y)$, Q controls the power of the heat source and σ is related with the size of the area of incidence of the heat source. V is the magnitude of the velocity $\mathbf{v} = V\mathbf{u}_x$ where \mathbf{u}_x is the unitary vector of the coordinate x . The starting point of the heat source is (x_c, y_c) .

Let us assume homogeneous Dirichlet boundary conditions on Γ_{DH} and homoge-

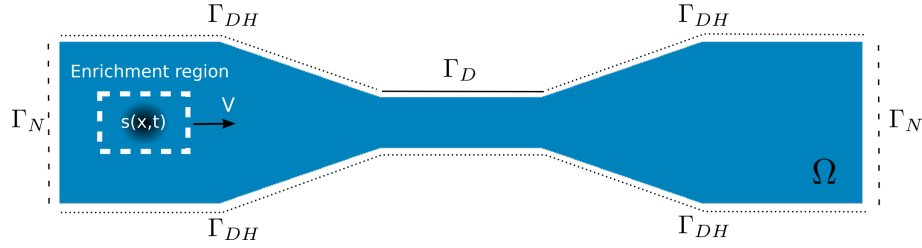


Figure 2.6: Scheme of the problem

neous Neumann boundary conditions on Γ_N . On Γ_D a Dirichlet boundary condition is imposed and its value depends on the example. The coefficient of diffusivity takes the value 1 and the other parameters will vary depending on the example.

To perform the V-GFEM, an enrichment region Ω_e is defined attached to the heat source, as can be seen in Fig. 2.6. This region, a subdomain of the global domain, moves with the source whilst retaining its shape and size. Then, in an off-line stage, the computational vademecum for this problem is computed in a moving reference frame. Moreover, the velocity of this reference frame is considered as an extra-coordinate.

In this example, the next parameters were introduced in the vademecum as extra-coordinates: the power of the heat source Q , the magnitude of the thermal source velocity V , the region of incidence of the heat source described by σ and the temperature at the boundary of the enrichment region u_{Γ_e} . To introduce the latter, a polynomial basis of order three was used. Thus, the parametric enrichment function reads:

$$\phi = \phi(\mathbf{x}, Q, V, \sigma, a_1, \dots, a_{12}) = \sum_{k=1}^N F^k(\mathbf{x}) G_i^k(Q) H_i^k(V) I_i^k(\sigma) \prod_{j=1}^{12} A_j^k(a_j).$$

In Fig. 2.7, the computational vademecum constructed for this example is presented. The visualization can be easily done with the ParaView open source plugin developed in our research group (Bordeu et al., 2013).

Then, the variational formulation of the problem (2.5) is constructed,

$$\left(u^{t+1*}, \frac{u^{t+1}}{\Delta t} \right) + a(u^{t+1*}, u^{t+1}) = \left(u^{t+1*}, \frac{u^t}{\Delta t} \right) + (u^{t+1*}, s^{t+1}) \quad (2.10)$$

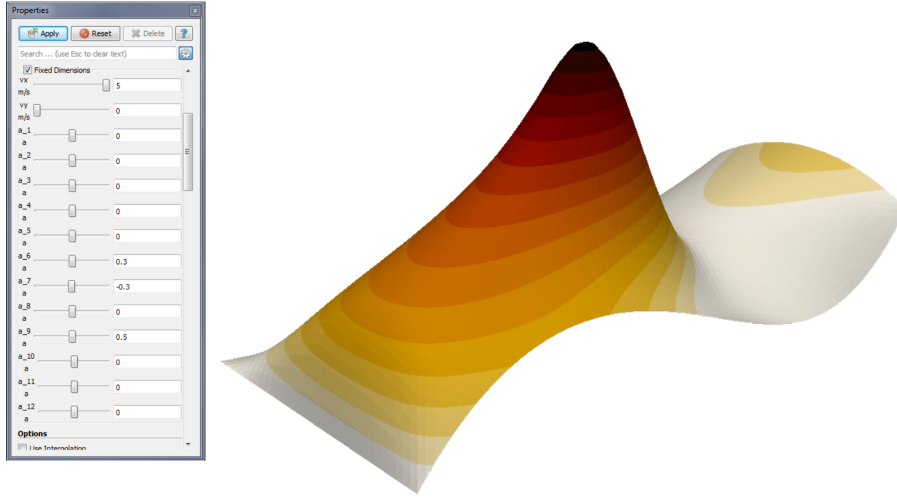


Figure 2.7: Computational Vademecum

where a Galerkin spatial discretization and an implicit α -method (with $\alpha = 1$) as a temporal scheme are used. For clarity, the argument of the functions have been omitted.

In Eq. (2.10), $a(u^{t+1*}, u^{t+1})$ is the Laplacian operator and the trial and test functions, u^{t+1} and u^{t+1*} respectively, are constructed using the approximation given by the V-GFEM in Eq. (2.3). It is important to realize that, exactly as in the GFEM^{gl} (O’Hara et al., 2009, 2011), in the V-GFEM the enrichment function is time-dependent. Thus, the operator $(u^{t+1*}, \frac{u^t}{\Delta t})$ on the right hand side should be carefully computed since it involves two functions, u^{t+1*} and u^t , which are represented using different approximation spaces. For this purpose, two particularizations of the vademecum must be stored when using this temporal integration scheme.

In this example, in order to perform the numerical integration, the coarse mesh equipped with a large number of integration points (of the order of 100) in the enriched elements has been used. The number of points has been determined by numerical tests as in (O’Hara et al., 2009). Advanced integration strategies, taking into account the offline/online nature of the presented work are still in progress.

In the next section we will analyze the solution of this problem solved with the

V-GFEM formulation under different scenarios. The computational vademecum, computed offline, is the same and the algorithm described in Fig. 2.2 was followed in all of these cases.

2.4.2 V-GFEM VS FEM

Let us start illustrating the important improvement that can be achieved with an enriched trial space in comparison with a traditional FEM space. In this example the following boundary conditions and technological parameters were selected: $Q = 10 \text{ W/m}^2$, $V = 1 \text{ m/s}$, $\sigma = \sqrt{0.05}$ and $u = 0$ on Γ_D .

The V-GFEM and the FEM simulations were carried out using the same coarse mesh depicted in Fig. 2.8. For clarity, the temperature field is represented as a relief map. As can be seen in Fig. 2.8, the V-GFEM solution, in solid color, significantly improves the FEM solution, wire-frame represented, in the vicinity of the heat source. Differences up to 30% in the maximum temperature value were observed.

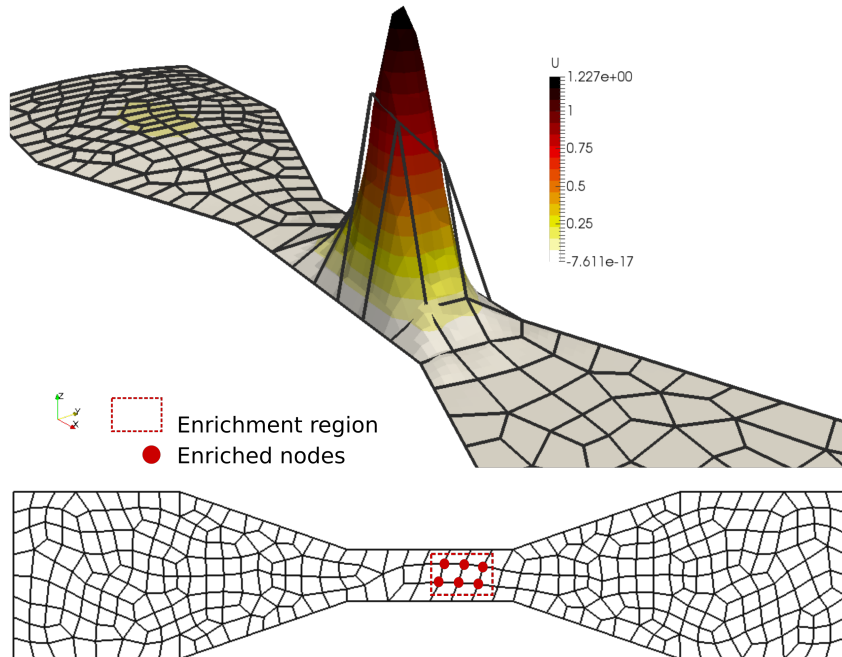


Figure 2.8: V-GFEM solution vs FEM solution

Here, the enrichment function is trivially updated, since the technological parameters are constant and the temperature field on the border of the enriched region does not change significantly during the simulation. Thus, in this case, the advantage of having a computational vademecum is the possibility of performing just one calculation for a given family of problems.

Adaptation to the boundary conditions

Let us now consider different boundary conditions of the global problem, setting $u = 1$ on Γ_D in the upper part of the narrow zone. Then, when the source enters in this narrow region, the global essential boundary conditions affect the optimal trial space. With the V-GFEM, due to the fact that the enrichment function is an explicit function of u_{Γ_e} , the best approximation space is always achieved. In Fig. 2.9 one can observe how the vademecum generates different enrichment functions ϕ in different instants during the simulations according to global boundary conditions.

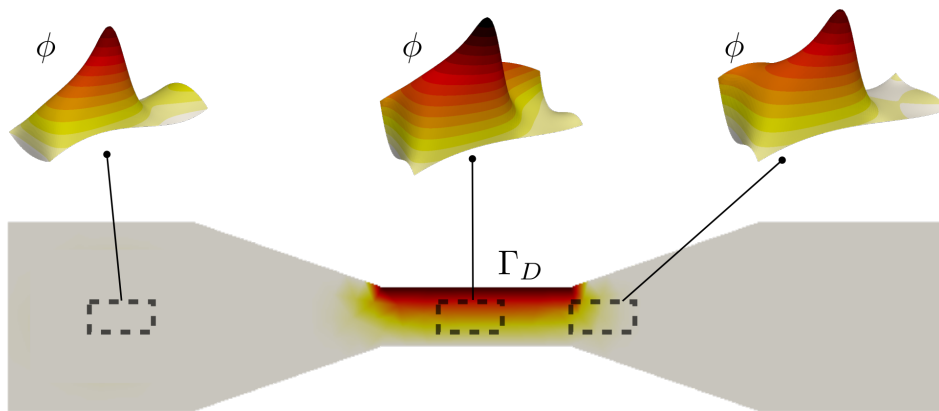


Figure 2.9: Adaptivity of the enrichment function

This allows us to obtain a considerably improved solution with respect to the FEM one using the same coarse mesh, as is shown in Fig. 2.10. The V-GFEM solution, in wire-frame, is equipped with the optimal trial space in the current time step. In solid color, the FEM solution using the same coarse mesh is represented. If the enrichment function is not updated as it is indicated in Fig. 2.9, the improve-

ment obtained with the V-GFEM will be reduced by 15%-20% as we will see in the following sections.

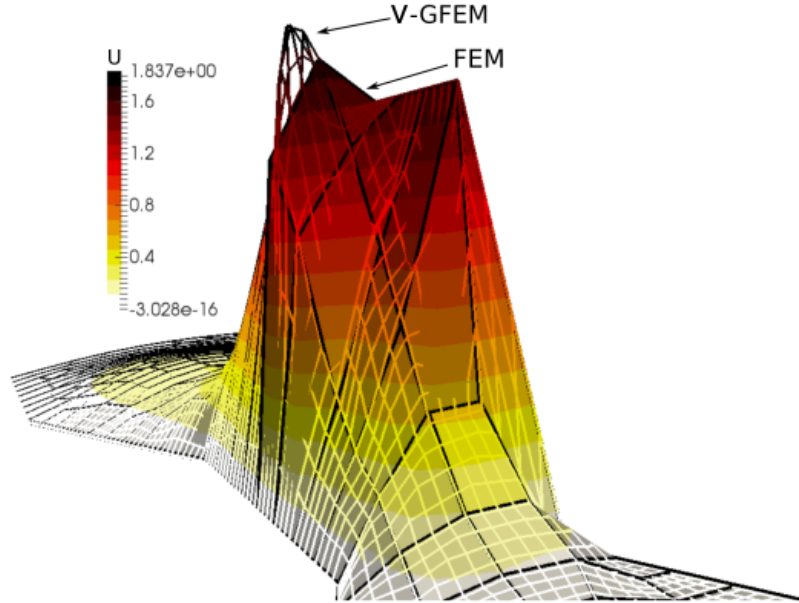


Figure 2.10: V-GFEM solution vs FEM solution with change in BCs

2.4.3 Accounting for variable technological parameters

We move forward now to analyze the key feature of the V-GFEM: the adaptation in real time to changes in the technological parameters of the simulation.

Let us consider a thermal source velocity which changes from 30 m/s to 5 m/s at a certain point during the process. The other technological parameters take the fixed values $Q = 10 \text{ W/m}^2$ and $\sigma = \sqrt{0.025}$. All the Dirichlet and Neumann BCs are homogeneous.

In Fig. 2.11, the two enrichment functions generated by the vademecum with those two different velocities are shown. The function ϕ_1 was particularized at 30 m/s and the function ϕ_2 at 5 m/s .

Then, two simulations were carried out. In the first one, we chose $\phi = \phi_1$ and we keep it constant during the complete simulation. In the second one, on the other

hand, ϕ was updated conveniently to the thermal source velocity change. In Fig. 2.12 the relative errors of both of the simulations are presented. It can be seen that updating the enrichment function diminishes the maximum relative error from 27% to 5% with respect to a reference solution (a FEM solution with a very fine mesh).

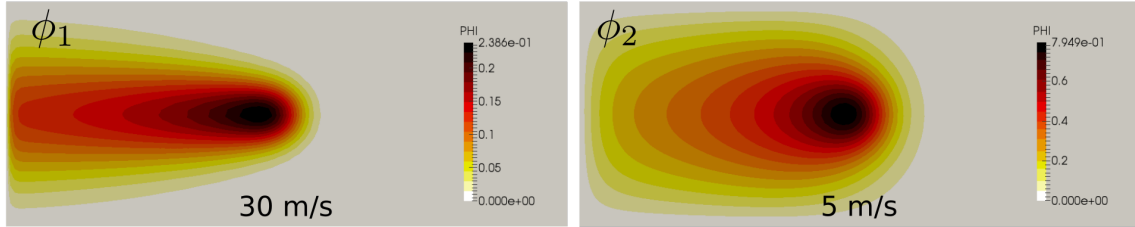


Figure 2.11: Enrichment functions at different advance velocities

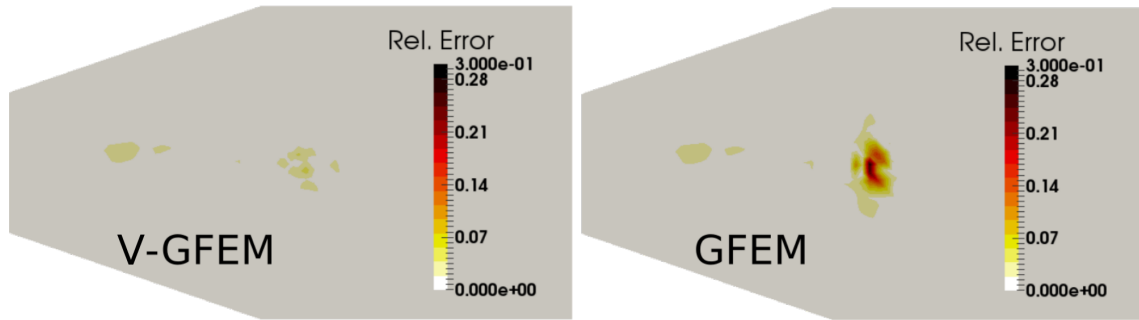


Figure 2.12: Relative errors with and without adapting the enrichment function

Let us now see another example. In this case, it is the area of incidence of the heat source, controlled by the parameter σ , which changes during the simulation. The essential and natural boundary conditions are homogeneous again. We set the other technological parameters, $Q = 10 \text{ W/m}^2$, $V = 10 \text{ m/s}$. We started the simulation with $\sigma = \sqrt{0.05}$ and at a certain point it changes to $\sigma = \sqrt{0.005}$. The two enriched functions generated by the computational vademecum at those instants are ϕ_1 and ϕ_2 respectively as can be seen in Fig. 2.13.

As before, we performed two simulations. In the first one, we set $\phi = \phi_1$ and we keep it constant during the entire simulation. In the second one, ϕ was updated conveniently, adapting it to the change of area of incidence. In this case, the fact of updating or not the enrichment function results in a difference of 25% in maximum

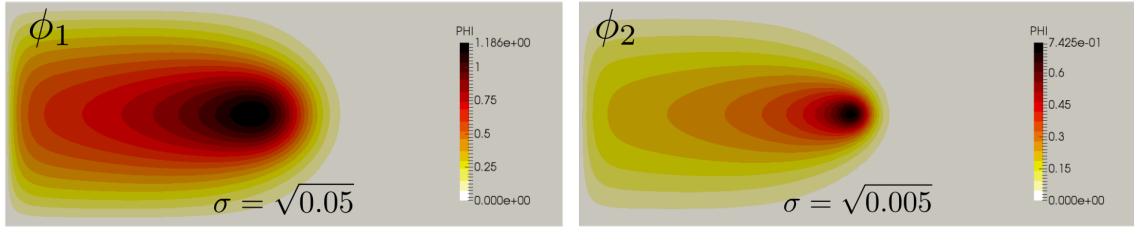


Figure 2.13: Enrichment functions in different areas of incidence of the heat source

temperature with respect to the reference solution, as can be observed in Fig. 2.14. In this figure, the reference FEM solution is in wire-frame and in solid color the solution without updating the enrichment function and by updating it within the V-GFEM framework.

In the last example, one can see that the thermal history of a given point could be significantly affected if an adaptation of the enrichment function is not carried out. If a GFEM without updating is considered, the maximum temperature at the point drops around a 25% with respect to the reference solution. Conversely, if the V-GFEM is used, the results are in very good agreement with the reference solution as can be observed in Fig. 2.15. It should be noted that, since updating the vademecum has a negligible cost, this improvement is obtained with no additional computational effort.

In simulation of welding, the thermal analysis is usually coupled with a metallurgical model to obtain changes in phases and in the microstructure of the material. For this analysis, a thermal history with errors of the order of 25% may represent in practice (see Fig. 2.15) obtaining a completely wrong numerical prediction of metallurgical and consequently mechanical properties.

2.4.4 Timing

In order to obtain a measure of the relative computational savings we obtain with the just presented technique, we solved the problems with a sequence of FEM meshes refined by bisection (i.e., each mesh contained four times the number of degrees of freedom of its parent mesh.)

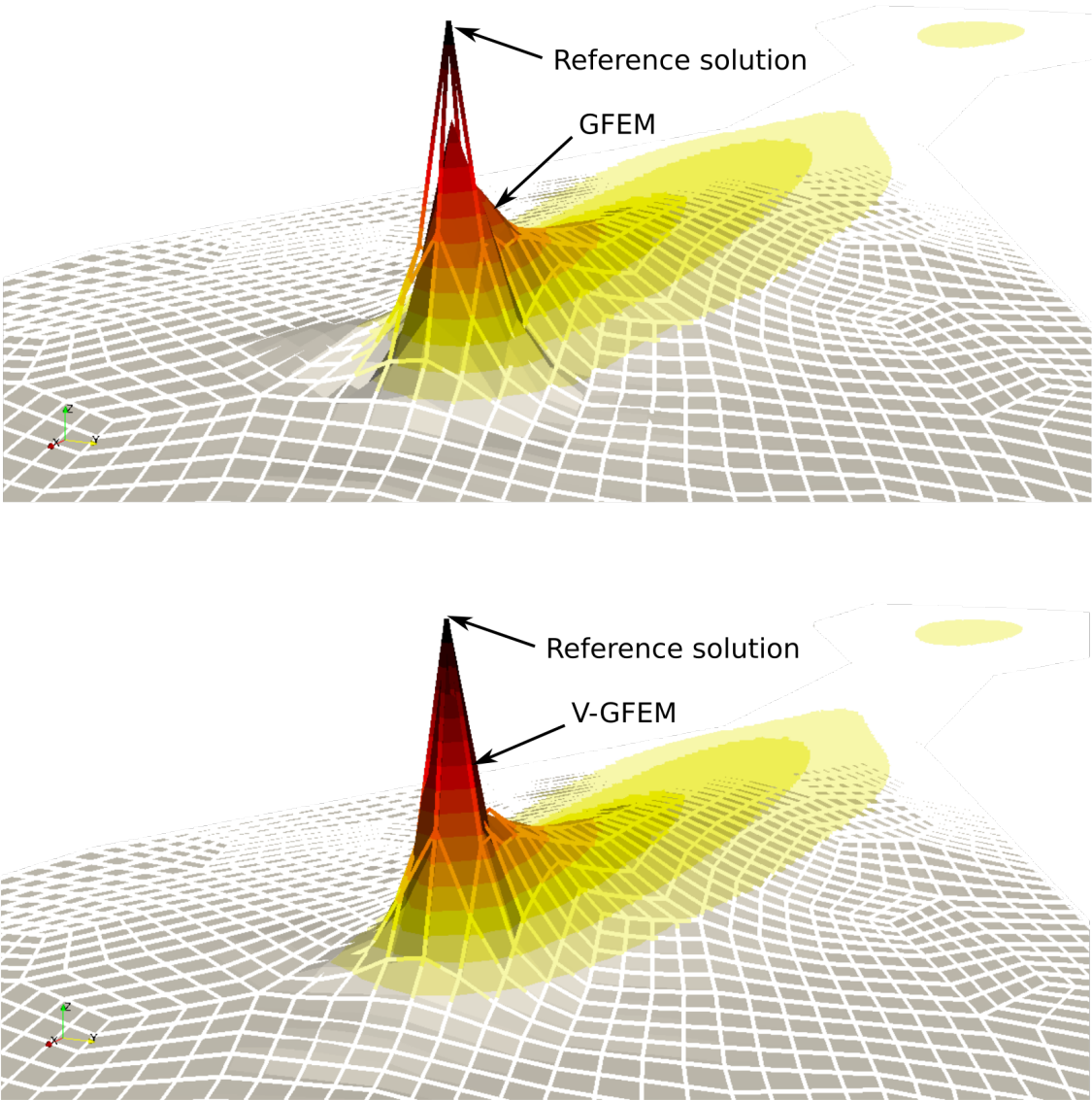


Figure 2.14: Difference between solution with and without updating the enrichment function

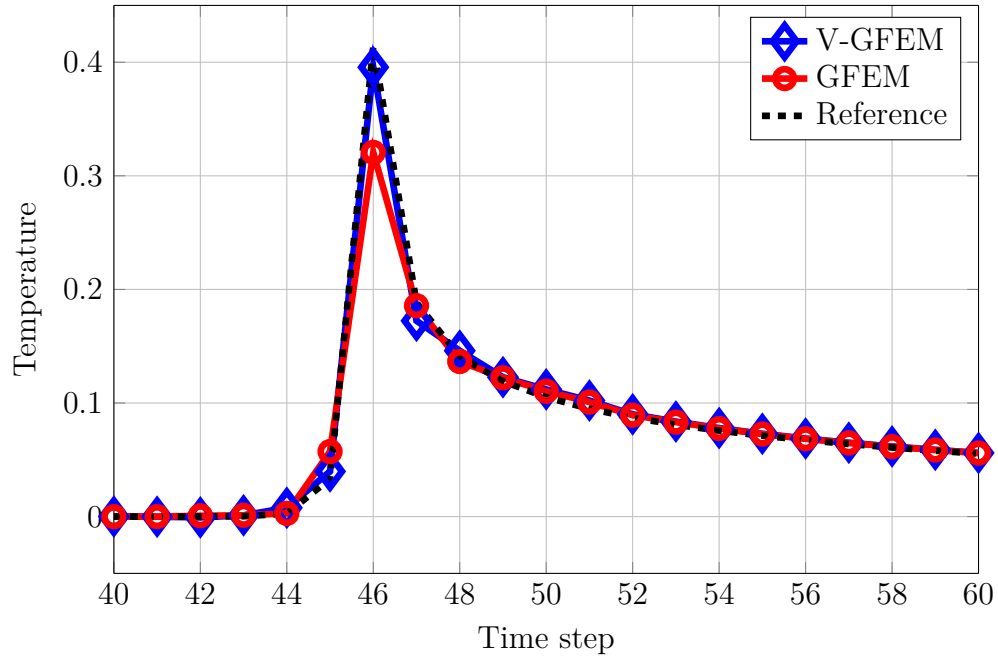


Figure 2.15: Thermal history of a material point

Our conclusion is that, in general, the proposed V-GFEM technique could obtain the same level of accuracy of its equivalent FEM mesh, but refined twice more. The resulting CPU savings turns out to be of one order of magnitude.

We strongly believe, nevertheless, that the advantages to be obtained in three-dimensional meshes will be even more important. Moreover, due to the fact that the enrichment function is known (computed offline), advanced integration strategies, as in (Olmos et al., 1996), can be used to significantly reduce the number of integration points with the consequent saving in computational time.

Chapter 3

Metalocal-global method for the analysis of large welded structures

In this chapter, the Metalocal-global is proposed as an efficient method to estimate final distortions and residual stresses in large structures where repetitive welded joints are performed. This method is based on the local-global method circumventing its main issue: the consideration of the influence of the global structure over the local region in an efficient manner. The Metalocal-global method substitutes the local simulation for a computational vademecum which provides the local solution for any elastic influence of the global domain over the local one. This methodology provides a systematic way to construct a database of computational vademecums that can be stored and used for different global geometries and global boundary conditions.

Contents

3.1	Introduction	65
3.2	Metalocal-Global Method	69
3.2.1	Identification of the equivalent stiffness coefficients	69
3.2.2	General Algorithm of the Metalocal-global method	73
3.3	Numerical examples	75

- 3.3.1 Linear thermo-elastic benchmark 75
- 3.3.2 Thermo elasto-plastic example and computational vade-
mecum 78

3.1 Introduction

Welding is a clear example of how numerical simulation has played a fundamental role in industry. According to Painter et al. (Bachorski et al., 1999), numerical experiments can be used to simulate a process or to gain a deeper understanding of its physics, depending on the scope of the model used. Computational Welding Mechanics (CWM) is not an exception and both types of studies can be found in literature. In this chapter we focus in improving the efficiency of a numerical strategy used for the simulation of welding in large structures where a high number of welded joints are performed (see Fig. 3.1). The main objective in these simulations is the prediction of residual stresses and distortion caused by the welding process.

This problem involves the use of models and hypothesis according to the variables of interest and their length scales. For numerical simulations at structural (or macro) length scale, the Finite Element method is *de facto* the standard method used. In the case of CSW, the thermo-mechanical models used are fairly consolidated in literature (Bergheau and Fortunier, 2013; Goldak and Akhlaghi, 2006) and can be found in several commercial codes.



Figure 3.1: Large welded structure

However, a detailed transient analysis (DTA) of welding in large structures, despite the important means of calculation available today, requires prohibitive calcu-

lation time. This is of particular importance when the aim is to optimize the welding strategy in order to minimize the distortion and the residual stresses. Indeed, the number of parameters to be considered (technological variables, paths, welding sequence, grips positions, etc.) is so large that makes it unfeasible to perform DTAs to explore the complete design space.

The application of model order reduction for a detail transient mechanical analysis of a welding process is a real challenge. We know from the Idelsohn's benchmark studied in (Allier et al., 2015) that the separability of problems involving moving heat sources is an issue. Moreover, because the trajectory of the source is not assumed *a priori* and inelasticities evolve in regions far from the heat source lead to the impossibility of following a similar strategy as developed in the previous chapter. Thus, we are interested in improving a simplified analysis of the mechanical simulation of welding.

Several simplified methods to provide approximate solutions with a computational cost of orders of magnitude lower than the DTA have been proposed. First, the Shrinkage method of Tsai et al. (Tsai et al., 1995) came up with variations like Lump-Pass method (Yang et al., 2002). These strategies neglect the contribution of the heat-up phase introducing the hypothesis that residual stresses are mainly due to the cooling of the material once welding has occurred (shrinkage). This is not very accurate when it comes to obtain the final distortion of the structure because these methods consider neither the direction of welding nor the transient effect of the motion of the source. In other words, the shrinkage is applied to the complete weld line instantly. Furthermore, the mechanical history of material points and phase changes cannot be calculated properly and certain calibration with experimental measures is needed to achieve good results. Even with these constraints, the shrinkage analysis provides valuable information in early phase of design, being widely used in industry today (Jackson and Darlington, 2011). A. Mendizabal et al. have recently proposed an improved shrinkage method in which the welding strategy is considered (Mendizabal et al., 2016).

The second family of simplified methods is composed of the so-called elastic methods. They are based on the Inherent Strain Method, proposed by Y. Ueda et

al. in 1979 (Ueda et al., 1979). The behavior of the large structure is obtained through an elastic calculation in which some known local plastic deformations are introduced into the weld line and an elastic global problem is solved. Hence, the principle of virtual works,

$$\int_{\Omega} \boldsymbol{\sigma} : \boldsymbol{\varepsilon}(\mathbf{w}) dV = \int_{\Omega} \mathbf{f} \cdot \mathbf{w} dV + \int_{\Gamma_t} \bar{\mathbf{t}} \cdot \mathbf{w} dA,$$

must be satisfied for any compatible displacement \mathbf{w} when a volumetric force \mathbf{f} and certain tractions $\bar{\mathbf{t}}$ on the boundary Γ_t are considered. The stress field reads $\boldsymbol{\sigma} = \mathbf{D}(\boldsymbol{\varepsilon} - \boldsymbol{\varepsilon}^p)$, where \mathbf{D} is the elasticity tensor and the plastic strain field, $\boldsymbol{\varepsilon}^p$, comes from analytical results, experiments or numerical simulations.

Subsequently, G. Jun generalized this idea leading to the Plasticity-Based Distortion Analysis (PDA) (Jung, 2003), also known as Mapped Plastic Strain Method. Here, the inherent strains come from a local simulation model and they are mapped into an elastic overall problem solved in a coarser discretization mesh. Its fundamental contribution is showing that the various components of distortions (and residual stresses) cannot be obtained by only considering one associated component of the inherent strain field because it is a coupled problem.

Finally, the so-called local-global method proposed by Souloumiac et al. in (Souloumiac et al., 2002) where the introduction of local plastic strains in the global linear simulation is made through a local subdomain rather than a mapping. This allows the use of degenerated elements in the global elastic problem (typically shell elements) instead of 3D solid elements that can be reserved only for the local one. Moreover, this strategy facilitates its implementation in commercial codes. Some industrial applications can be found in (Duan et al., 2007). Those families of CMW methods are schematized in the Fig. 3.2.

The main shortcoming of the PDA and the local-global methods is that the boundary conditions of the local problem should reflect the mechanical influence of the rest of the structure in order to obtain a reliable local solution. The importance of the correct choice of the local problem boundary conditions has been noted by different authors (Mendizabal et al., 2016; Souloumiac et al., 2002) and studied in detail by Duan et al. in (Duan et al., 2007). Their choice is critical because the

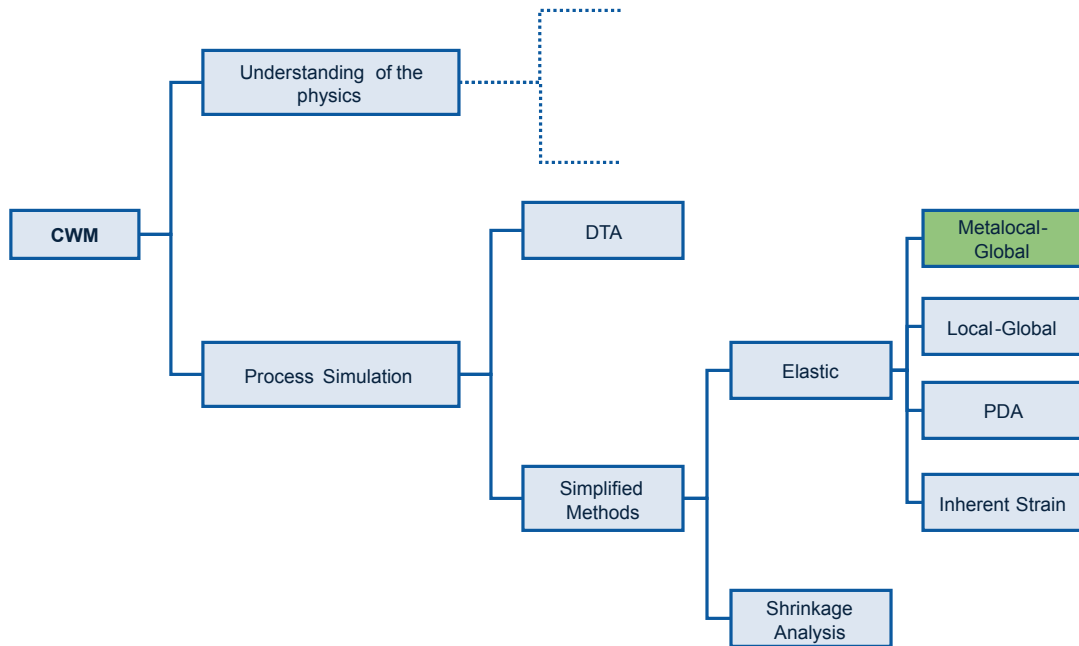


Figure 3.2: Scheme of CMW methods.

local plasticity depends on them and cannot be corrected later in the elastic global calculation.

Moreover, in the PDA and the local-global methods the local problem must be recalculated whenever these boundary conditions need to be changed, the initial conditions are not the same or the technological parameters vary. This limits the interest of these methods because finally the total simulation, including the local resolutions, results in high computational cost. This problem has been pointed out by Yang et al. in (Yang and Athreya, 2013), proposing the creation of a database of local problems. However, up to our knowledge, it is not clear in literature how to efficiently construct this database.

In this work, a new local-global method able to circumvent the forementioned limitations is presented. After this introduction the chapter is organized as follows. The proposed method and its different ingredients are elaborated in Section 3.2. Then, numerical examples of this technique are described in Section 3.3.

3.2 Metalocal-Global Method

Computational vademecums can also be an interesting ingredient to improve preexisting methods such as the Vademecum-GEFM introduced in Chapter 2, the numerical integrator presented in (González et al., 2014) and the Metalocal-global method elaborated in this chapter.

The Metalocal-global method circumvents both the main limitations of the PDA and the local-global strategy thanks to the introduction of a computational vademecum, offline precomputed, as a local metamodel. In this local metamodel, the influence of the global domain over the local domain is parametrized and it is part of the solution in an explicit form. This allows instant access to an approximated local elasto-plastic solution for any global geometry and any global boundary conditions. Furthermore, the computational vademecum construction is non-intrusive, facilitating the introduction of this method in commercial simulation platforms.

We move forward to the elaboration of the two main bricks of the method: the identification of the mechanical influence of the global structure over the local domain, and the construction of a non-intrusive computational vademecum for the local model. At the end of this section, a general scheme of the method is presented.

3.2.1 Identification of the equivalent stiffness coefficients

As described in the introduction, local-global techniques for welding simulations assume that complex physics only take place in a local region around the weld line. Thus, a costly detailed transient model is solved in a little local domain. The rest of the structure, the global domain, is considered just as an elastic structure where neither metallurgical changes nor plastic deformations occur.

However, the influence of the global domain over the local one cannot be neglected in the detailed transient calculation. In the Metalocal-global method this influence is parametrized in order to construct the local meta-model.

Let us consider a general structure Ω with certain essential boundary conditions Γ_D (fixed displacements) and certain natural boundary conditions Γ_N (applied

loads). This domain is divided into two subdomains, the local domain, Ω_l , and the global one, Ω_G , as depicted in Fig. 3.3.

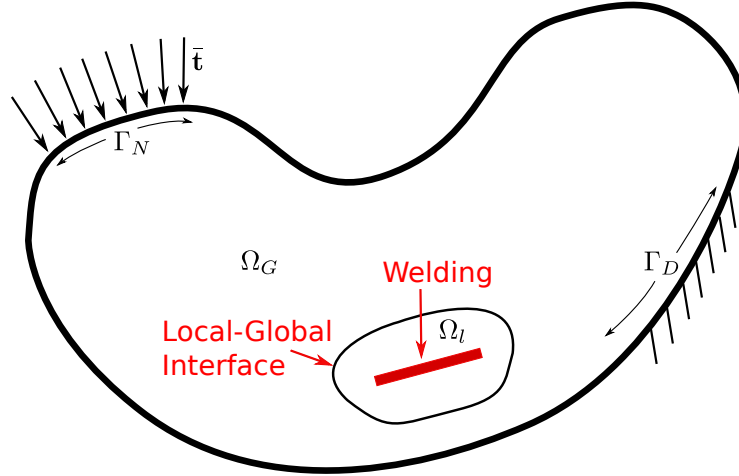


Figure 3.3: General local-global problem.

From the local-global hypothesis it follows that, after the discretization, the elastic contribution of the global domain can be seen as a static condensation of the global degrees of freedom (DOFs) over the degrees of freedom of the local-global interface,

$$\tilde{\mathbf{K}}_{ii} = \mathbf{K}_{ii} - \mathbf{K}_{iG} \mathbf{K}_{GG}^{-1} \mathbf{K}_{Gi},$$

where the subindices i and G denote the block of the stiffness matrix corresponding to the DOFs of the interface and to the DOFs of the global domain respectively. This is nothing but a superelement technique where the non-singularity of \mathbf{K}_{GG} is needed. The boundary conditions should preclude all rigid body motions: if this condition is not verified, the superelement is called *floating* and especial techniques such as projections and generalized inverses must be used. Without loss of generality, we consider in this chapter that the global domain is not a floating domain and no loads are applied on this region. This is the case of most of the situations in practice where the thermal loads come from the heat source situated in the local region and several areas of the global domain must be clamped in order to perform quality welds.

Once the stiffness condensation has been carried out, the nonlinear problem is solved in the local domain taking into account this contribution. Typically, if a

generic Newton-Raphson method is used, each iteration (k) requires the solution of the standard linear system for an increment of displacements $\delta\mathbf{u}^{(k)}$,

$$\mathbf{K}_T \delta\mathbf{u}^{(k)} = -\mathbf{r}^{(k-1)}, \quad (3.1)$$

where \mathbf{K}_T is the tangent operator and $\mathbf{r}^{(k-1)}$ is the residual of the precedent iteration. The tangent operator must include the contribution of the global superelement, $\tilde{\mathbf{K}}_{ii}$, with a proper assembly of the DOFs of the interface.

Obviously, an exact parametrization of the influence of the global domain over the local one implies defining one parameter for each $\tilde{\mathbf{K}}_{ii}$ term. This leads to the same number of parameters as the number of degrees of freedom of the interface. The construction of a computational vademecum with such a number of parameters is unfeasible from a practical point of view. Thus, a simplified strategy to reduce this number to a few of them is proposed below.

Let us consider an auxiliary local problem where a layer of elements around the local domain is introduced as depicted in Fig. 3.4. The external boundary of the layer is fixed and the internal nodes coincide with the nodes of the local-global interface. The aim is to construct a stiffness matrix associated to the layer, \mathbf{K}^{lay} , that should reproduce as best as possible the condensed stiffness matrix, $\tilde{\mathbf{K}}_{ii}$, of the original problem. This can be done, for example, changing the elastic properties, of the elements of the layer, their section properties or introducing some multiplicative factors in \mathbf{K}^{lay} . In any case, two fundamental requirements must be fulfilled: firstly, it should be a small number of parameters, and secondly a simple and generalized strategy to fit these parameters must be defined.

It should be noted that this strategy is not a general domain decomposition technique. In fact, one could formulate a plethora of complex mechanical problems where this equivalence cannot be, in general, achieved using just a few number of parameters. However, in this case, the global influence can be seen as a restriction to the local free dilatation (and contraction) by a heat source. In other words, the global domain acts as a structural rig of the local domain. Therefore, it is reasonable to establish a certain equivalence between $\tilde{\mathbf{K}}_{ii}$ and \mathbf{K}^{lay} though some simple and general mechanical tests.

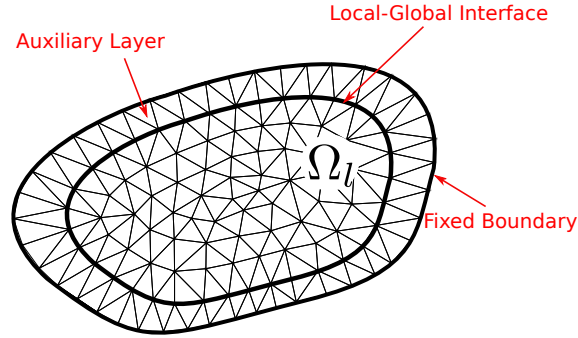


Figure 3.4: Auxiliary local problem.

Let us define $\hat{\mathbf{K}}^{lay}$ as the stiffness matrix of the assembled layer using some arbitrary element properties (elastic parameters and section), for example the same as those of the global domain. Then, this stiffness matrix is multiplied by a uniform displacement vector in each direction, $\mathbf{U}_j \in \mathbb{R}^{ni}$ with $j \in \{x, y, z\}$. \mathbf{U}_j contains an arbitrary constant value at each degree of freedom associated to the j direction and it is null in the degrees of freedom associated to the others. These products lead to the nodal force vectors \mathbf{F}_j^{lay} which represent the nodal forces needed to obtain the nodal displacements given by \mathbf{U}_j . In the 3D case we obtain:

$$\begin{aligned}\hat{\mathbf{K}}^{lay} \cdot \mathbf{U}_x &= \mathbf{F}_x^{lay} \\ \hat{\mathbf{K}}^{lay} \cdot \mathbf{U}_y &= \mathbf{F}_y^{lay} \\ \hat{\mathbf{K}}^{lay} \cdot \mathbf{U}_z &= \mathbf{F}_z^{lay}.\end{aligned}$$

The same procedure is carried out with the condensed stiffness matrix $\tilde{\mathbf{K}}_{ii}$, using the same displacement vectors \mathbf{U}_j to compute the nodal force vectors \mathbf{F}_j^{cond} . In the 3D case they read,

$$\begin{aligned}\tilde{\mathbf{K}}_{ii} \cdot \mathbf{U}_x &= \mathbf{F}_x^{cond} \\ \tilde{\mathbf{K}}_{ii} \cdot \mathbf{U}_y &= \mathbf{F}_y^{cond} \\ \tilde{\mathbf{K}}_{ii} \cdot \mathbf{U}_z &= \mathbf{F}_z^{cond}.\end{aligned}$$

Thereafter, the equivalent stiffness coefficients α_j can be defined as the ratio

between the norms of the nodal forces \mathbf{F}_j^{cond} and \mathbf{F}_j^{lay} ,

$$\alpha_j = \frac{\|\mathbf{F}_j^{cond}\|}{\|\mathbf{F}_j^{lay}\|}. \quad (3.4)$$

Finally, the condensed stiffness matrix $\tilde{\mathbf{K}}_{ii}$ is approximated by \mathbf{K}^{lay} which is the assembly of the matrices $\alpha_j \hat{\mathbf{K}}_j^{lay}$, where $\hat{\mathbf{K}}_j$ represents the extraction of the degrees of freedom in the j direction of $\hat{\mathbf{K}}^{lay}$, in a 3D problem,

$$\tilde{\mathbf{K}}_{ii} \simeq \mathbf{K}^{lay} = \sum_{j=1}^3 \alpha_j \hat{\mathbf{K}}_j^{lay}.$$

The coefficients α_j are computed *a priori* for a certain application, so the intervals $\alpha_j \in [\alpha_j^{min}, \alpha_j^{max}]$ are known and a computational vademecum taking into account these coefficients as parameters can be constructed. For this application, due to the not too large number of parameters and we are interested in a non-intrusive method, the SSL method, elaborated in Section 1.1.4 has been chosen.

3.2.2 General Algorithm of the Metalocal-global method

Once the two main ingredients of the Metalocal-global method have been introduced, for the sake of clarity, the general strategy is developed below in a concise manner.

Let us consider a large structure where an important number of welded joints must be performed at different positions l . All the welded joints must be described with the same local geometry, Ω_l , as depicted in Fig. 3.5.

Since the local geometry is constant, an auxiliary problem is created adding a layer of elements to the local domain, as explained in Section 3.2.1. The computational vademecum can be created considering α_j as parameters, using this auxiliary problem.

For each position l , a static condensation is carried out and all the associated equivalent stiffness coefficients α_j^l are identified.

Finally, the computational vademecum is particularized and the local plastic

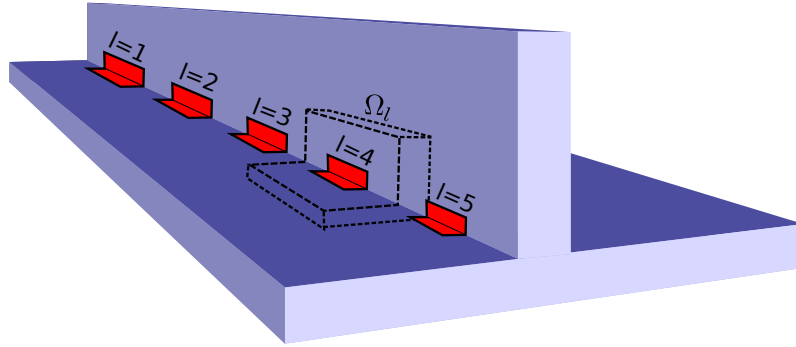


Figure 3.5: Scheme of a large structure welded at different regions.

strain field is computed for each particular position. These plastic strains can be inserted into the global structure through a local subdomain (which coincides with the local domain of the computational vademecum) or by projection in a coarse mesh. This decision does not affect the strategy presented in this work.

It should be noted that the welding sequence can be taken into account since the coefficients α_j^l of the position l are computed after the introduction of the local solution of the position $l - 1$. Thus, if this previous local welding has an influence in the global stiffness of the structure, the coefficients α_j^l will take account on it. The general steps of the method are presented below:

1. For each local position l , an static condensation is carried out.
2. The equivalent stiffness coefficients, α_j^l are identified.
3. The computational vademecum, computed offline, is particularized for those coefficients. So, the local plastic strain field is provided.
4. The local plastic strain field, ϵ^p , is introduced in the global structure.
5. A linear elastic problem is solved.

3.3 Numerical examples

In this section, two simple benchmarks are presented: a linear thermo-elastic problem first and then a thermo elasto-plastic one. In both of them, a symmetrical thin plate is submitted to a Gaussian temperature distribution on its center. A local-global domain division is carried out and the Metalocal-global strategy is studied. These examples do not try to reproduce the real physics of a welding simulation but to study the feasibility of the proposed strategy from a numerical point of view.

3.3.1 Linear thermo-elastic benchmark

This first example is aimed to verify whether, for a linear thermo-elastic problem, the auxiliary problem is able to reproduce the elastic solution in the local domain for different global geometries and for different global boundary conditions. The auxiliary problem is defined in Section 3.2.1 equipped with the equivalent stiffness coefficients.

Let us consider a symmetrical thin plate submitted to a Gaussian temperature distribution in its local domain as depicted in Fig. 3.6. Under the plane stress hypothesis the problem to be solved reads,

$$\int_{\Omega} \boldsymbol{\varepsilon}(\mathbf{w})^T \cdot \mathbf{D} \cdot \boldsymbol{\varepsilon} dV = \int_{\Omega} \mathbf{w}^T \cdot \mathbf{D} \cdot \boldsymbol{\varepsilon}^{th} dV \quad (3.5)$$

with

$$\boldsymbol{\varepsilon} \equiv \begin{bmatrix} \varepsilon_{11} & \varepsilon_{22} & 2\varepsilon_{12} \end{bmatrix}^T, \quad \mathbf{D} \equiv \frac{E}{1-\nu^2} \begin{bmatrix} 1 & \nu & 0 \\ \nu & 1 & 0 \\ 0 & 0 & \frac{1-\nu}{2} \end{bmatrix} \quad \text{and} \quad \boldsymbol{\varepsilon}^{th} = \alpha_t \Delta T.$$

The value of the dilatation coefficient α_t is $23 \cdot 10^{-6} K^{-1}$ and $\Delta T = 10^5 / (18\pi) \exp(-(x^2 + y^2)/18) K$ is the imposed temperature field. The elastic parameters are $E = 70$ GPa and $\nu = 0.2$.

The geometry of the local domain, Ω_l , will remain constant and the geometry and boundary conditions of the global domain, Ω_G and Γ_G respectively, will be modified.

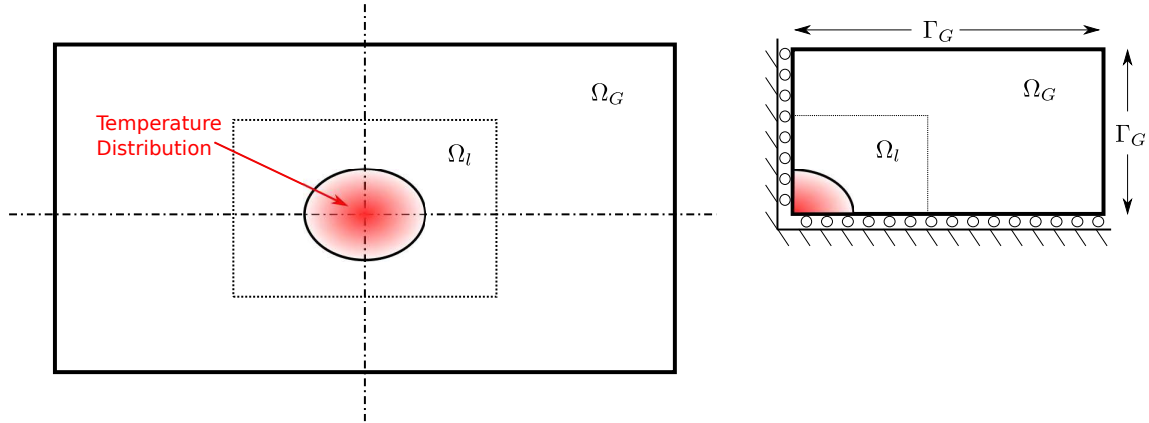


Figure 3.6: Linear thermo-elastic example.

Let's begin by examining the local solution for different Γ_G . In Fig. 3.7, the norm of the displacement field is presented for both the reference solution for the case of fixed boundaries and the case of traction-free condition. If the auxiliary problem is constructed and the equivalent stiffness coefficients are identified, the local solutions are conveniently approximated in both cases, as it can be seen in Fig. 3.8.

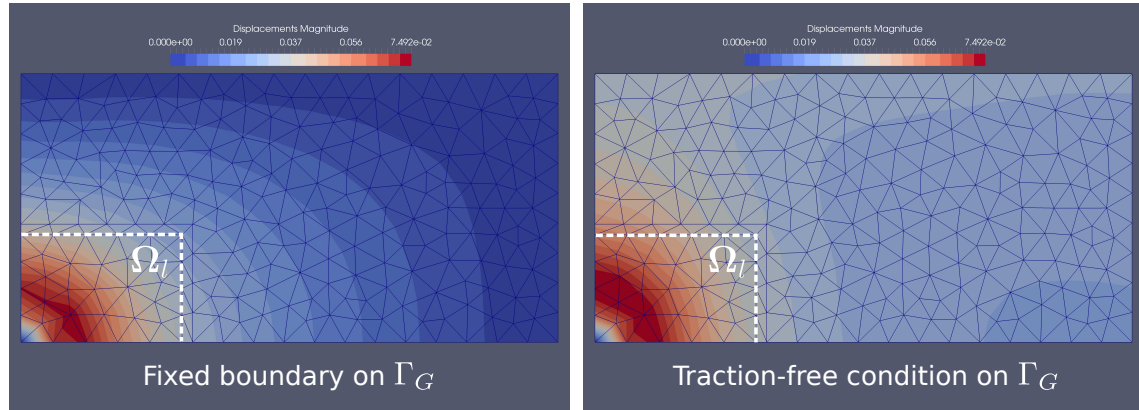


Figure 3.7: Linear thermo-elastic reference solutions.

In the previous examples, the equivalent stiffness coefficients took the values $\alpha_x = 0.094$, $\alpha_y = 0.1127$ for Γ_G fixed, and $\alpha_x = 0.0681$, $\alpha_y = 0.0522$ for the traction-free condition. The local problem is frequently solved in practice with fixed boundary conditions to avoid performing repetitive local simulations. This choice leads to less accurate results, as can be seen in Fig. 3.9 and 3.10, where this strategy

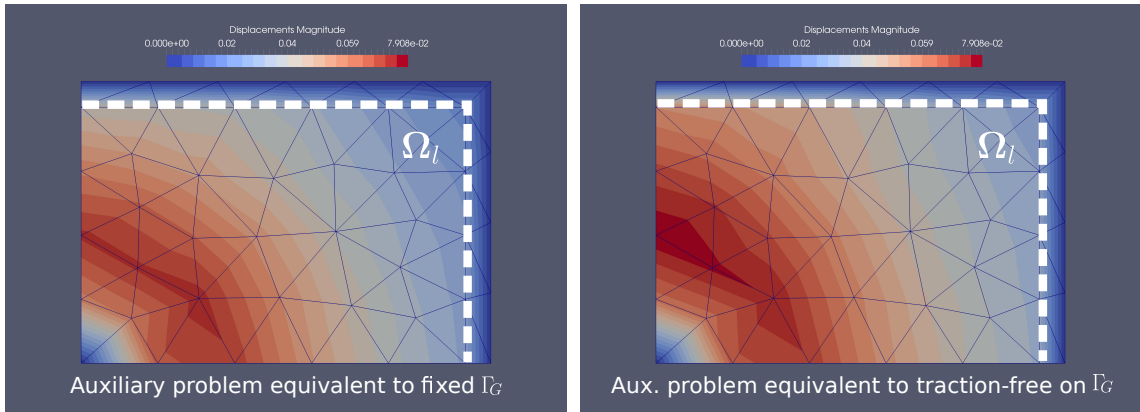


Figure 3.8: Linear thermo-elastic local solutions with equivalent stiffness coefficients.

is compared with the equivalent stiffness approach. The equivalent stiffness approach provides relative errors inferior to 10% in almost the complete local domain, while with fixed boundary conditions relative errors are between 50% and 100% in most than half of the plate.

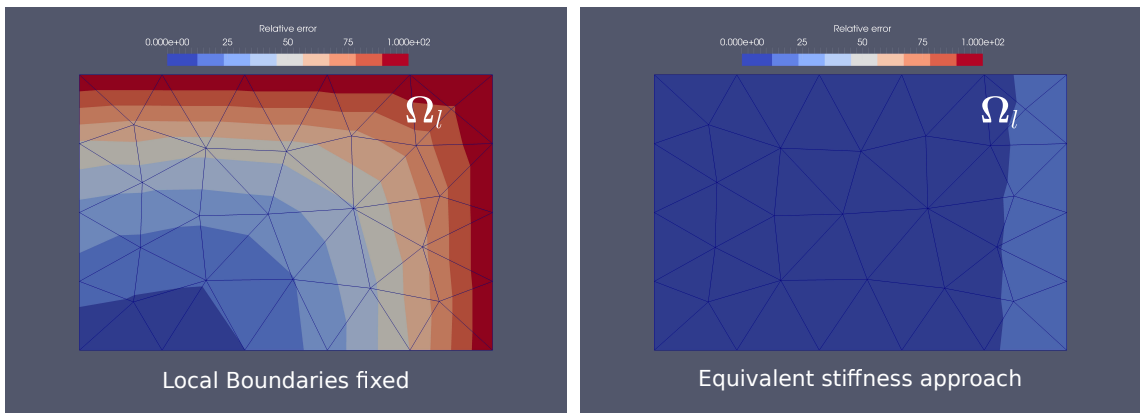


Figure 3.9: Relative errors for fixed Γ_G .

Finally, if another global geometry is considered, the presented strategy is able to provide an accurate approximated local solution, as it can be seen in Fig. 3.11.

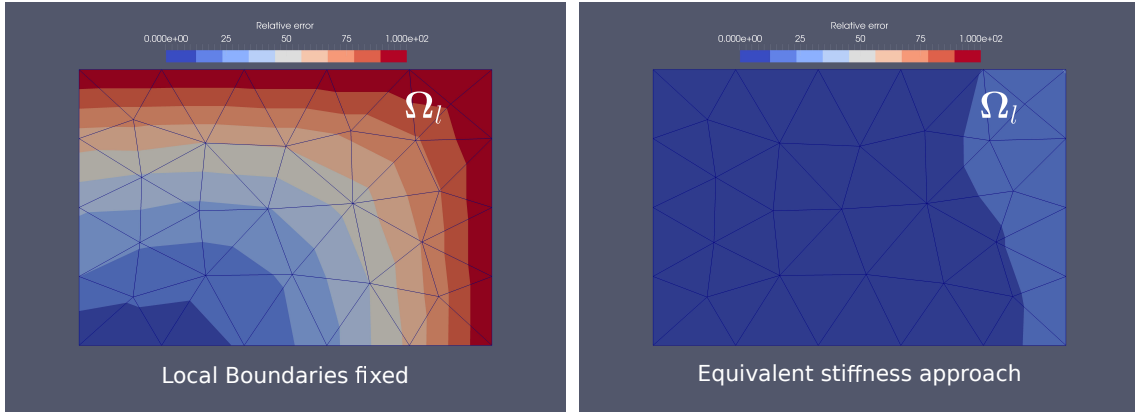


Figure 3.10: Relative errors for traction-free Γ_G .

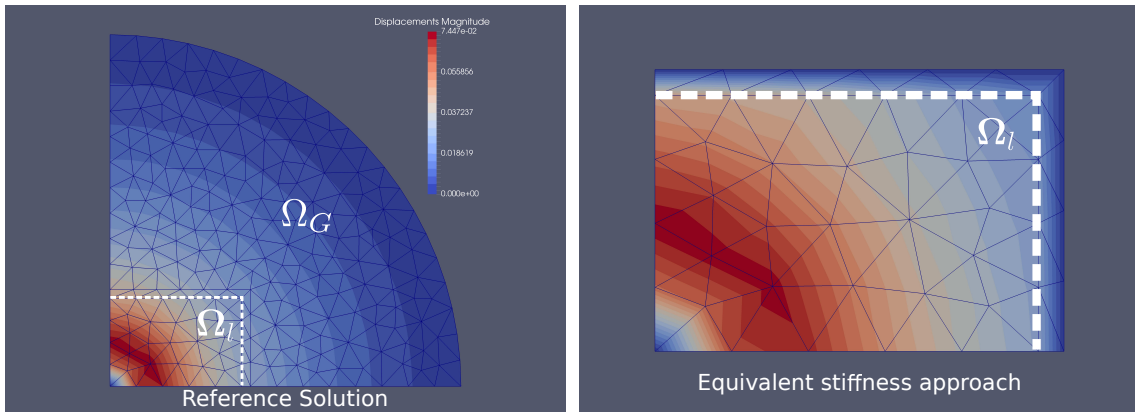


Figure 3.11: Equivalent stiffness approach in a circular plate.

3.3.2 Thermo elasto-plastic example and computational vademecum

Then, let us move on to a new benchmark solution where the real local-global hypothesis is introduced: a thermo elasto-plastic problem is solved in the local domain while the global domain is considered purely elastic.

For the local model, a plane stress projected von Mises model with linear isotropic hardening is solved. The implicit elastic predictor/return-mapping algorithm used can be found in (de Souza Neto et al., 2011). It is interesting to note that, if a plane stress model is used, the equation that must be solved to compute the

plastic multiplier is nonlinear even if a linear hardening is used. For the sake of completeness, the govern equations of this plastic model are enumerated below.

1. Elastoplastic strain split

$$\dot{\boldsymbol{\varepsilon}} = \dot{\boldsymbol{\varepsilon}}^e + \dot{\boldsymbol{\varepsilon}}^p$$

2. Elastic law

$$\boldsymbol{\sigma} = \mathbf{D}\boldsymbol{\varepsilon}^e$$

3. Yield function definition

$$\Phi = \frac{1}{2}\boldsymbol{\sigma}^T \mathbf{P}\boldsymbol{\sigma} - \frac{1}{3}\sigma_y^2(\bar{\boldsymbol{\varepsilon}}^p); \quad \mathbf{P} \equiv \frac{1}{3} \begin{bmatrix} 2 & -1 & 0 \\ -1 & 2 & 0 \\ 0 & 0 & 6 \end{bmatrix}$$

4. Plastic flow rule

$$\dot{\boldsymbol{\varepsilon}}^p = \dot{\gamma} \frac{\partial \Phi}{\partial \boldsymbol{\sigma}} = \dot{\gamma} \mathbf{P}\boldsymbol{\sigma}$$

5. Hardening variable evolution

$$\dot{\bar{\boldsymbol{\varepsilon}}}^p = \dot{\gamma} \sqrt{\frac{2}{3}\boldsymbol{\sigma}^T \mathbf{P}\boldsymbol{\sigma}}$$

6. Loading/unloading criterion

$$\dot{\gamma} \geq 0, \quad \Phi \leq 0, \quad \dot{\gamma}\Phi = 0$$

where $\dot{\gamma}$ is the plastic multiplier.

The nonlinear problem is formulated incrementally in displacements following a Newton-Raphson method, as Eq. (3.1) indicates. The tangent operator \mathbf{K}_T must be conveniently assembled in the global domain, where it remains constant, and in the local domain, where it evolves according with the plastic model. The Newton Raphson algorithm is initialized with the trial strains that results from the linear predictor, given by the solution of Eq. (3.5). On this occasion, a negative increment

of temperature has been imposed. This increment of temperature is constant $\Delta T = 1200K$ inside an ellipse centered in the middle of the plate.

Let us consider a fixed geometry Ω_G with different boundary conditions Γ_G and see how the equivalent stiffness coefficients are able to approximate the reference solution in the local domain. To that purpose, the equivalent plastic strains are used for comparisons.

In the first example, the global boundaries are considered fixed, $\mathbf{u} = 0$ at Γ_G . The reference solution is computed and is compared with the approximated solution created with the coefficients $\alpha_x = 1.1713$ and $\alpha_y = 1.1671$. A good agreement between them can be seen in Fig. 3.12.

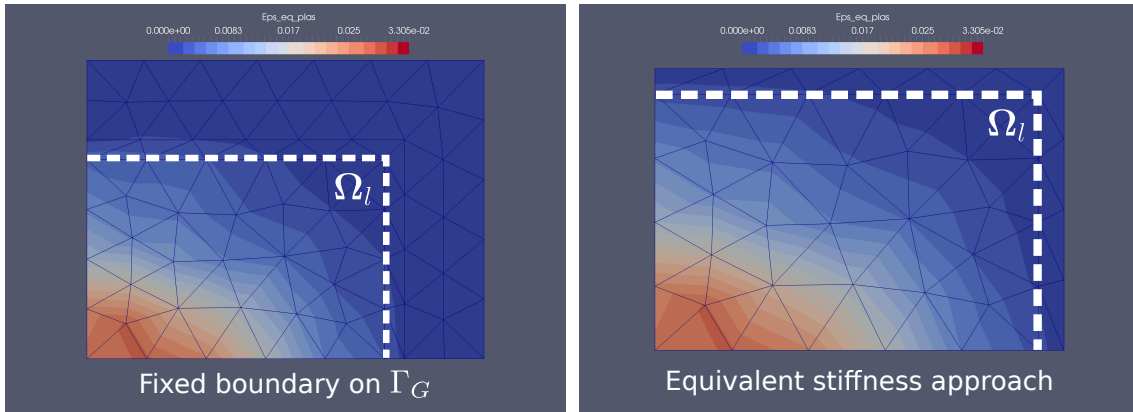


Figure 3.12: Equivalent stiffness approach with fixed Γ_G .

For the second example, the global boundaries are free, $\frac{\partial \mathbf{u}}{\partial \mathbf{n}} = 0$ at Γ_G . Again, with the identification of coefficients given by Eq. 3.4, a good approximation solution is reached, as Fig. 3.13 shows. In this case, the values of the equivalent stiffness coefficients are $\alpha_x = 0.2484$ and $\alpha_y = 0.2283$.

For the case of fixed Γ_G , the absolute of the equivalent stiffness approach and the strategy of fixing the local domain with respect to the reference solution are presented in Fig. 3.14.

The above examples show that it is possible to reproduce the local solution for very different geometries and boundary conditions of the global domain with a few number of parameters in a systematic way. Since the local domain is invariable

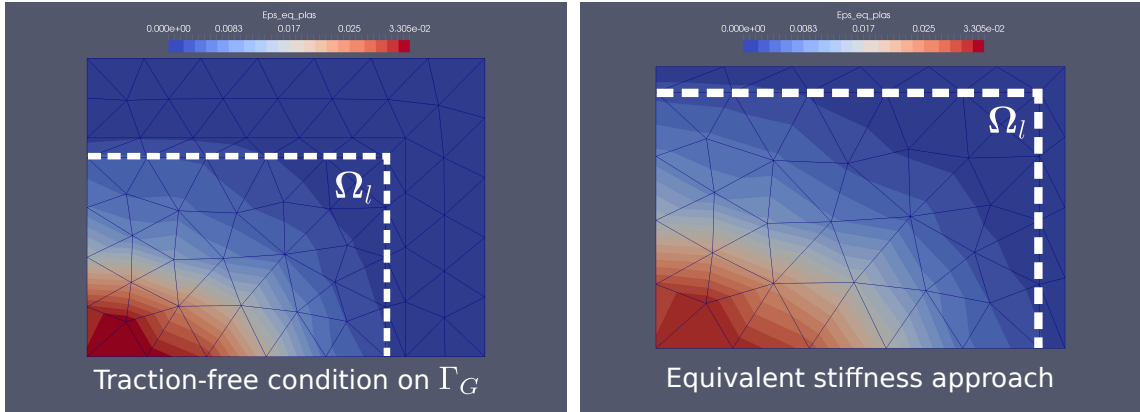


Figure 3.13: Equivalent stiffness approach with traction-free condition.

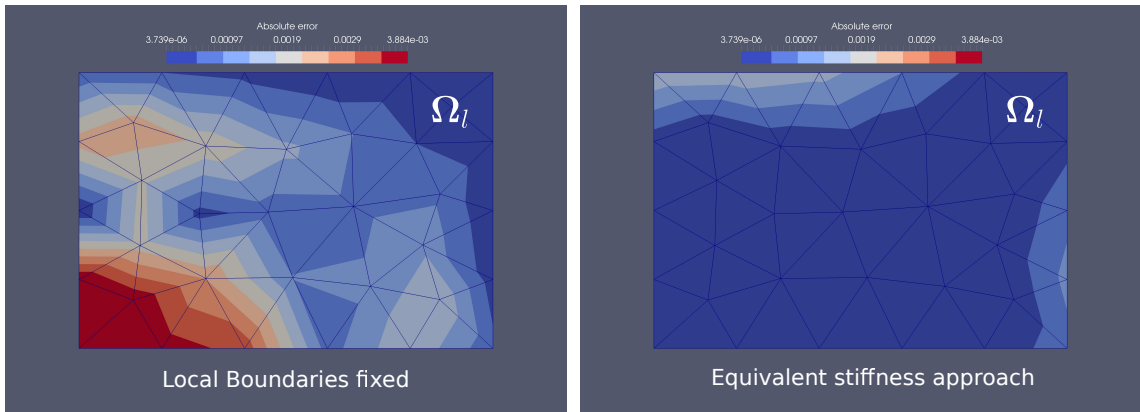


Figure 3.14: Absolute errors of fixed local domain and equivalent stiffness approach for Γ_G fixed.

as well as the added layer of elements, a computational vademecum can be built for certain intervals of the parameters, $\alpha_x = [0.01, 3]$ and $\alpha_y = [0.01, 3]$ in this case, following the SSL method. It has to be remarked that the intervals can be constructed as $\alpha_i = (0, 1]$ if the elements of boundary layers have the same properties as the elements of the global region, since the local cannot be stiffer than the global. This is not the case in these examples, where unitary thickness for the layer has been chosen, different to the global region one and $\alpha_i > 1$ can be obtained.

The separated solution associated to the vademecum is composed of 8 modes:

$$\varepsilon_p(\mathbf{x}, \alpha_1, \alpha_2) = \sum_{m=1}^8 c_m \psi_s^m(\mathbf{x}) \psi_1^m(\alpha_1) \psi_2^m(\alpha_2),$$

In the Fig. 3.15, 3.16 and 3.17, the first four modes of each dimension are presented. To construct this computational vademecum, 385 collocation points were needed, obtaining an estimated relative error of 0.02%. Not all of the collocation points must be computed (see (Borzacchiello et al., 2017)) and once it has been built it can be stored and reused for very different global geometries and boundary conditions if the local region remains identical.

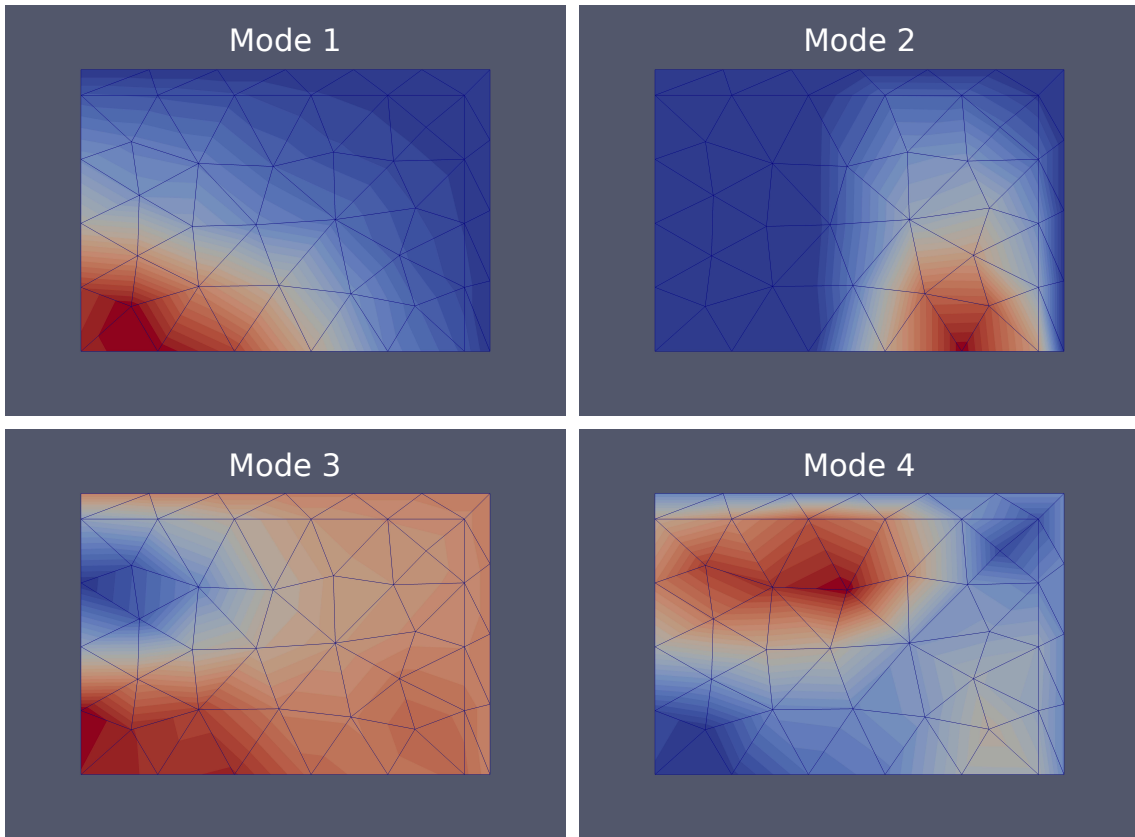


Figure 3.15: The first four spatial modes of the computational vademecum.

It is also possible to explore the vademecum with an intuitive ParaView interface developed by Bordeau (Bordeau et al., 2013). A screenshot of this interface with the

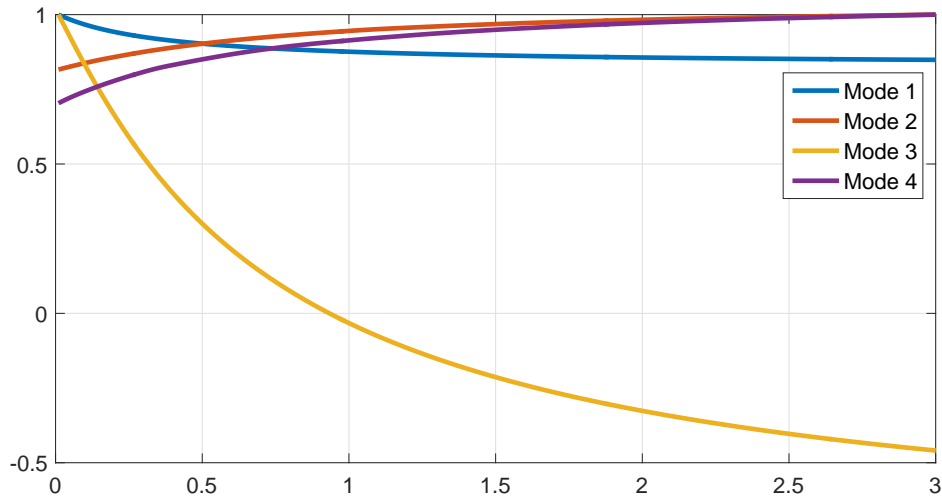


Figure 3.16: The first four modes of parameter α_1 of the computational vademecum.

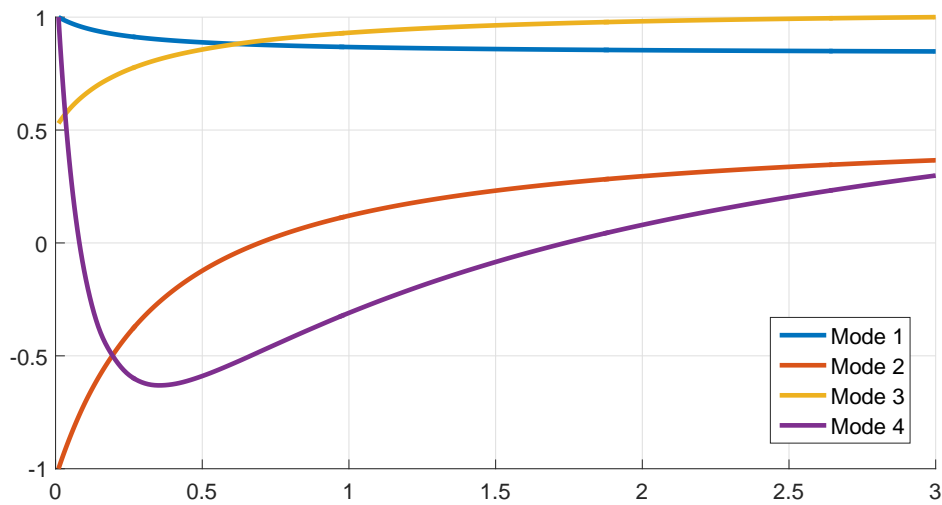


Figure 3.17: The first four modes of parameter α_2 of the computational vademecum.

vademecum constructed for this example is shown in Fig. 3.18.

The presented examples are devoted to the identification of equivalent stiffness coefficients, the construction of the local metamodel and the verification of the goodness of the local solution. The last step in the Metalocal-global strategy is the inclusion of the plastic strain field into the global structure. This step, not included



Figure 3.18: Screenshot of the ParaView interface to visualize computational vademecums.

in this work, is completely equivalent to that of the original local-global method and can be carried out using the same local-global domains or through a projection of the local plastic strain field into a coarse global mesh that discretize the entire domain.

Chapter 4

Vademecums for steady-state welding

As has been mentioned in the previous chapters, when a detailed transient analysis is carried out the costs of the simulation of welding processes involving thermal, metallurgical and mechanical analysis can be high. In Chapter 3 we have introduced different families of methods that try to reduce the computational effort of the mechanical analysis by introducing simplifying hypotheses. An improvement of one of these approaches, the local-global, that can be combined with a computational vademecum to gain efficiency has been elaborated.

In this chapter we propose to revisit one of the strongest simplifications that can be made in welding simulation: the steady-state hypothesis. Although, in principle, these models can have a very restricted use in real applications we will see that they will be quite helpful to adjust some parameters used in practice and for pre-design stages. As it will be seen below, it is especially appealing the possibility of building a computational vademecum of these processes, which is the purpose of this chapter.

Contents

4.1 Introduction	87
4.2 Steady-state formulations	90

Chapter 4. Computational Vademecums for steady-state welding simulations

4.2.1 Thermal and metallurgical formulation 90

4.2.2 Mechanical formulation 91

4.3 Numerical example 94

4.1 Introduction

The steady-state simulation of welding is one of the first applications found in the literature led by the first work of modeling the heat source in welding carried out by Rosenthal (Rosenthal, 1946) and Rykalin (Rykalin, 1976). This Eulerian formulation uses spatial coordinates: the material points move through the observed domain, which is fixed in space. The reference mesh and the arc are fixed and the material moves relative to the mesh at the welding speed, as is schematized in Fig. 4.1.

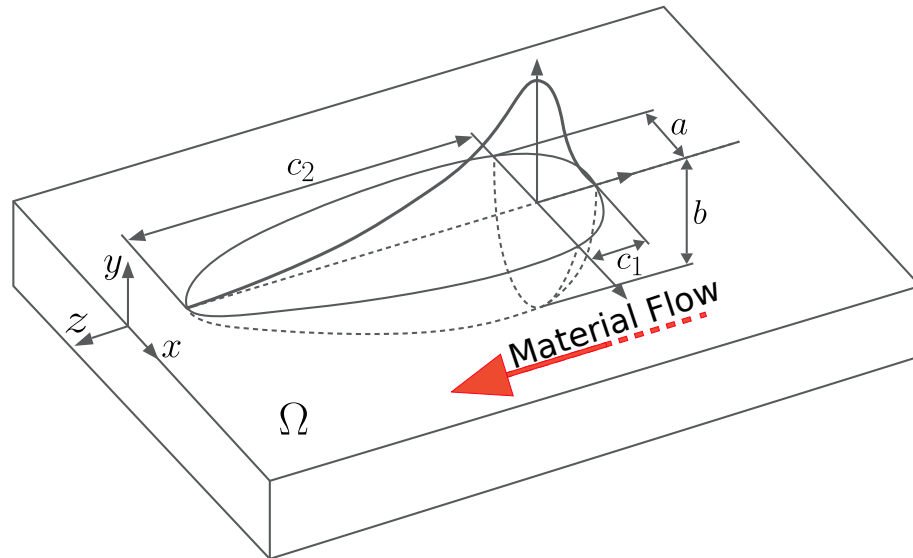


Figure 4.1: Eulerian framework and Goldak ellipsoid

With these first models it was possible to reproduce quite approximately the temperature distribution in a zone sufficiently far from the weld pool in thick plates. With a second generation of heat source models, in which the Goldak ellipsoid (Goldak et al., 1985) stands out, more accurate temperature distributions are achieved and nonlinearities and metallurgical processes could be included in the analysis. The double Goldak ellipsoid, shown in Fig. 4.1, is perhaps the most commonly used model in welding simulations at structural level and can be used for both stationary and non-stationary simulations. In this model, the physics of the weld pool is not reproduced and as a result the temperature that appears in it is

fictitious. The power density distribution in the front quadrant of the double Goldak ellipsoid becomes:

$$q_f(x, y, z) = \frac{6\sqrt{3}f_f Q}{abc\pi\sqrt{\pi}} \exp\left(-3\left(\frac{x^2}{a_1^2} + \frac{y^2}{b_1^2} + \frac{z^2}{c_1^2}\right)\right),$$

and for the rear quadrant becomes:

$$q_r(x, y, z) = \frac{6\sqrt{3}f_r Q}{abc\pi\sqrt{\pi}} \exp\left(-3\left(\frac{x^2}{a_2^2} + \frac{y^2}{b_2^2} + \frac{z^2}{c_2^2}\right)\right).$$

In Fig. 4.1 $a_1 = a_2 = a$ and $b_1 = b_2 = b$, but in general the parameters are independent. In this model the fractions f_f and f_r of the heat deposited in the front and rear quadrants are needed, where $f_f + f_r = 2$. The results obtained using this model are valid for the prediction of distortions and residual stresses, which is the aim of the welding simulation at this length scale. More sophisticated models with more realistic weld pool physics have been proposed in (Radaj, 2000; Ohji et al., 1992; Weiss et al., 1995; Sudnik et al., 1998, 2000).

The steady-state mechanical analysis came later, emphasizing the pioneering works of Bergheau et al. (Bergheau et al., 1992) and Gu et al. (Gu et al., 1993), where Eulerian formulations were elaborated. These first works are based on an Eulerian framework where the Gauss points follow the streamlines, needing a certain pre-processing and data structure adapted to the simulation. Other formulations such as those of Shanghvi et al. (Shanghvi and Michaleris, 2002) permit relaxing these requirements, although they present other inconveniences of complexity that cause that the former methods are the most used in industry.

The steady-state simulations, as long as they can be applied, allow to dramatically diminish the computational cost in comparison with a detailed transient analysis. This gaining normally represents several orders of magnitude, while keeping a reasonable level of precision (Goldak and Akhlaghi, 2006).

That is, the following would be the application scenarios:

- Simulations where a steady-state (or a succession of several steady-states) is sufficiently representative of the physics of the problem. The starting and final

transient stages should be negligible. Moreover, the welding process must be performed in a prismatic body where the source travels parallel to the axis of the prism. Convection and radiation boundary conditions must be invariant with respect the welding direction. This situation could appear when welding standard long structural components like beams.

- *Pre-design analysis.* These simulations can be very useful for having preliminary results before launching the full transient model.
- *Source fitting.* As mentioned, Goldak's ellipsoid provides good results, but since it does not represent the physics of the weld pool, its parameters must be adjusted. A first coarse-tuning can be performed ensuring that, in the simulation, the internal temperature of the weld pool corresponds to the melting point of the material. This guarantees achieving a good penetration of the weld. However, if more accuracy is required, a fine-tune of the heat source parameters must be performed with the aid of experimental testing (Fig. 4.2). This process is the so-called *source fitting* and it is performed with steady-state simulations. In this case the mechanical calculation is not needed.



Figure 4.2: Experimental measure for source fitting

In all of these scenarios, the construction of a non-intrusive computational vademecums can provide enormous advantages since, with a traditional approach, either

for a predesign stage or a source fitting, the stationary simulation must be launched on numerous occasions leading to a high computational time. In addition, the construction of a computational vademecums opens the possibility of an optimization and sensitivity analysis of a quantity of interest, an information of great value that is not available through a conventional trial-error approach (Chinesta et al., 2013b). Finally, a non-intrusive computational vademecum, such as the one presented here, can be updated over time through the accumulated experienced of new simulations, enriching the parametric range of the current vademecum.

4.2 Steady-state formulations

In this section the classic thermal and mechanical steady-state formulations for welding are briefly reviewed. We focus on the formulations that have been used in the numerical example of Section 4.3, although other steady-state formulations (Shanghvi and Michaleris, 2002) can be found in related literature.

4.2.1 Thermal and metallurgical formulation

The heat conduction equation in an Eulerian reference frame reads,

$$\rho c \mathbf{v} \cdot \nabla T - \nabla \cdot (k \nabla T) = \dot{q},$$

where c is the heat capacity, k is the thermal conductivity, \mathbf{v} is the velocity vector of the mass flow with respect to the co-moving coordinate system ($-\mathbf{v}$ is the velocity of the heat source) and \dot{q} is the heat generation per unit volume. The stress power is usually neglected in practice, decoupling thermal and mechanical problems.

Microstructure evolution is associated with a material point. In a Lagrangian formulation, Gauss points are material points and hence one simply solves the equations for microstructure evolution as a function of temperature. However, in a steady-state formulation, Gauss points are spatial points and not material points. Thus, because the velocity field is constant, one must compute the streamlines to

capture the thermal cycle of each material particle. This methodology needs a special data structure to identify for each Gauss point $n + 1$ its precedent, not necessary consecutive, integration point (spatial point) n in the streamline (see Fig. 4.3).

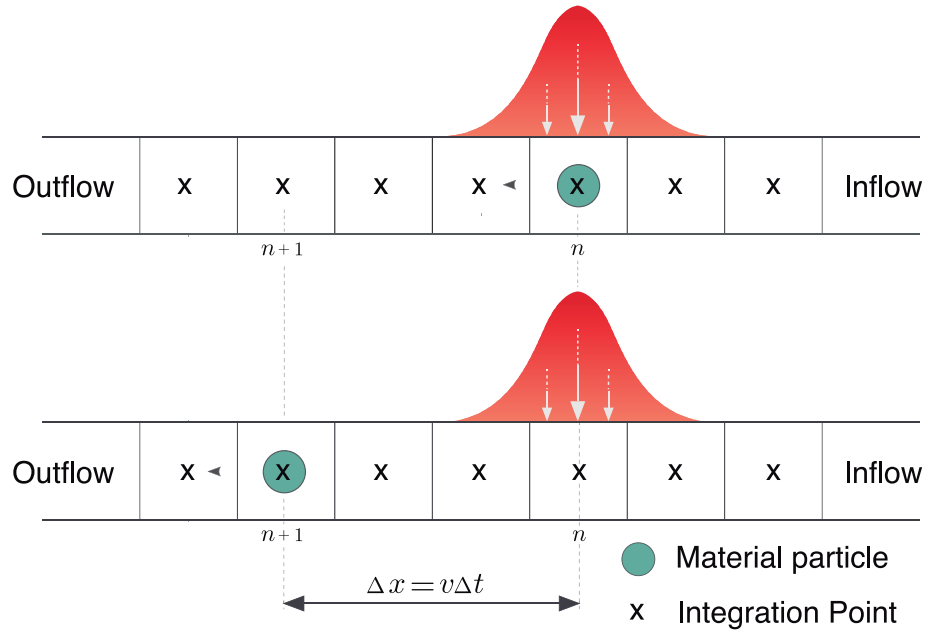


Figure 4.3: Relationship between material and integration points

It should be noted that thermal and metallurgical calculations are fully coupled: at each temperature, phase proportions are calculated.

4.2.2 Mechanical formulation

Taking into account that we are working with an Eulerian reference system, the temporal derivative of any tensorial magnitude \mathbf{F} attached to the material points reads:

$$\dot{\mathbf{F}} = \frac{\partial \mathbf{F}}{\partial t}(\mathbf{x}, t) - \nabla_{\mathbf{x}} \mathbf{F} \cdot \mathbf{v}(\mathbf{x}, t).$$

Since inertial terms are neglected, the equilibrium equation does not change with respect to a Lagrangian formulation,

$$\nabla \cdot \boldsymbol{\sigma}(\mathbf{x}, t) + \mathbf{f}(\mathbf{x}, t) = 0.$$

Considering classical small strain plasticity (Simo and Hughes, 2006), an additive decomposition of strains is introduced,

$$\boldsymbol{\varepsilon} = \boldsymbol{\varepsilon}^e + \boldsymbol{\varepsilon}^p,$$

and considering the thermal dilatation, the constitutive law reads,

$$\boldsymbol{\sigma}(\mathbf{x}, t) = \mathbf{D} : [\boldsymbol{\varepsilon}(\mathbf{x}, t) - \boldsymbol{\varepsilon}^p(\mathbf{x}, t) - \alpha(T(\mathbf{x}, t) - T_0(\mathbf{x}))\mathbf{I}] + \boldsymbol{\sigma}_0(\mathbf{x}).$$

Compatibility equation,

$$\boldsymbol{\varepsilon}(\mathbf{x}, t) = \frac{1}{2} [\nabla \mathbf{u}(\mathbf{x}, t) + \nabla^t \mathbf{u}(\mathbf{x}, t)]$$

also remains the same with regard to a material reference system.

The plastic flow rule in the Eulerian reference system reads,

$$\frac{\partial \boldsymbol{\varepsilon}^p}{\partial t}(\mathbf{x}, t) - \nabla \boldsymbol{\varepsilon}^p(\mathbf{x}, t) \cdot \mathbf{v}(\mathbf{x}, t) = \lambda \frac{\partial f}{\partial \boldsymbol{\sigma}}(\mathbf{x}, t).$$

Analogously, the hardening law in this reference system is

$$\frac{\partial \alpha_k}{\partial t}(\mathbf{x}, t) - \nabla \alpha_k(\mathbf{x}, t) \cdot \mathbf{v}(\mathbf{x}, t) = \lambda \frac{\partial f}{\partial \mathbf{A}_k}(\mathbf{x}, t).$$

An associative flow rule has been considered, since the yield function, f , is also the flow potential. The loading/unloading criterion remains identical to the Lagrangian case,

$$\phi \leq 0, \quad \dot{\gamma} \geq 0, \quad \dot{\gamma} \phi = 0,$$

and appropriate boundary conditions must be introduced into the Ω spatial domain.

For the temporal discretization, an explicit Euler scheme is used. As an example, the discretized flow plastic rule reads,

$$\frac{\boldsymbol{\varepsilon}^p(\mathbf{x}, t + \Delta t) - \boldsymbol{\varepsilon}^p(\mathbf{x}, t)}{\Delta t} + v \frac{\boldsymbol{\varepsilon}^p(\mathbf{x}, t) - \boldsymbol{\varepsilon}^p(\mathbf{x} + \Delta x, t)}{\Delta x} = \lambda \frac{\partial f}{\partial \boldsymbol{\sigma}(\mathbf{x}, t + \Delta t)}.$$

Once the temporal and spatial discretization are performed, the iterative resolution only differs from a classic elastoplastic problem in the expression of plastic deformations. In the Eulerian case, a material particle situated in the spatial point $n + 1$ at time $t + 1$ it was situated in the point n at the previous instant, and this fact must be conveniently taken into account. In practice, these spatial points are the Gauss points and then, the precedence relation between them must be known.

For the sake of clarity and without loss of generality, the algorithm of this methodology is presented in Alg. 1 for a thermoelastoplastic problem with a linear kinematic hardening law. It is quite straightforward to include another hardening law, always taking into account that internal variables must be integrated over the streamlines as indicated. In the case of considering a nonlinear plastic law, the calculation of the plastic multiplier can be done by the classical procedures developed in (Simo and Hughes, 2006).

Algorithm 1 Steady-state mechanical algorithm

- 1: Data known at instant t : $\{\boldsymbol{\sigma}_0, \boldsymbol{\varepsilon}_0, \boldsymbol{\varepsilon}_0^p, T_0\}$
 Data known at instant $t + \Delta t$: $\{\Delta T\}$
 Initialization: $\{\Delta \boldsymbol{\sigma}_j, \Delta \boldsymbol{\varepsilon}_j, \Delta \boldsymbol{\varepsilon}_j^p\} = \{\mathbf{0} \quad \mathbf{0} \quad \mathbf{0}\}$
 - 2: Incremental variables at t_j : $\{\Delta \boldsymbol{\sigma}_j, \Delta \boldsymbol{\varepsilon}_j, \Delta \boldsymbol{\varepsilon}_j^p\}$
 - 3: Solving global equilibrium to obtain the elastic predictor: $\Delta \boldsymbol{\varepsilon}_{j+1}$
 - 4: Check plastic admissibility

$$\boldsymbol{\xi}_{j+1}^* = \mathbf{s}_0 - H \boldsymbol{\varepsilon}_0^p + 2\mu \Delta \boldsymbol{\varepsilon}_{j+1} + (2\mu + H) \frac{v \Delta t}{\Delta x} (\boldsymbol{\varepsilon}_0^p - \boldsymbol{\varepsilon}_0^p(n))$$
 - 5: **if** $\|\boldsymbol{\xi}_{j+1}^*\| \leq k$, **then**
 Process is elastic: $\boldsymbol{\varepsilon}_{j+1}^p = \boldsymbol{\varepsilon}_0^p - \frac{v \Delta t}{\Delta x} (\boldsymbol{\varepsilon}_0^p - \boldsymbol{\varepsilon}_0^p(n))$
 - 6: **else**
 Process is plastic: $\boldsymbol{\varepsilon}_{j+1}^p = \boldsymbol{\varepsilon}_0^p - \frac{v \Delta t}{\Delta x} (\boldsymbol{\varepsilon}_0^p - \boldsymbol{\varepsilon}_0^p(n)) + \frac{1}{2\mu + H} \left(1 - \frac{k}{\|\boldsymbol{\xi}_{j+1}^*\|}\right) \boldsymbol{\xi}_{j+1}^*$
 - 7: **end if**
 - 8: $\boldsymbol{\sigma}_{j+1} = \boldsymbol{\sigma}_0 + \mathbf{D} : \left[\left(\Delta \boldsymbol{\varepsilon}_{j+1} - \Delta \boldsymbol{\varepsilon}_{j+1}^p \right) - \alpha \Delta T \mathbf{I} \right]$
 - 9: **if** $\|\boldsymbol{\sigma}_{j+1} - \boldsymbol{\sigma}_j\| \leq \text{Tol}$, **then**
 Go to 1
 - 10: **else**
 Go to 2
 - 11: **end if**
-

4.3 Numerical example

In this section several computational vademecums for the welding of a steel T-beam are presented. The example is realistic and the black-box solver was Sysweld, one of the most used welding software in industry.

These vademecums (thermal, mechanical and metallurgical), would be useful for the three purposes introduced above: simulating an almost steady welding condition, predesign analysis and source fitting.

We illustrate this methodology selecting three parameters associated to the heat source (a Goldak ellipsoid): The energy per unit length, $E_p \in [150, 250]J/mm$, the source velocity, $V \in [5, 15]mm/s$ and the total length of the ellipsoid, $A = c_1 + c_2$, with $A \in [2, 6]mm$.

The geometry of the steel T-beam is shown in Fig. 4.4. The material is a Manganese Carbon Steel S355J2G3 and its properties are extracted from the proprietary Sysweld database. These properties are temperature-dependent, including the hardening law. For the thermal problem radiation and convective boundary conditions were introduced. The radiation coefficient varies with temperature while the convection coefficient $h = 25W/m^2/K$ was fixed. A constant temperature of $20^\circ C$ is imposed at the entrance nodes. For the mechanical problem, spring boundary conditions in wing extremities of the beam have been imposed (red arrows in Fig. 4.4) with $K = 500N/mm$, simulating the typical weld fixture clamps used in these processes.

To obtain the vademecums, 297 snapshots were calculated corresponding to the first four levels of the SSL method elaborated in Section 1.1.4. The estimated relative error was less than 2% for the thermal abacus, and less than 5% for the mechanic and metallurgical ones. The solution, can be re-compacted by the PGD, obtaining a separated representation solution of only 15 modes that preserves the previous relative error,

$$u \approx \sum_{i=1}^{15} \psi_s^i(\mathbf{x}) \psi_{E_p}^i(E_p) \psi_V^i(V) \psi_A^i(A),$$

where u represent any variable of interest (a computational vademecum is con-

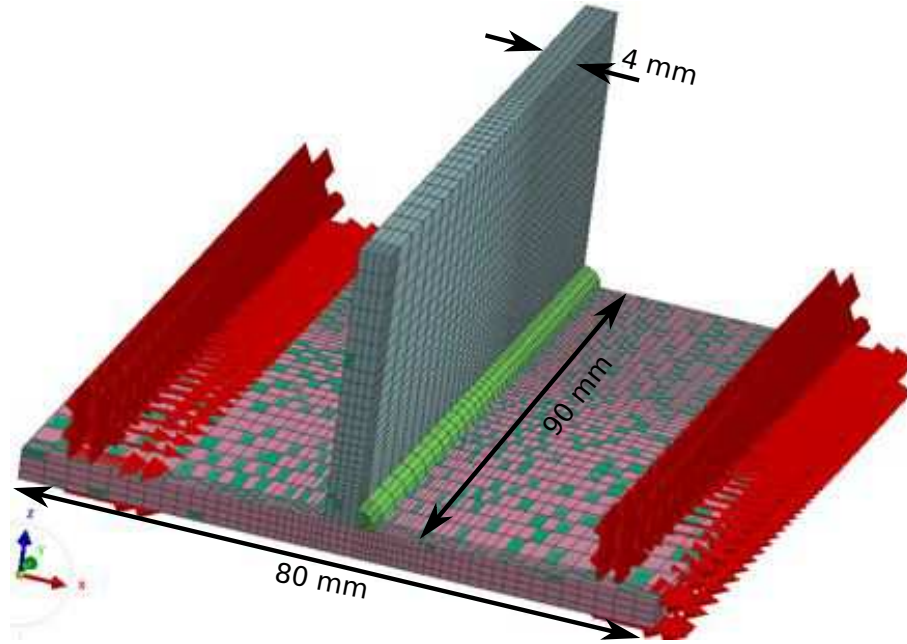


Figure 4.4: Fixed displacements in the T beam

structured for each variable). In Fig. 4.5 and Fig. 4.6 the first two spatial and parametric modes are shown.

Thanks to the *pxdmf* format and its ParaView plugin (Bordeu et al., 2013), these vademecums can be easily visualized and manipulated. Fig. 4.7 shows a screenshot of the thermal vademecum for the parameter values $E_p = 200$, $V = 11.124$ and $A = 3.769$ (shown in the picture). The updating of these parameters can be performed continuously using the sliders shown in Fig. 4.8.

This vademecum can be used to perform the source fitting, as shown in Fig. 4.9, where it can be observed, by an orthogonal cut, if the selected parametric values provide the desired penetration. Likewise, optimization analysis can be envisioned by representing the sensitivity of one quantity of interest with respect the variations of the parameters. For example, one can visualize the sensitivity of the thermal field with respect to the parameter A ($\partial T/\partial A$), as depicted in Fig. 4.10.

The mechanical and metallurgical vademecums, which may be of great interest for pre-design analysis, are shown in Fig. 4.11 and Fig. 4.12 respectively. From among all the possible variables to be shown of the mechanical problem, the equiv-

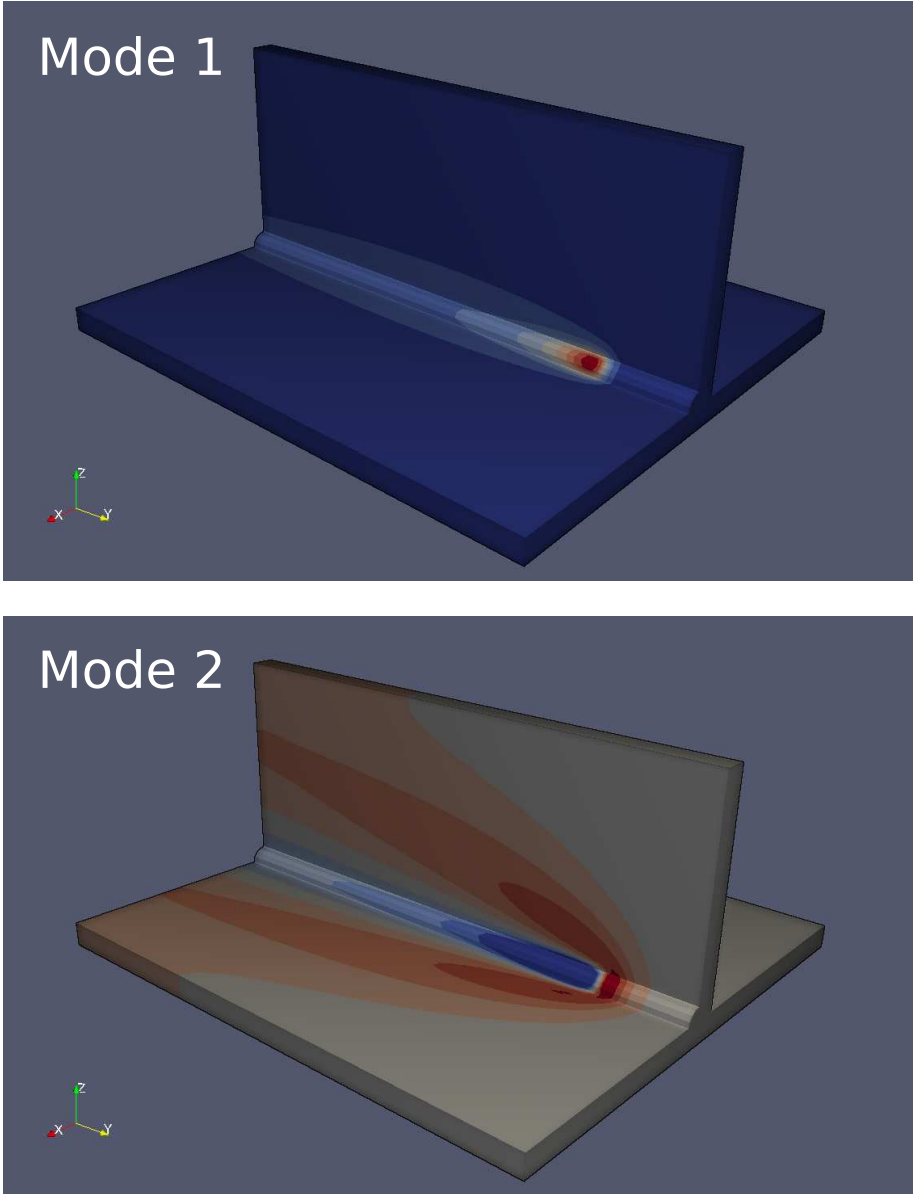


Figure 4.5: First two modes of spatial dimension

4.3. Numerical example

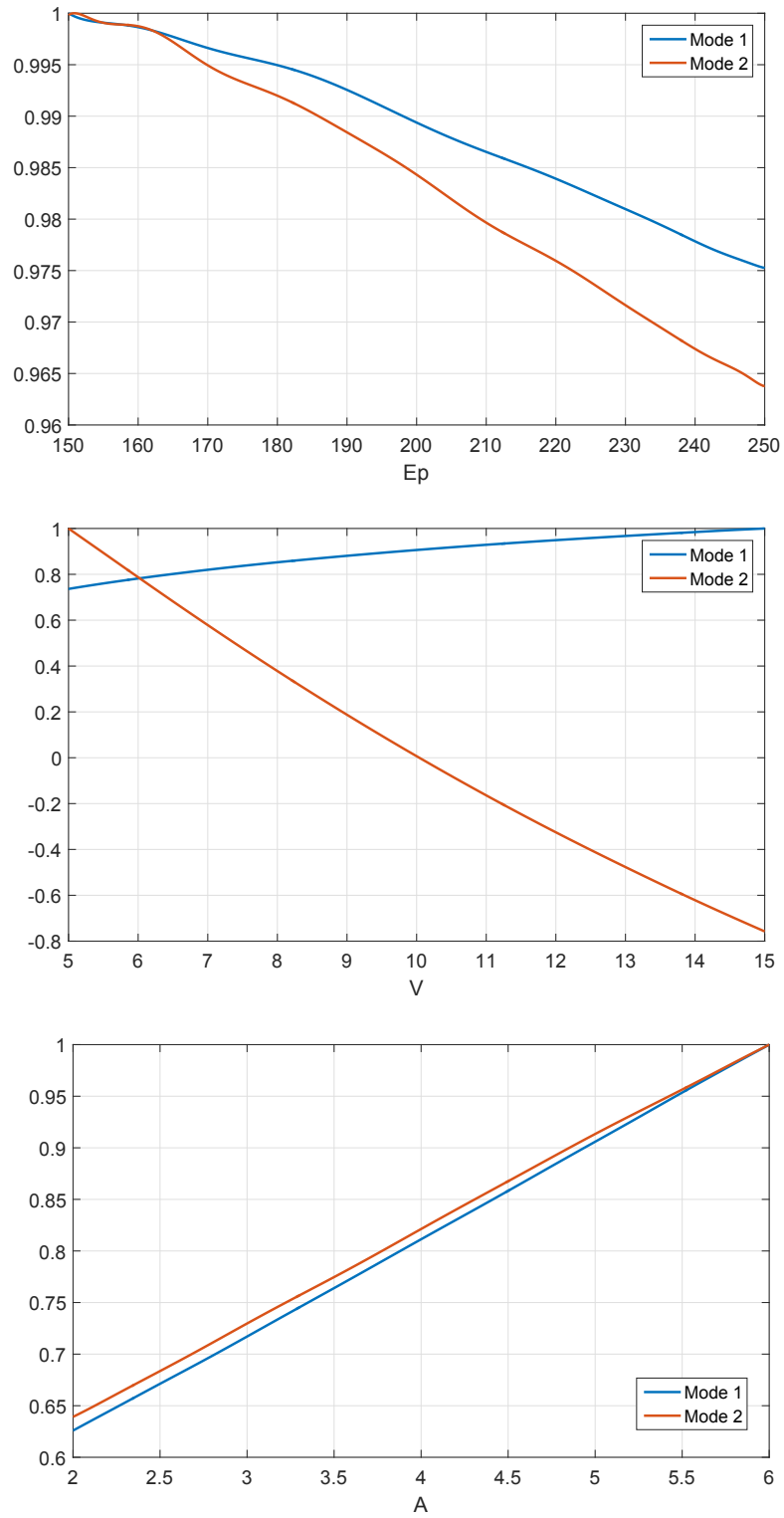


Figure 4.6: First two modes of each parametric dimension
97

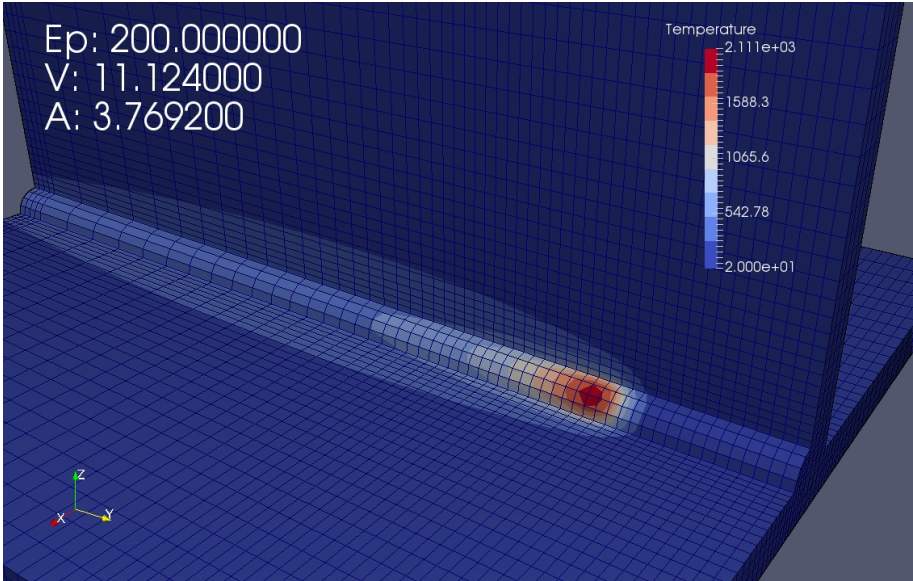


Figure 4.7: Thermal vademecum

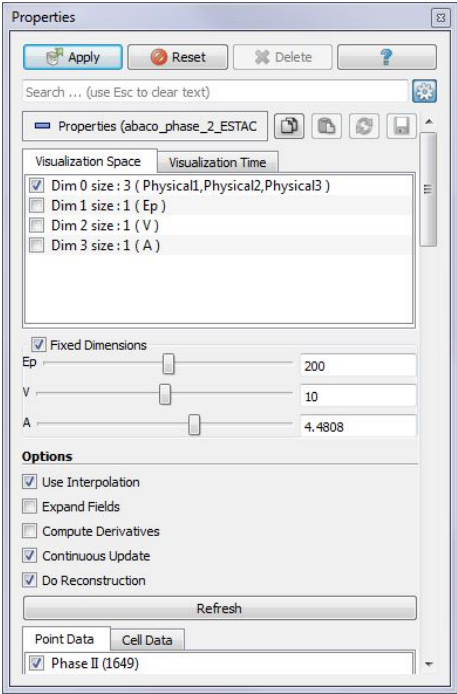


Figure 4.8: Parametric sliders

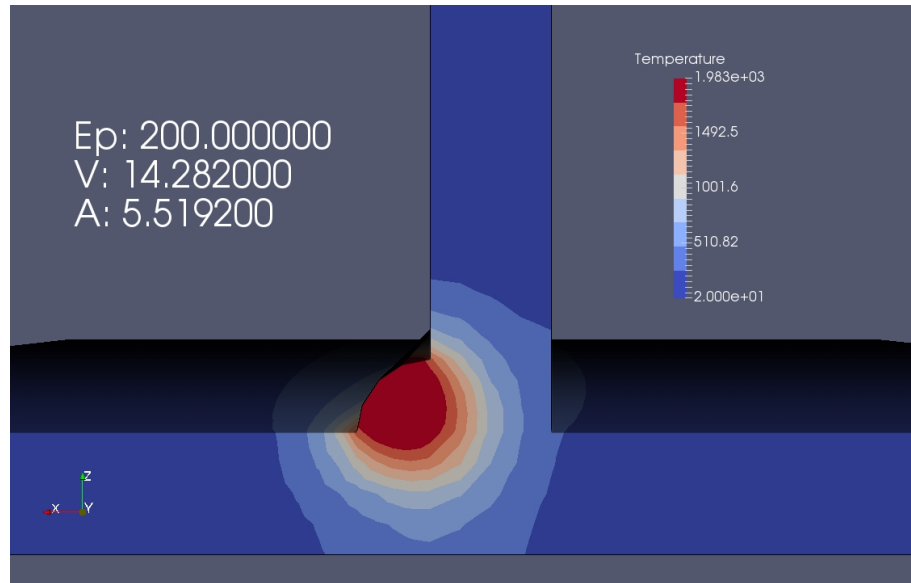


Figure 4.9: Orthogonal cut of thermal vademecum for source fitting

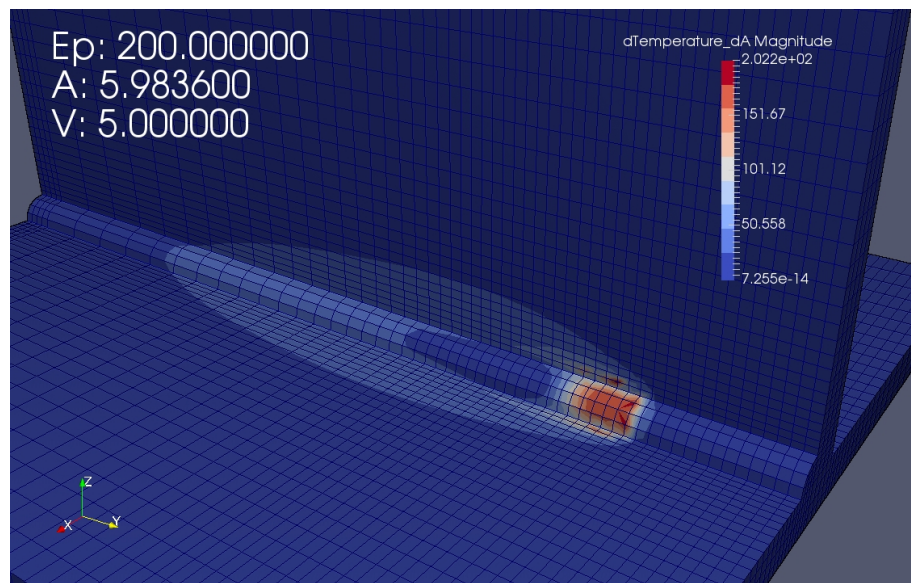


Figure 4.10: Sensitivity of temperature with respect A

alent plastic deformations generated by the welding process are shown in Fig. 4.11. In order to show the feasibility of the construction of metallurgical vademecum, the volumetric ratio of phase II (Bainite) after the welding operation is shown in Fig. 4.12. Both vademecums can be updated continuously using the sliders shown in Fig. 4.8.

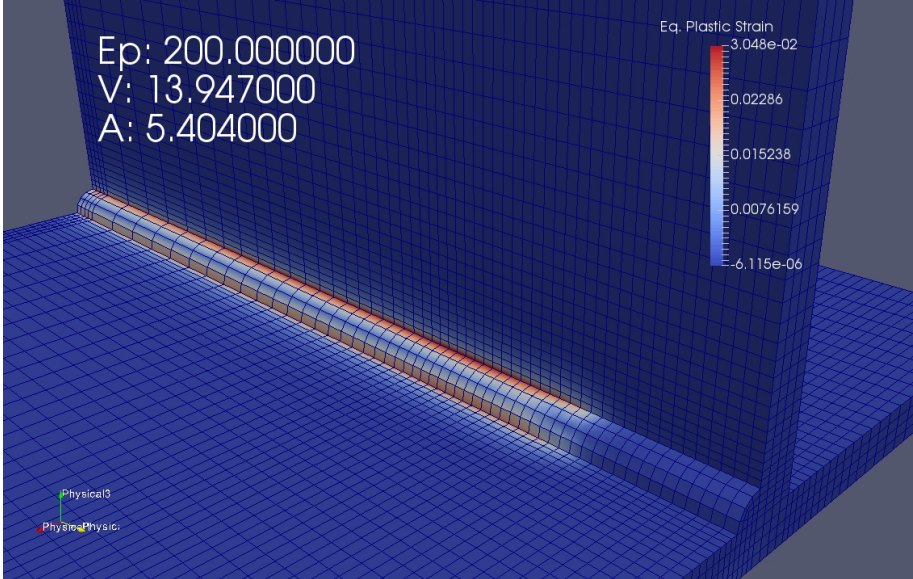


Figure 4.11: Equivalent plastic strains vademecum

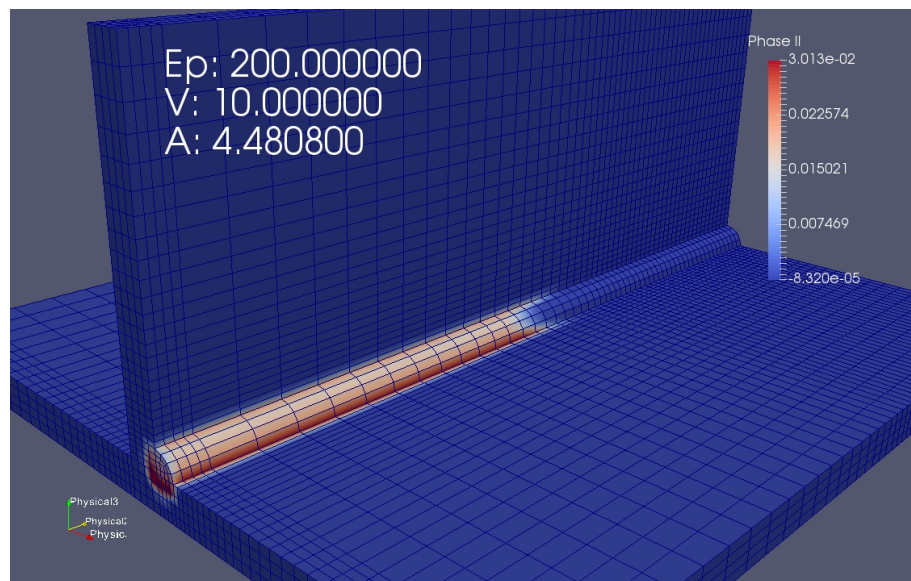


Figure 4.12: Proportion of phase II (Bainite) vademecum

Chapter 5

PGD solver for thermomechanical models defined in plate domains: application to FSW

In this chapter, a new efficient updated Lagrangian strategy for numerical simulations of material forming processes is presented and illustrated with the simplified simulation of a non-conventional welding process: the Friction Stir Welding (FSW). The basic ingredient is the tensorial decomposition of the velocity field into a finite sum of in-plane and an out-of-plane components that leads to an equivalent computational complexity similar to a set of two-dimensional problems. This is efficiently achieved by using the Proper Generalized Decomposition (PGD), which is here employed as a solver as it was introduced in Section 1.1.3.2. The resulting strategy is of general purpose, although it is especially well suited for addressing thermomechanical models defined in plate or shell (in general, parallelepipedic) domains, such as the case in FSW.

Contents

5.1	Introduction	105
5.2	Proposed strategy	107

- 5.2.1 The in-plane/out-of-plane decomposition in an updated Lagrangian framework 109
- 5.2.2 FE-SCNI 112
- 5.3 Validation of the strategy 114**
- 5.3.1 Revisiting PGD through a Poisson’s problem 114
- 5.3.2 Unsteady convection-diffusion equation 115
- 5.4 FSW-like kinematics 120**

5.1 Introduction

Numerical simulation of material forming processes is a fundamental tool in industry but it continues being a very challenging task. These simulations are specially complex due to the following:

- The multiphysic nature of the problem that leads to coupled thermomechanical problems with non-trivial boundary conditions.
- The presence of large deformations and strains.
- The emergence of voids and flaws.
- The presence of evolving free surfaces and fixed or moving interfaces.
- The need of knowledge of the thermomechanical history of each material particle to evaluate properties depending on each thermomechanical history.

In general, three numerical simulation frameworks can be found in literature to simulate thermomechanical processes. Choosing a particular one depends on the specific application. Briefly, we can summarize the following frameworks:

- Eulerian. The discretization mesh is fixed. This means that the mesh does not evolve in time. In practice, with this approach, no mesh distortion occurs. This is, in principle, the easiest approach to simulate fluid-like materials with no free boundaries.

Unfortunately, the material derivative in a fixed reference frame will contain a convective term. This convective term, when it dominates the problem, leads to numerical instabilities and the problem should be stabilized (Donea and Huerta, 2003). Additionally, the path and thermomechanical history of the material particles should be reconstructed *a posteriori*, involving numerical inaccuracies. Besides, this reconstruction is frequently performed since the physics of the problem depends on the material distribution (Dialami et al., 2013). Finally, the treatment of both free surfaces and evolving boundary conditions is a tricky issue within the Eulerian framework.

- Lagrangian. Discretization nodes are attached to material particles. The mesh evolves in time following material motion, obtaining their thermomechanical history in a direct manner. Free surfaces are easily tracked and boundary conditions can be easily imposed (Martínez et al., 2004; Alfaro et al., 2006b,c,a). However, this approach leads to distorted meshes when large deformations occur, and therefore, a frequent remeshing is needed. 3D-remeshing could be very expensive in practice, constituting for some applications a true simulation bottleneck. In addition, frequent projections of fields between old and new meshes are required, introducing numerical diffusion.
- Arbitrary Lagrangian-Eulerian (ALE). This framework was developed in order to avoid the main issues of the former approaches while preserving their main advantages. Discretization nodes are attached neither to the space nor to material points. The mesh moves in a prescribed way to avoid an excessive distortion, alleviating remeshing procedures.

However, convective terms associated with the relative velocity between the mesh and the material remain in the formulation, implying again numerical difficulties. ALE-based methods can be very expensive computational-wise, and the field projection between meshes is not completely avoided. Moreover, they require certain “know-how”: the mesh velocity depends on specific application and its determination is not a trivial task. In any case, computational codes based on ALE approaches are successfully employed for numerical simulation of material forming processes such as FSW (Feulvarch et al., 2013; Guerdoux and Fourment, 2009).

The choice of one or another approach will depend on specific application. A deeper analysis of these frameworks can be found in (Donea et al., 2004). For FSW, hybrid strategies combining different frameworks in the different regions (ALE around the pin, Lagrangian or Eulerian faraway) show accurate results (Feulvarch et al., 2013) .

Updated-Lagrangian frameworks are very appealing since material particles can be tracked without any approximation and without postprocessing. However, its

computational cost remains sometimes too high, basically due to reiterative remeshings. Indeed, the main goal of this chapter is to explore a new strategy to enhance updated Lagrangian simulations reducing substantially its computational cost. To that end, in Section 5.2 the main ingredients of the proposed technique are introduced, namely the in-plane-out-of-plane decomposition based on PGD (Chinesta et al., 2013a). In the same section, the use of efficient stabilized nodal conforming integration (Yoo et al., 2004) to allow for minimal loss of accuracy despite mesh distortion (Cueto and Chinesta, 2015; Quak et al., 2011) is elaborated. In Section 5.3, the proposed strategy is validated, while in Section 5.4 the possibility of employing the proposed technique for FSW simulation is envisioned.

5.2 Proposed strategy

The proposed strategy can be seen as a natural extension of the in-plane/out-of-plane decomposition based on the Proper Generalized Decomposition (PGD) in an updated Lagrangian framework. The idea of decomposing three-dimensional (here, velocity) fields into a sequence of two-dimensional and one-dimensional fields was initially developed to analyze plates by Bognet *et al.* (Bognet et al., 2012a) and has been introduced in Chapter 1.

The main idea of the approach here developed is to take advantage of updated Lagrangian methods, very convenient for material forming simulations, in which the thermomechanical history is of major interest, but obtaining a significant reduction of its computational complexity using the in-plane/out-of-plane PGD-based decomposition. The material particles' position and all the variables attached to them are projected onto a plane and onto the thickness axis (step1). Using these nodal projections two functional spaces are constructed, 2D and 1D respectively. The intensive variables are projected on these spaces using a PGD approximation, equivalent to a singular value decomposition (SVD) (step 2). Then, the thermomechanical problem is solved as a series of 2D and 1D problems in these spaces thanks to the in-plane/out-of-plane PGD-based formulation (step 3). Once the solution is obtained, the primary variables can be reconstructed in the material particles in the

3D domain (step 4) and their positions updated (step 5). This reconstruction does not involve any interpolation or projection stage, avoiding the numerical diffusion and other numerical difficulties. These steps are repeated until the end of the simulation. In Fig. 5.1, a general scheme of the strategy with its different steps is shown. Note that mechanical and thermal parts of the problem can be solved using spatial decomposition regardless the coupling scheme used.

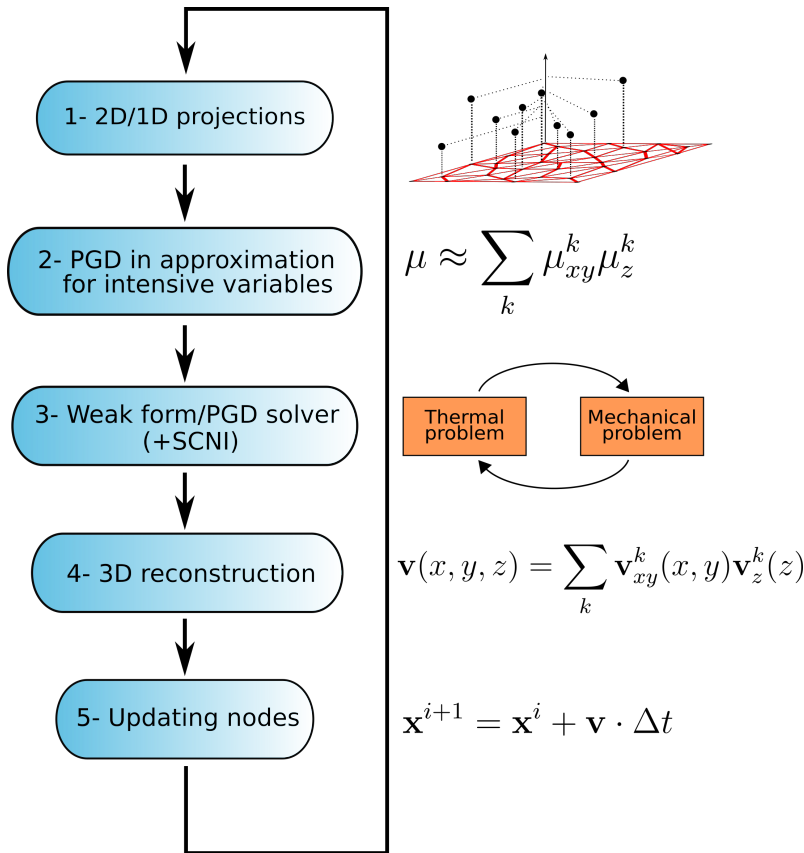


Figure 5.1: General scheme of the proposed strategy

The main ingredients of the proposed strategy are presented in detail below. In Section 5.2.1 the space decomposition in the updated Lagrangian framework is described. A general flow model for material forming processes is presented considering linear and nonlinear behavior laws. In Section 5.2.2, stabilized conforming nodal integration (SCNI) is briefly reviewed, which allow performing accurate integration of the operators even in very distorted meshes (Yoo et al., 2004; Quak et al., 2011).

5.2.1 The in-plane/out-of-plane decomposition in an updated Lagrangian framework

Let us describe this updated Lagrangian strategy through a generic viscoplastic flow model (Oh and Altan, 1989) in a domain Ω .

The balance of momentum and mass equations without inertia and the assumed incompressibility of the flow read:

$$\nabla \cdot \boldsymbol{\sigma} = \mathbf{0}, \quad \nabla \cdot \mathbf{v} = 0 \quad \text{in } \Omega. \quad (5.1)$$

To calculate the temperature field, the viscoplastic flow model is coupled with the heat transfer equation:

$$\nabla \cdot (k \nabla T) + \dot{r} - (\rho c_p \dot{T}) = 0 \quad \text{in } \Omega. \quad (5.2)$$

The rate of heat generation due to plastic deformation is obtained from

$$\dot{r} = \beta \boldsymbol{\sigma} : \mathbf{d},$$

where β is the fraction of mechanical energy transformed to heat and \mathbf{d} the strain rate tensor.

Together with these equations, a constitutive law and the appropriate boundary conditions should be considered. The mechanical and thermal problem will be solved iteratively.

Considering a plate domain $\Omega = \Xi \times \mathcal{I}$ with $(x, y) \in \Xi$ and $z \in \mathcal{I}$, we assume the separated approximation of the velocity field

$$\mathbf{v}(x, y, z) = \begin{pmatrix} u(x, y, z) \\ v(x, y, z) \\ w(x, y, z) \end{pmatrix} \approx \sum_{i=1}^N \begin{pmatrix} u_{xy}^i(x, y) \cdot u_z^i(z) \\ v_{xy}^i(x, y) \cdot v_z^i(z) \\ w_{xy}^i(x, y) \cdot w_z^i(z) \end{pmatrix},$$

where $u_{xy}(x, y)$, $v_{xy}(x, y)$ and $w_{xy}(x, y)$ are functions of the in-plane coordinates

whereas $u_z(z)$, $v_z^i(z)$ and $w_z(z)$ are functions involving the thickness coordinate. Similarly, the strain rate tensor can be expressed in a separated form. If viscosity is not constant its separated representation is needed in order to preserve the 2D/1D complexity. This can be performed by invoking again the PGD approximation:

$$\mu(x, y, z) \approx \sum_{k=1}^M \mu_{xy}^k(x, y) \cdot \mu_z^k(z).$$

Two different constitutive laws have been considered. In the linear case the constitutive equation reads:

$$\begin{cases} \nabla p = \mu \nabla \cdot (\nabla \mathbf{v}) \\ \nabla \cdot \mathbf{v} = 0 \end{cases},$$

where p and μ are the pressure and the viscosity of the fluid respectively.

To circumvent the problems related to the development of stable mixed formulations (i.e., approximations verifying the LBB condition) within the separated representation, a penalty formulation is considered that modifies mass balance by introducing a penalty coefficient λ small enough

$$\nabla \cdot \mathbf{v} + \lambda p = 0,$$

or, more explicitly,

$$p = -\frac{1}{\lambda} \left(\frac{\partial u}{\partial x} + \frac{\partial v}{\partial y} + \frac{\partial w}{\partial z} \right) = -\frac{\nabla \cdot \mathbf{v}}{\lambda}.$$

By replacing it into the momentum balance (first equation in (5.1)) we obtain

$$\nabla (\nabla \cdot \mathbf{v}) + \xi \Delta \mathbf{v} = \mathbf{0},$$

with $\xi = \mu\lambda$. After some elementary algebra, it results

$$\left(\begin{array}{c} \frac{\partial^2 u}{\partial x^2} + \frac{\partial}{\partial x} \frac{\partial v}{\partial y} + \frac{\partial}{\partial x} \frac{\partial w}{\partial z} \\ \frac{\partial}{\partial y} \frac{\partial u}{\partial x} + \frac{\partial^2 v}{\partial y^2} + \frac{\partial}{\partial y} \frac{\partial w}{\partial z} \\ \frac{\partial}{\partial z} \frac{\partial u}{\partial x} + \frac{\partial}{\partial z} \frac{\partial v}{\partial y} + \frac{\partial^2 w}{\partial z^2} \end{array} \right) + \xi \left(\begin{array}{c} \frac{\partial^2 u}{\partial x^2} + \frac{\partial^2 u}{\partial y^2} + \frac{\partial^2 u}{\partial z^2} \\ \frac{\partial^2 v}{\partial x^2} + \frac{\partial^2 v}{\partial y^2} + \frac{\partial^2 v}{\partial z^2} \\ \frac{\partial^2 w}{\partial x^2} + \frac{\partial^2 w}{\partial y^2} + \frac{\partial^2 w}{\partial z^2} \end{array} \right) = 0.$$

The *flow model* can readily be extended to power-law fluids:

$$\begin{cases} \nabla p = \nabla \cdot \mathbf{T} \\ \nabla \cdot \mathbf{v} = 0 \end{cases},$$

where the extra-stress tensor \mathbf{T} writes:

$$\mathbf{T} = 2K\bar{d}^{n-1}\mathbf{d}, \quad (5.3)$$

with K and n two rheological parameters and the equivalent strain rate \bar{d} given by:

$$\bar{d} = \sqrt{2(\mathbf{d} : \mathbf{d})},$$

where “ : ” denotes the tensor product twice contracted.

In order to perform the in-plane/out-of-plane decomposition, the system of PDEs defined by Eqs.(5.1)-(5.2) should be written in its variational form. For instance, assuming linear behavior and a penalty formulation, the variational formulation writes:

$$a(\mathbf{w}, \mathbf{v}) + \xi b(\mathbf{w}, \mathbf{v}) = \mathbf{0}, \quad (5.4)$$

with

$$a(\mathbf{w}, \mathbf{v}) = \int_{\Omega} \nabla \cdot \mathbf{w} \nabla \cdot \mathbf{v} \, d\Omega \quad \text{and} \quad b(\mathbf{w}, \mathbf{v}) = \int_{\Omega} \nabla \mathbf{w} : \nabla \mathbf{v} \, d\Omega,$$

where a and b are the bilinear forms related to the incompressibility and viscous terms ; \mathbf{v} and \mathbf{w} are the trial and test functions respectively.

Then, it is assumed that the first $n - 1$ modes of the PGD solution have been previously obtained. To further enrich this solution with another functional product

the following problem needs to be solved:

$$\mathbf{v}(x, y, z) = \begin{pmatrix} u(x, y, z) \\ v(x, y, z) \\ w(x, y, z) \end{pmatrix} \approx \sum_{i=1}^{n-1} \begin{pmatrix} u_{xy}^i(x, y) \cdot u_z^i(z) \\ v_{xy}^i(x, y) \cdot v_z^i(z) \\ w_{xy}^i(x, y) \cdot w_z^i(z) \end{pmatrix} + \mathbf{R}(x, y) \circ \mathbf{S}(z), \quad (5.5)$$

where the second term on the right-hand side represents the enrichment and the symbol ‘ \circ ’ denotes the so-called entry-wise Hadamard or Schur multiplication for vectors.

The test function is defined by:

$$\mathbf{w} = \mathbf{R}^*(x, y) \circ \mathbf{S}(z) + \mathbf{R}(x, y) \circ \mathbf{S}^*(z). \quad (5.6)$$

Introducing Eqs. (5.5) and (5.6) into Eq. (5.4), a nonlinear problem results due the presence of the products of the unknown PGD modes. As we have seen in Chapter 1, this is the case even when the original problem is linear. To solve this nonlinearity, the already explained alternated direction fixed-point algorithm is used.

5.2.2 FE-SCNI

In the proposed strategy, after nodal position updating, their orthogonal projections into a 2D domain defined by the in-plane coordinates and the 1D projection onto the domain thickness, constitute the nodal position of the interpolant spaces used for the PGD solution. An additional problem is faced, since the 2D mesh will eventually be very distorted, and the numerical integration of the discrete operators may be not accurate enough.

Chen *et al.* (Yoo et al., 2004) introduced the SCNI technique to perform an accurate nodal integration in meshless methods. Indeed, it has been observed that SCNI can be incorporated into traditional FE formulations to produce a very robust method to deal with highly distorted meshes with almost no loss of accuracy (Cueto and Chinesta, 2015).

The SCNI is based on the assumed strain method, in which a modified gradient is introduced at the integration point (node):

$$\tilde{\nabla} \mathbf{v}(\mathbf{x}_i) = \frac{1}{A_i} \int_{\Omega_i} \nabla \mathbf{v}(\mathbf{x}) \, d\Omega,$$

where \mathbf{x}_i are the coordinates of node n_i and A_i the area defined by the cell Ω_i . The set of cells defines a partition of the 2D domain. Typically a Voronoi tessellation is used (see Fig. 5.2), although any type of non-overlapping tiling can be used.

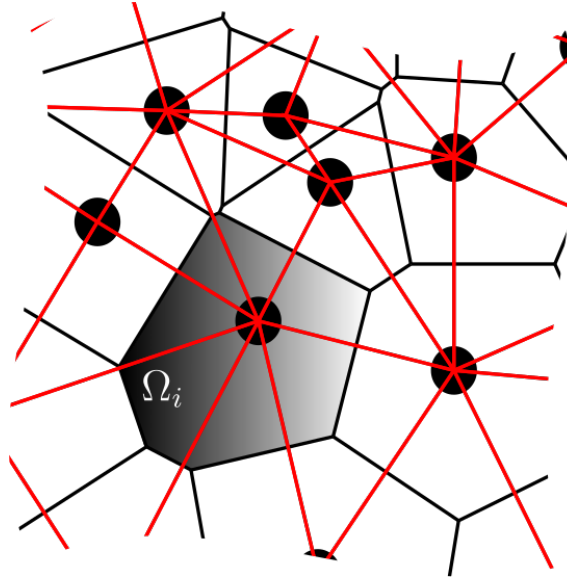


Figure 5.2: Voronoi tessellation to perform the SCNI

The modified strain rate tensor is given by

$$\tilde{\mathbf{d}}(\mathbf{x}_i) = \frac{1}{A_i} \int_{\Omega_i} \mathbf{d}(\mathbf{x}) \, d\Omega = \frac{1}{A_i} \int_{\Omega_i} \begin{pmatrix} \frac{\partial u}{\partial x} & \frac{1}{2} \left(\frac{\partial u}{\partial y} + \frac{\partial v}{\partial x} \right) & \frac{1}{2} \left(\frac{\partial u}{\partial z} + \frac{\partial w}{\partial x} \right) \\ \frac{1}{2} \left(\frac{\partial u}{\partial y} + \frac{\partial v}{\partial x} \right) & \frac{\partial v}{\partial y} & \frac{1}{2} \left(\frac{\partial v}{\partial z} + \frac{\partial w}{\partial y} \right) \\ \frac{1}{2} \left(\frac{\partial u}{\partial z} + \frac{\partial w}{\partial x} \right) & \frac{1}{2} \left(\frac{\partial v}{\partial z} + \frac{\partial w}{\partial y} \right) & \frac{\partial w}{\partial z} \end{pmatrix} d\Omega.$$

Applying the divergence theorem, it results in:

$$\tilde{\mathbf{d}}(\mathbf{x}_i) = \frac{1}{A_i} \int_{\Gamma_i} \begin{pmatrix} u(\mathbf{x})n_x & \frac{1}{2}(u(\mathbf{x})n_y + v(\mathbf{x})n_x) & \frac{1}{2}(u(\mathbf{x})n_z + w(\mathbf{x})n_x) \\ \frac{1}{2}(u(\mathbf{x})n_y + v(\mathbf{x})n_x) & v(\mathbf{x})n_y & \frac{1}{2}(v(\mathbf{x})n_z + w(\mathbf{x})n_y) \\ \frac{1}{2}(u(\mathbf{x})n_z + w(\mathbf{x})n_x) & \frac{1}{2}(v(\mathbf{x})n_z + w(\mathbf{x})n_y) & w(\mathbf{x})n_z \end{pmatrix} d\Gamma.$$

Thus, in order to compute the strain rate at each node considered to integrate the weak form it suffices to approximate the different components of the velocity field in each element by using standard shape functions such as piecewise linear interpolants, and then evaluate the integral on the boundary of the cell associated to each node. When Voronoi cells are considered, the numerical quadrature can be calculated evaluating the boundary integral on each face of the polyhedral cell.

5.3 Validation of the strategy

5.3.1 Revisiting PGD through a Poisson's problem

This first example analyzes the PGD acting as a differential solver in separated dimensions with a 2D Poisson's problem:

$$\left\{ \begin{array}{ll} \Delta u = f & \text{in } \Omega = (0, 2) \times (0, 1) \\ u = 0 & \text{on } x = 0 \\ u = 0 & \text{on } y = 0 \\ u = -y(y - 1) & \text{on } x = 2 \\ \frac{\partial u}{\partial y} = g(x) & \text{on } y = 1, \end{array} \right.$$

where the source term has been considered as

$$f(x, y) = -20 \exp((1 - x)^2/0.1) \exp((0.5 - y)^2/0.1).$$

The function associated to natural boundary condition reads

$$g(x) = \begin{cases} 0, & \text{if } x \leq 0.5 \\ 1, & \text{if } x > 0.5. \end{cases}$$

The most typical structure of a PGD approximation to the problem is to look

for a solution of the form:

$$u(x, y) \approx \sum_{i=1}^N F_i(x) \cdot G_i(y).$$

Here, a stopping criterion was set at 10^{-4} as tolerance for the residual. This leads to around 40 PGD functional pairs or “modes”, depending on the number of the 2D points considered. When new points are introduced, the solution becomes richer and more PGD modes are necessary to capture the finest solution features.

In Fig. 5.3 the absolute error (in infinity norm) of the PGD solution is presented. A 2D standard FEM solution in a fine enough mesh was considered as the reference solution. Obviously, the more points are considered in the domain, the more information we get and the less error is obtained. This method is approximately of order one with respect to the number of points used.

Both the reference solution and the reconstructed PGD solution in the points of the 2D domain are presented in Fig. 5.4, where the reference solution is represented as a continuous surface, and the PGD solution as spheres in the introduced points. The PGD solution is in very good agreement with the fully 2D solution while it is computed only with the cost of a set of 1D problems.

5.3.2 Unsteady convection-diffusion equation

In this section, the updated Lagrangian framework is considered and analyzed. For that purpose, the transient rotating pulse (advection-diffusion) example proposed in (Donea and Huerta, 2003) is solved. The problem reads:

$$\begin{cases} u_t + \mathbf{a} \cdot \nabla u - \nabla \cdot (\nu \nabla u) = s & \text{in } \Omega = (0, 1) \times (0, 1) & (5.8a) \\ u = 0 & \text{on } \partial\Omega & (5.8b) \\ u = 0 & \text{at } t = 0 & (5.8c) \end{cases}$$

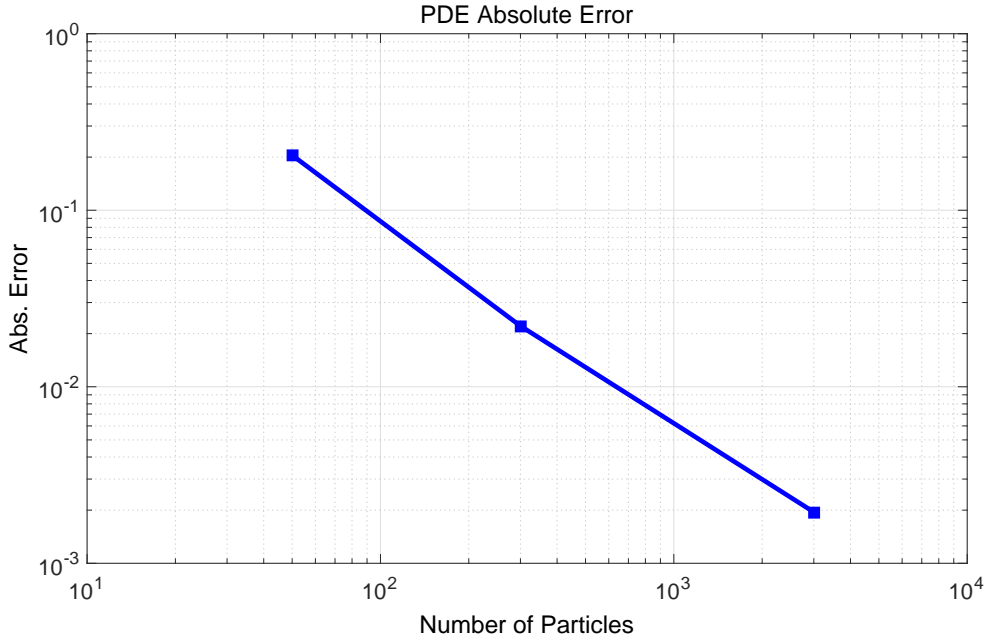


Figure 5.3: PDE absolute error.

with a small diffusion $\nu = 10^{-5}$, $\mathbf{a} = (-y + 0.5, x - 0.5)$ and

$$s = \begin{cases} \cos(\pi/2\sqrt{x_c^2 + y_c^2}), & \text{if } \sqrt{x_c^2 + y_c^2} \leq 1 \\ 0, & \text{otherwise} \end{cases},$$

with $(x_c, y_c) = (x - 0.2, y - 0.2)$.

It is well-known that an Eulerian FEM solution requires stabilization regardless the selected time integration scheme. Here we have used, as a reference solution, a streamline-upwind Petrov-Galerkin (SUPG) discretization in space and an implicit multistage Padé method $R_{2,2}$ as time integration scheme (Donea and Huerta, 2003). The stabilized weak form of the time discretized problem is given by

$$\left(w, \frac{\Delta \mathbf{u}}{\Delta t} \right) - (w, \mathbf{W} \Delta \mathbf{u}_t) + \sum_e (\boldsymbol{\tau} \mathcal{P}(w), \mathcal{R}(\Delta \mathbf{u}))_{\Omega^e} = (w, \mathbf{g} u_t^n),$$

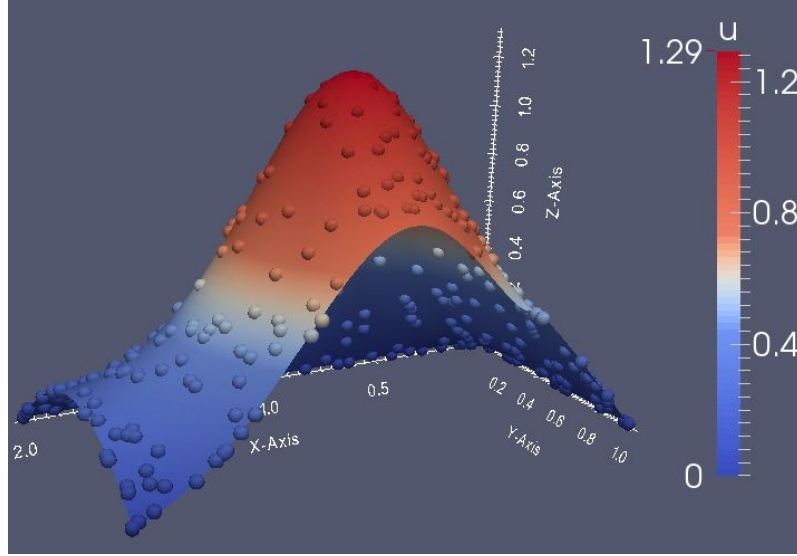


Figure 5.4: Reference solution (continuous) versus PGD solution (spheres)

where

$$\Delta \mathbf{u} = \begin{pmatrix} u^{n+\frac{1}{2}} - u^n \\ u^{n+1} - u^{n+\frac{1}{2}} \end{pmatrix}, \quad \Delta \mathbf{u}_t = \begin{pmatrix} u_t^{n+\frac{1}{2}} - u_t^n \\ u_t^{n+1} - u_t^{n+\frac{1}{2}} \end{pmatrix}.$$

$\Delta \mathbf{u}$ is the primary variable, w is the test function and Δt the chosen time step. The partial time derivatives are obtained from the governing Eq. (5.8a),

$$u_t^n = s^n - \mathcal{L}(u^n)$$

where \mathcal{L} is the associated linear differential operator.

The matrix \mathbf{W} and the vector \mathbf{g} are useful to express the Padé scheme in a compact form and they read:

$$\mathbf{W} = \frac{1}{24} \begin{pmatrix} 7 & -1 \\ 13 & 5 \end{pmatrix}, \quad \mathbf{g} = \frac{1}{2} \begin{pmatrix} 1 \\ 1 \end{pmatrix}.$$

The operator $\mathcal{P}(w)$ characterizes the stabilization technique, in this case a SUPG,

$$\mathcal{P}(w) := \mathbf{W}(\mathbf{a} \cdot \nabla)w.$$

The time-dependent residual \mathcal{R} reads

$$\mathcal{R}(\Delta \mathbf{u}) = \frac{\Delta \mathbf{u}}{\Delta t} - \mathbf{W} \Delta \mathbf{u}_t - \mathbf{g} u_t^n$$

Finally, $\boldsymbol{\tau}$ is the intrinsic time scale matrix which in this example reads:

$$\boldsymbol{\tau} = \frac{h}{2a} \left[\coth(Pe) - \frac{1}{Pe} \right] \mathbf{W}^{-1},$$

where h is the mesh size, a is the convection magnitude and Pe the Péclet number.

It is important to note that, even when using standard SUPG techniques, the solution exhibits oscillations near the boundary. In the updated Lagrangian approach, the convective term does not appear, and therefore stabilization is not necessary since oscillations do not occur. In an updated Lagrangian approach, the problem reads:

$$u_t - \nu \nabla^2 u = s,$$

where u_t represents the material derivative calculated along the flow streamlines related to the velocity field \mathbf{a} .

If an implicit temporal scheme is used, and the increment of u , $\Delta u = u^{n+1} - u^n$, is selected as primary variable, the semi-discretized equation to solve at each time step, reads:

$$\frac{\Delta u}{\Delta t} - \nu \nabla^2 (\Delta u) = s^{n+1} + \nu \nabla^2 u^n.$$

To solve this problem using the PGD, the trial and test functions are constructed as in the previous example, as

$$\Delta u(x, y) \approx \sum_{i=1}^{n-1} \Delta u_x^i(x) \cdot \Delta u_y^i(y) + R(x) \cdot S(y)$$

and

$$w = R^*(x) \cdot S(y) + R(x) \cdot S^*(y).$$

respectively. Moreover, in the time step $n + 1$ the known fields u^n and s^{n+1} should be expressed in a separated form by invoking a standard SVD.

This problem has been solved by the proposed strategy for different times in $[0, \pi]$ and compared with a reference FEM solution with no oscillations thanks to a higher diffusion coefficient. In Fig. 5.5 relative errors in L^2 norm for a value of the diffusion coefficient of 10^{-3} are presented. It can be seen that even with a not too high number of points (about 1000), the errors are small, between 2% and 10% throughout the complete simulation. These values are reasonable in an industrial context.

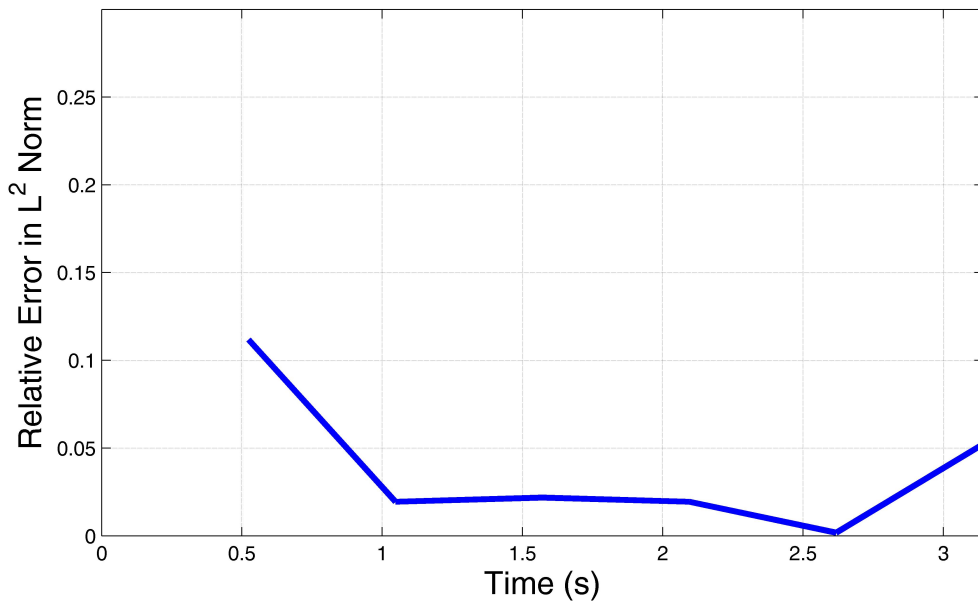


Figure 5.5: Relative errors in L^2 norm

It is also remarkable that the method has a greater robustness in problems where convection is dominant. Indeed, if the diffusion coefficient is set to 10^{-5} , the FEM solution presents oscillations near the boundary, regardless of the time integration scheme used (Donea and Huerta, 2003). However, it can be seen in Fig. 5.6 that the proposed strategy provides a solution which does not present these oscillations on the border. The SUPG solution is presented as a continuous surface while the PGD solution is presented with spheres in the material points positions. Moreover, thanks to the separation of variables, the problem solution exhibits roughly a 1D computational cost.

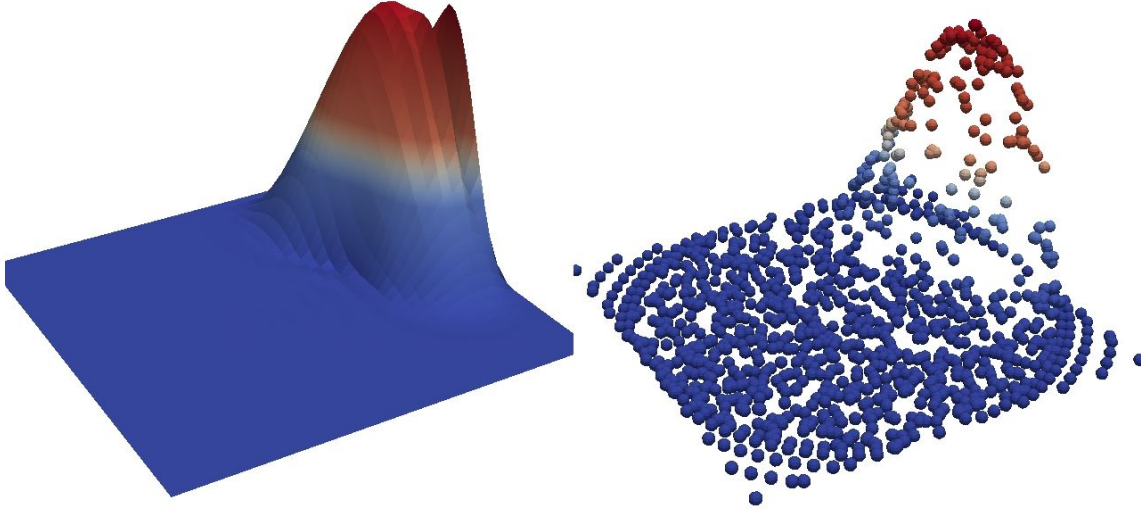


Figure 5.6: FEM solution versus PGD solution in a convection-dominated problem

5.4 FSW-like kinematics

FSW is a solid state welding technique which since its invention in 1991 is of great interest to the industry (Mishra and Ma, 2005). The FSW welding process is conceptually simple. A non-consumable rotating tool with a specially designed pin and shoulder is inserted into the abutting edges of sheets or plates to be joined and traversed along the line of joint. The tool heats the workpiece and its stir movement produces the joint.

In this work, a simplified model of the kinematics of this process has been tested with the proposed strategy. The viscous flow expressed in Eq. (5.1) has been solved considering a nonlinear behavior law (a Power Law, Eq. (5.3)). For the sake of simplicity and without loss of generality, the thermal problem has been omitted, considering an isothermal process without mechanical dissipation. The boundary conditions consist of an imposed velocity (\mathbf{V}_{adv}) far away from the tool ($\partial\Omega$), and an imposed tangential velocity (\mathbf{V}_{tg}) on the tool surface ($\partial\Lambda$). In Fig. 5.7 a scheme

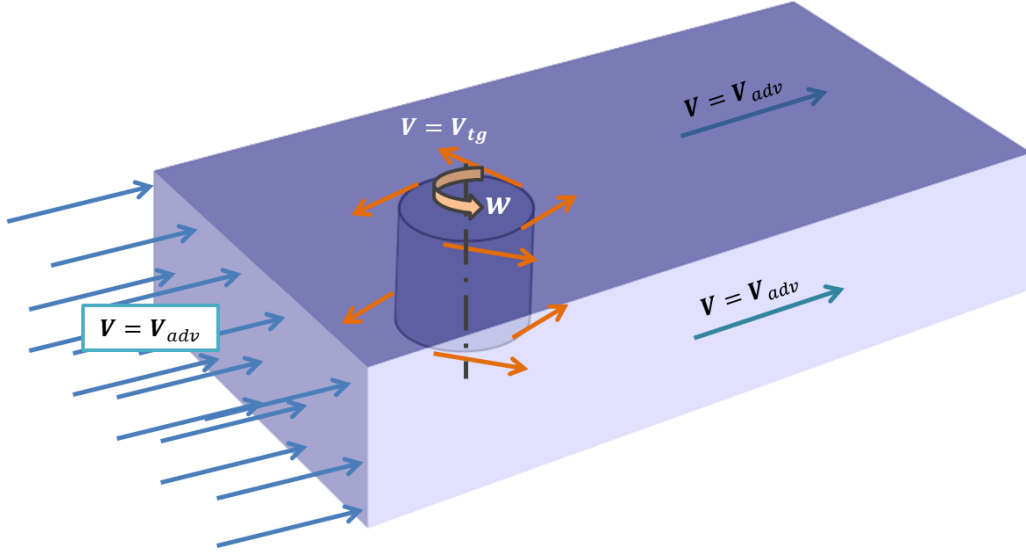


Figure 5.7: FSW kinematics model

of the problem is depicted. Thus, the problem reads,

$$\begin{cases} \nabla \cdot \boldsymbol{\sigma} = \mathbf{0} & \text{in } \Omega \\ \nabla \cdot \mathbf{v} = 0 & \text{in } \Omega \\ \mathbf{v} = \mathbf{V}_{adv} & \text{on } \partial\Omega \\ \mathbf{v} = \mathbf{V}_{tg} & \text{on } \partial\Lambda, \end{cases}$$

Even when neither the real technological parameters (constitutive model, friction law, etc.) nor the actual geometry of the tools are implemented, the feasibility of the numerical algorithm is proved: a 3D flow model can be solved in an updated Lagrangian framework with a computational cost characteristic of 2D simulations. Moreover, the thermomechanical history (mechanical history in this case) of the material particles is computed directly from the simulation. For instance, we can study the evolution of the viscosity of a material particle during the process. In Fig. 5.8, we can observe how the viscosity of the material particle decreases when it approaches the tool, where the strain rates are high due to the rotation of the pin.

The streamlines are not computed *a posteriori*: they are simply the different positions of the material particles obtained during the simulation. In Fig. 5.9, the paths of some of these material points are shown. Moreover, it is well known from literature (Mishra and Ma, 2005) that the material flow plays a fundamental role in the quality of the welding, and some typical defects such as the tunnel effect can be predicted with its analysis. This method provides a direct way to perform this study, indeed the material particles of both welded plates are easily tracked just attaching an scalar value to them. In Fig. 5.10, this application is shown using two colors to represent the two different plates to joint. The relative position between the particles of the two plates behind the tool could indicate, using the appropriate techniques, the existence of defects.

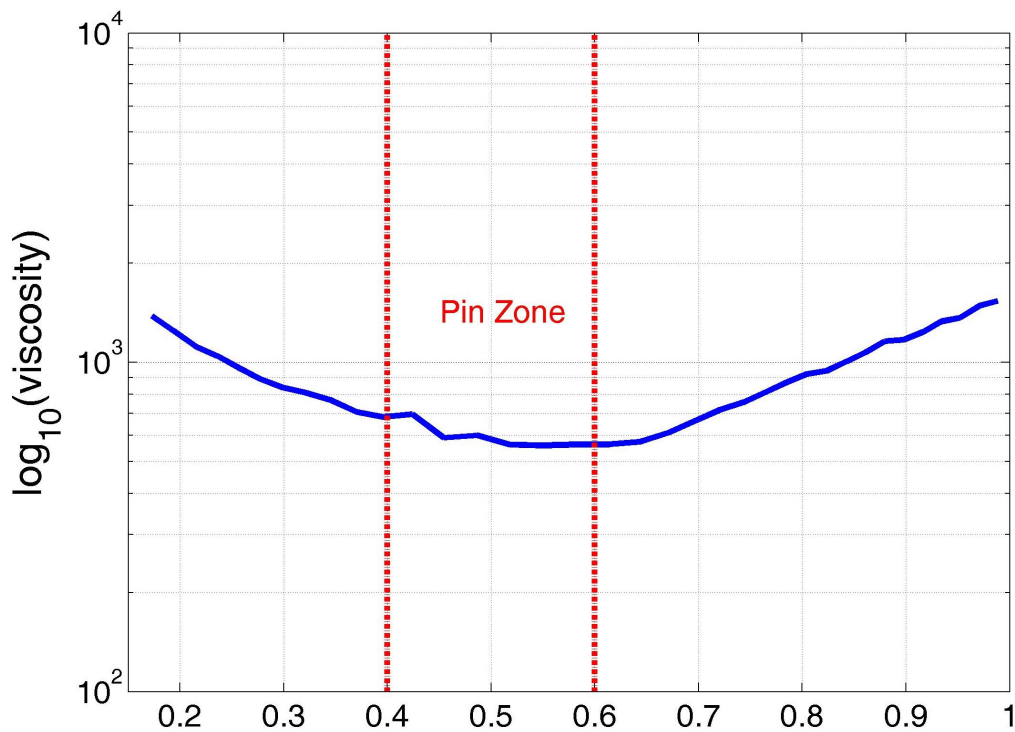


Figure 5.8: Viscosity of a material particle with respect to the distance to the entrance

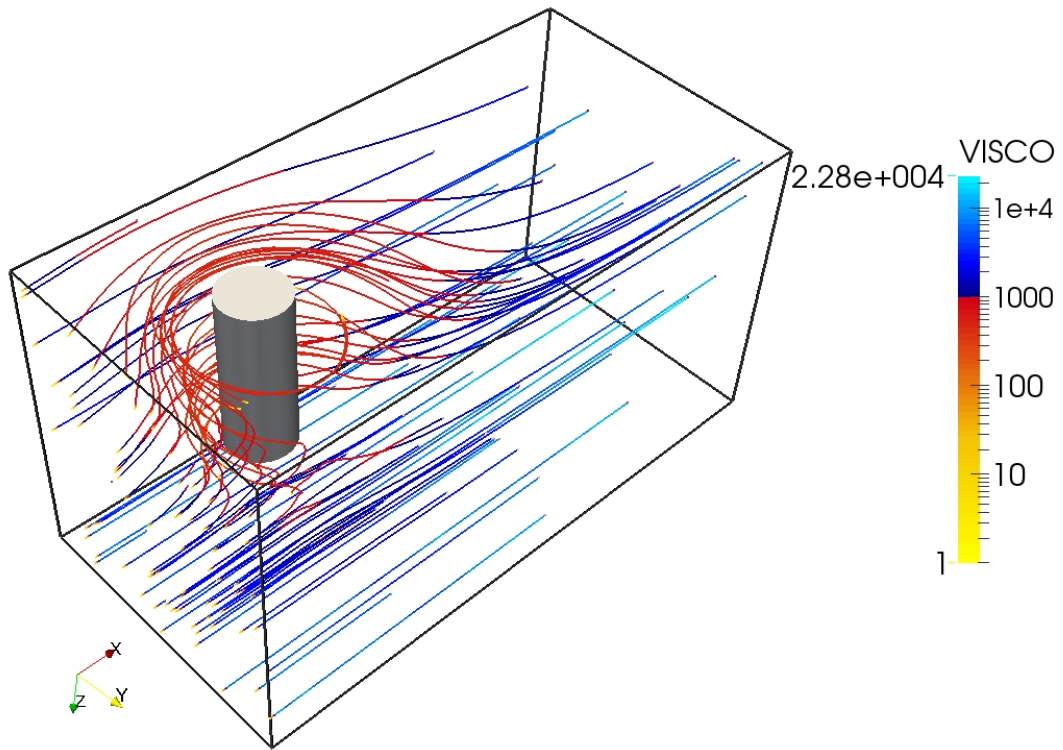


Figure 5.9: Material viscosity along some material pathlines

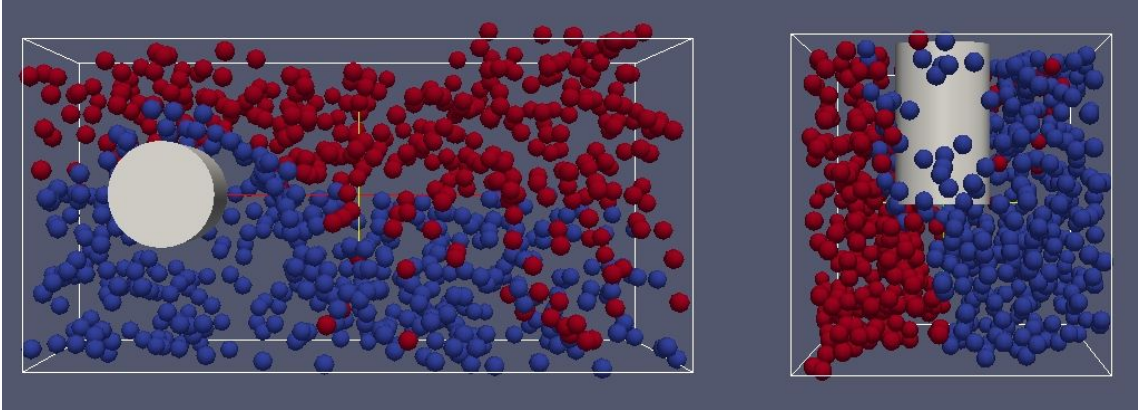


Figure 5.10: Direct visualization of material mixing

Conclusion

In this thesis, different strategies for the efficient simulation of conventional and non-conventional welding processes have been proposed. The originality of this work resides in the use of MOR techniques with different approaches seeking its best industrial applicability: improving classic and robust techniques and easing their integration in preexistent computational platforms. Its main contributions, conclusions and lines of research are summarized here.

The V-GFEM, for efficient simulations of transient thermal models, has been introduced. Its main advantage consists in adapting the trial space in real-time to approximate the solution of the problem optimally. This is achieved thanks to the key ingredient of V-GFEM, the computational vademecum, which is computed offline. Not only does the V-GFEM inherit the good features of the GFEM formulations such as local approximability, conforming and meshless character of the enrichment, but also brings an important advantage: it only needs one enrichment function which is the best possible for a given family of problems at any instant of the simulation. The computational cost of the V-GFEM is the same as any other GFEM approach in which only one analytical enrichment function is used. In the examples presented here, we have generally obtained a difference of an order of magnitude between the V-GFEM solution and FEM solution with a h -adapted mesh to obtain the same accuracy.

The Metalocal-global method has been proposed as an efficient one to estimate final distortions and residual stresses in large structures where repetitive welded joints are performed. This strategy is based on the local-global method circumventing its main issue: the consideration of the influence of the global structure over the

local region in an efficient manner. The Metalocal-global method substitutes the local simulation for a computational vademecum, which provides the local solution for any elastic influence of the global domain over the local one. This methodology constitutes a systematic way to construct a database of computational vademecums that can be stored and used for different global geometries and global boundary conditions.

The complete simulation of conventional welding has been treated in a simplified scenario: steady-state. It has been seen how computational vademecum opens the door to new applications of great industrial applicability, such as predesign, sensitivity analysis or source fitting. In that chapter, special emphasis has been placed on the consideration of non-intrusive methodologies for the construction of these vademecums, showing numerical examples carried out using Sysweld as a black-box solver for thermal, metallurgical and mechanical analysis. Finally, the PGD has been presented as an efficient solver that reduces the computational complexity of models defined in 3D plate-like geometries, very suitable for the simulation of unconventional welding processes like FSW.

Many lines of research remain open. The most significant one is perhaps how to introduce model reduction in mechanical welding simulations without any additional hypothesis. Although this objective has been completed for the thermal analysis (at least as a demonstrator with an academic code), for the mechanical analysis our proposal lays on simplifying hypothesis: local-global hypothesis or steady-state. The complexity in considering this analysis without any simplification lies in the fact that, from the mechanical point of view, welding is not a local problem: plastic deformations and introduced residual stresses evolve for a considerable time after the passage of the heat source. This fact, together with the possibility of considering an infinity of possible trajectories, entails that the strategies above introduced cannot be straightforwardly applied.

A second open research area concerns to the use of PGD as an in-plane-out-of-plane solver in industry. This MOR technique, as presented here, is too intrusive for its implementation on preexisting computing platforms. This opens the door to envisioning less intrusive formulations that continue to take advantage of this high-

performance spatial decomposition. This line of research is well advanced in our group and it is possible that in the near future current limitations will be solved.

Conclusion

Bibliography

- Abbott, B. P., Abbott, R., Abbott, T., Abernathy, M., Acernese, F., Ackley, K., Adams, C., Adams, T., Addesso, P., Adhikari, R., et al. (2016). Observation of gravitational waves from a binary black hole merger. *Physical review letters*, 116(6):061102. *cited on page 1*
- Aguado, J. (2016). *Advanced strategies for the separated formulation of problems in the Proper Generalized Decomposition framework*. PhD thesis, École Centrale de Nantes. *cited on page 7, 9, and 15*
- Aguado, J. V., Borzacchiello, D., Ghnatios, C., Lebel, F., Upadhyay, R., Binetruy, C., and Chinesta, F. (2017). A simulation app based on reduced order modeling for manufacturing optimization of composite outlet guide vanes. *Advanced Modeling and Simulation in Engineering Sciences*, 4(1):1. *cited on page 31*
- Alfaro, I., Bel, D., Cueto, E., Doblaré, M., and Chinesta, F. (2006a). Three-dimensional simulation of aluminium extrusion by the alpha-shape based natural element method. *Computer Methods in Applied Mechanics and Engineering*, 195(33-36):4269–4286. *cited on page 106*
- Alfaro, I., González, D., Bel, D., Cueto, E., Doblaré, M., and Chinesta, F. (2006b). Recent advances in the meshless simulation of aluminium extrusion and other related forming processes. *Archives of Computational Methods in Engineering*, 13(1):3–44. *cited on page 106*
- Alfaro, I., Yvonnet, J., Cueto, E., Chinesta, F., and Doblaré, M. (2006c). Meshless methods with application to metal forming. *Computer Methods in Applied Mechanics and Engineering*, 195(48-49):6661–6675. *cited on page 106*

- Allier, P.-E., Chamoin, L., and Ladevèze, P. (2015). Proper generalized decomposition computational methods on a benchmark problem: introducing a new strategy based on constitutive relation error minimization. *Advanced Modeling and Simulation in Engineering Sciences*, 2(1):17. *cited on page 66*
- Ammar, A., Chinesta, F., and Cueto, E. (2011). Coupling finite elements and proper generalized decompositions. *International Journal for Multiscale Computational Engineering*, 9(1). *cited on page 37*
- Ammar, A., Mokdad, B., Chinesta, F., and Keunings, R. (2006). A new family of solvers for some classes of multidimensional partial differential equations encountered in kinetic theory modeling of complex fluids. *Journal of Non-Newtonian Fluid Mechanics*, 139(3):153–176. *cited on page 7 and 15*
- Ammar, A., Pruliere, E., Férec, J., Chinesta, F., and Cueto, E. (2009). Coupling finite elements and reduced approximation bases. *European Journal of Computational Mechanics/Revue Européenne de Mécanique Numérique*, 18(5-6):445–463. *cited on page 37*
- Aquino, W., Brigham, J., Earls, C., and Sukumar, N. (2009). Generalized finite element method using proper orthogonal decomposition. *International journal for numerical methods in engineering*, 79(7):887–906. *cited on page 40*
- Babuška, I., Caloz, G., and Osborn, J. E. (1994). Special finite element methods for a class of second order elliptic problems with rough coefficients. *SIAM Journal on Numerical Analysis*, 31(4):945–981. *cited on page 35 and 37*
- Bachorski, A., Painter, M., Smailes, A., and Wahab, M. A. (1999). Finite-element prediction of distortion during gas metal arc welding using the shrinkage volume approach. *Journal of Materials Processing Technology*, 92:405–409. *cited on page 65*
- Barasinski, A., Tertrais, H., Ghnatios, C., and Chinesta, F. (2016). Processing of a carbon fiber reinforced polymer (cfrp) laminate part by microwaves. In *Electromagnetic Field Computation (CEFC), 2016 IEEE Conference on*, pages 1–3. IEEE. *cited on page 31*

-
- Barrault, M., Maday, Y., Nguyen, N. C., and Patera, A. T. (2004). An ‘empirical interpolation’ method: application to efficient reduced-basis discretization of partial differential equations. *Comptes Rendus Mathematique*, 339(9):667–672.
cited on page 13
- Bellman, R. (1956). Dynamic programming and lagrange multipliers. *Proceedings of the National Academy of Sciences*, 42(10):767–769. *cited on page 15*
- Belytschko, T., Gracie, R., and Ventura, G. (2009). A review of extended/generalized finite element methods for material modeling. *Modelling and Simulation in Materials Science and Engineering*, 17(4):043001. *cited on page 35*
- Belytschko, T., Moës, N., Usui, S., and Parimi, C. (2001). Arbitrary discontinuities in finite elements. *International Journal for Numerical Methods in Engineering*, 50(4):993–1013. *cited on page 35*
- Benner, P., Gugercin, S., and Willcox, K. (2013). A survey of model reduction methods for parametric systems. *cited on page 7*
- Benner, P. and Sokolov, V. I. (2006). Partial realization of descriptor systems. *Systems & Control Letters*, 55(11):929–938. *cited on page 15*
- Bergheau, J., Pont, D., and Leblond, J. (1992). Three-dimensional simulation of a laser surface treatment through steady state computation in the heat source’s comoving frame. In *Mechanical Effects of Welding*, pages 85–92. Springer. *cited on page 88*
- Bergheau, J.-M. and Fortunier, R. (2013). *Finite element simulation of heat transfer*. John Wiley & Sons. *cited on page 51 and 65*
- Bognet, B., Bordeu, F., Chinesta, F., Leygue, A., and Poitou, A. (2012a). Advanced simulation of models defined in plate geometries: 3d solutions with 2d computational complexity. *Computer Methods in Applied Mechanics and Engineering*, 201:1–12. *cited on page 23 and 107*
- Bognet, B., Leygue, A., and Chinesta, F. (2012b). On the fully 3d simulations of thermoelastic models defined in plate and shell geometries. *European Journal*

- of Computational Mechanics/Revue Européenne de Mécanique Numérique*, 21(1-2):40–51. *cited on page 23*
- Bordeu, F., Chinesta, F., Cueto, E., and Leygue, A. (2013). Abaqes numériques: Visualisation et post-traitement de solutions à variable séparée. application au temps réel non linéaire. *cited on page 53, 82, and 95*
- Borzacchiello, D., Aguado, J., and Chinesta, F. (2016). Reduced order modelling for efficient numerical optimisation of a hot-wall chemical vapour deposition reactor. *International Journal of Numerical Methods for Heat and Fluid Flow*, 27(4). *cited on page 11*
- Borzacchiello, D., Aguado, J., and Chinesta, F. (2017). Non-intrusive sparse subspace learning for parametrized problems. *Archive of Computational Methods in Engineering*, Accepted. *cited on page 11, 26, and 82*
- Chaturantabut, S. and Sorensen, D. C. (2010). Nonlinear model reduction via discrete empirical interpolation. *SIAM Journal on Scientific Computing*, 32(5):2737–2764. *cited on page 13*
- Chinesta, F., Keunings, R., and Leygue, A. (2013a). *The proper generalized decomposition for advanced numerical simulations: a primer*. Springer Science & Business Media. *cited on page 19, 40, and 107*
- Chinesta, F., Leygue, A., Bognet, B., Ghnatios, C., Poulhaon, F., Bordeu, F., Barasinski, A., Poitou, A., Chatel, S., and Maison-Le-Poec, S. (2014). First steps towards an advanced simulation of composites manufacturing by automated tape placement. *International journal of material forming*, 7(1):81–92. *cited on page 31*
- Chinesta, F., Leygue, A., Bordeu, F., Aguado, J. V., Cueto, E., González, D., Alfaro, I., Ammar, A., and Huerta, A. (2013b). Pgd-based computational vademecum for efficient design, optimization and control. *Archives of Computational Methods in Engineering*, 20(1):31–59. *cited on page 11, 18, 42, and 90*
- Cohen, A. and DeVore, R. (2015). Approximation of high-dimensional parametric pdes. *Acta Numerica*, 24:1–159. *cited on page 7 and 8*

-
- Cosimo, A., Cardona, A., and Idelsohn, S. (2014). Improving the k-compressibility of hyper reduced order models with moving sources: applications to welding and phase change problems. *Computer Methods in Applied Mechanics and Engineering*, 274:237–263. *cited on page 30*
- Courard, A., Néron, D., Ladevèze, P., and Ballere, L. (2016). Integration of pgd-virtual charts into an engineering design process. *Computational Mechanics*, 57(4). *cited on page 18*
- Cueto, E. and Chinesta, F. (2015). Meshless methods for the simulation of material forming. *International Journal of Material Forming*, 8(1):25–43. *cited on page 107 and 112*
- Cueto, E., González, D., and Alfaro, I. (2016). *Proper Generalized Decompositions: An Introduction to Computer Implementation with Matlab*. Springer International Publishing. *cited on page 19*
- Darema, F. (2004). Dynamic data driven applications systems: A new paradigm for application simulations and measurements. In *International Conference on Computational Science*, pages 662–669. Springer. *cited on page 7*
- de Souza Neto, E. A., Peric, D., and Owen, D. R. J. (2011). *Computational methods for plasticity: theory and applications*. John Wiley & Sons. *cited on page 78*
- Deane, A., Kevrekidis, I., Karniadakis, G. E., and Orszag, S. (1991). Low-dimensional models for complex geometry flows: Application to grooved channels and circular cylinders. *Physics of Fluids A: Fluid Dynamics*, 3(10):2337–2354. *cited on page 7*
- Dialami, N., Chiumenti, M., Cervera, M., and de Saracibar, C. A. (2013). An apropos kinematic framework for the numerical modeling of friction stir welding. *Computers and Structures*, 117(0):48 – 57. *cited on page 105*
- Dolbow, J. and Belytschko, T. (1999). A finite element method for crack growth without remeshing. *International journal for numerical methods in engineering*, 46(1):131–150. *cited on page 35, 37, and 40*

- Donea, J. and Huerta, A. (2003). *Finite element methods for flow problems*. John Wiley & Sons. *cited on page 105, 115, 116, and 119*
- Donea, J., Huerta, A., Ponthot, J.-P., and Rodriguez-Ferran, A. (2004). Encyclopedia of computational mechanics vol. 1: Fundamentals., chapter 14: Arbitrary lagrangian-eulerian methods. *cited on page 106*
- Duan, Y., Vincent, Y., Boitout, F., Leblond, J., and Bergheau, J. (2007). Prediction of welding residual distortions of large structures using a local/global approach. *Journal of mechanical science and technology*, 21(10):1700–1706. *cited on page 67*
- Duarte, C. A. and Kim, D.-J. (2008). Analysis and applications of a generalized finite element method with global–local enrichment functions. *Computer Methods in Applied Mechanics and Engineering*, 197(6):487–504. *cited on page 40*
- Duarte, C. A. and Oden, J. T. (1996). Hp clouds—an hp meshless method. *Numerical methods for partial differential equations*, 12(6):673–706. *cited on page 35 and 37*
- Farhat, C., Chapman, T., and Avery, P. (2015). Structure-preserving, stability, and accuracy properties of the energy-conserving sampling and weighting method for the hyper reduction of nonlinear finite element dynamic models. *International Journal for Numerical Methods in Engineering*, 102(5):1077–1110. *cited on page 13*
- Feulvarch, E., Roux, J.-C., and Bergheau, J.-M. (2013). A simple and robust moving mesh technique for the finite element simulation of Friction Stir Welding. *Journal of Computational and Applied Mathematics*, 246(2013):269–277. *cited on page 106*
- Fish, J. (1992). The s-version of the finite element method. *Computers & Structures*, 43(3):539–547. *cited on page 37*
- Fish, J. and Belytschko, T. (2007). A first course in finite elements. *cited on page 36*
- Fish, J. and Yuan, Z. (2005). Multiscale enrichment based on partition of unity. *International Journal for Numerical Methods in Engineering*, 62(10):1341–1359. *cited on page 37*

-
- Gatski, T. and Glauser, M. (1992). Proper orthogonal decomposition based turbulence modeling. In *Instability, Transition, and Turbulence*, pages 498–510. Springer. *cited on page 7*
- Ghnatios, C., Chinesta, F., and Binetruy, C. (2015). 3d modeling of squeeze flows occurring in composite laminates. *International Journal of Material Forming*, 8(1):73–83. *cited on page 23*
- Goldak, J., Bibby, M., and Chakravarti, A. (1985). *A double ellipsoid finite element model for welding heat sources*. International Institute of Welding. *cited on page 87*
- Goldak, J. A. and Akhlaghi, M. (2006). *Computational welding mechanics*. Springer Science & Business Media. *cited on page 65 and 88*
- Golub, G. H. and Van Loan, C. F. (2012). *Matrix computations*, volume 3. JHU Press. *cited on page 14*
- González, D., Cueto, E., and Chinesta, F. (2014). Real-time direct integration of reduced solid dynamics equations. *International Journal for Numerical Methods in Engineering*, 99(9):633–653. *cited on page 69*
- Gu, M., Goldak, J., Knight, A., and Bibby, M. (1993). Modelling the evolution of microstructure in the heat-affected zone of steady state welds. *Canadian metallurgical quarterly*, 32(4):351–361. *cited on page 88*
- Guerdoux, S. and Fourment, L. (2009). A 3D numerical simulation of different phases of friction stir welding. *Modelling and Simulation in Materials Science and Engineering*, 17(7):075001. *cited on page 106*
- Gupta, V., Kim, D.-J., and Duarte, C. A. (2012). Analysis and improvements of global–local enrichments for the generalized finite element method. *Computer Methods in Applied Mechanics and Engineering*, 245:47–62. *cited on page 49*
- Hernández, J., Caicedo, M., and Ferrer, A. (2017). Dimensional hyper-reduction of nonlinear finite element models via empirical cubature. *Computer Methods in Applied Mechanics and Engineering*, 313:687–722. *cited on page 13 and 30*

- Hibbeler, L. C., See, M. M. C., Iwasaki, J., Swartz, K. E., O'Malley, R. J., and Thomas, B. G. (2016). A reduced-order model of mould heat transfer in the continuous casting of steel. *Applied Mathematical Modelling*, 40(19):8530–8551. *cited on page 30*
- Jackson, K. and Darlington, R. (2011). Advanced engineering methods for assessing welding distortion in aero-engine assemblies. In *IOP Conference Series: Materials Science and Engineering*, volume 26, page 012018. IOP Publishing. *cited on page 66*
- Johnson, C. (2012). *Numerical solution of partial differential equations by the finite element method*. Courier Corporation. *cited on page 42*
- Jung, G. (2003). *Plasticity-based distortion analysis for fillet welded thin plate T-joints*. PhD thesis, The Ohio State University. *cited on page 67*
- Kolda, T. G. and Bader, B. W. (2009). Tensor decompositions and applications. *SIAM review*, 51(3):455–500. *cited on page 16*
- Ladeveze, P. (1985). New algorithms: mechanical framework and development. *Compte rendu de l'académie des Sci*, 300(2):41–44. *cited on page 15*
- Lumley, J. L. (1967). The structure of inhomogeneous turbulent flows. *Atmospheric turbulence and radio wave propagation*, 790:166–178. *cited on page 7*
- Maday, Y., Patera, A., and Turinici, G. (2002). Reliable real-time solution of parametrized partial differential equations: Reduced-basis output bound methods. *J. Fluids Eng*, 124(1):70–80. *cited on page 12*
- Martínez, M. A., Cueto, E., Alfaro, I., Doblaré, M., and Chinesta, F. (2004). Updated Lagrangian free surface flow simulations with Natural Neighbour Galerkin methods. *International Journal for Numerical Methods in Engineering*, 60(13):2105–2129. *cited on page 106*
- Melenk, J. (1995). *On Generalized Finite Element Methods*. PhD thesis, University of Maryland. *cited on page 35, 37, and 38*

-
- Melenk, J. M. and Babuška, I. (1996). The partition of unity finite element method: basic theory and applications. *Computer methods in applied mechanics and engineering*, 139(1-4):289–314. *cited on page 35 and 37*
- Mendizabal, A., González-Díaz, J., San Sebastián, M., and Echeverría, A. (2016). Improved accuracy of the inherent shrinkage method for fast and more reliable welding distortion calculations. *Journal of Materials Engineering and Performance*, 25(7):2670–2678. *cited on page 66 and 67*
- Merle, R. and Dolbow, J. (2002). Solving thermal and phase change problems with the extended finite element method. *Computational mechanics*, 28(5):339–350. *cited on page 40*
- Mishra, R. S. and Ma, Z. (2005). Friction stir welding and processing. *Materials Science and Engineering: R: Reports*, 50(1):1–78. *cited on page 120 and 122*
- Moës, N. and Belytschko, T. (2002). Extended finite element method for cohesive crack growth. *Engineering fracture mechanics*, 69(7):813–833. *cited on page 35*
- Niroomandi, S., Alfaro, I., Gonzalez, D., Cueto, E., and Chinesta, F. (2012). Real-time simulation of surgery by reduced-order modeling and x-fem techniques. *International journal for numerical methods in biomedical engineering*, 28(5):574–588. *cited on page 37*
- Nouy, A. (2010). A priori model reduction through proper generalized decomposition for solving time-dependent partial differential equations. *Computer Methods in Applied Mechanics and Engineering*, 199(23):1603–1626. *cited on page 18*
- Novak, J. and Ibáñez, J. M. (2000). Gravitational waves from the collapse and bounce of a stellar core in tensor-scalar gravity. *The Astrophysical Journal*, 533(1):392. *cited on page 1*
- Oden, J. T., Duarte, C., and Zienkiewicz, O. C. (1998). A new cloud-based hp finite element method. *Computer methods in applied mechanics and engineering*, 153(1-2):117–126. *cited on page 37*

- Oden, T., Belytschko, T., Babuska, I., and Hughes, T. (2003). Research directions in computational mechanics. *Computer Methods in Applied Mechanics and Engineering*, 192(7):913–922. *cited on page 2*
- Oden, T., Belytschko, T., Fish, J., Hughes, T., Johnson, C., Keyes, D., and Yip, S. (2006). A report of the National Science Foundation Blue Ribbon Panel on simulation-based engineering science: revolutionizing engineering science through simulation. *cited on page 1*
- Oden, T., Ghattas, O., King, J., and Schneider, B. (2011). A report of the National Science Foundation Advisory Committee for Cyberinfrastructure Task Force on Grand Challenges. *cited on page 2*
- Oh, S.-I. and Altan, T. (1989). *Metal forming and the finite-element method*. Oxford university press. *cited on page 109*
- O’Hara, P. (2010). *A Multi-scale Generalized Finite Element Method for Sharp, Transient Thermal Gradients*. PhD thesis. *cited on page 39, 40, 44, and 49*
- O’Hara, P., Duarte, C., and Eason, T. (2009). Generalized finite element analysis of three-dimensional heat transfer problems exhibiting sharp thermal gradients. *Computer Methods in Applied Mechanics and Engineering*, 198(21):1857–1871. *cited on page 40, 49, and 54*
- O’Hara, P., Duarte, C., and Eason, T. (2011). Transient analysis of sharp thermal gradients using coarse finite element meshes. *Computer Methods in Applied Mechanics and Engineering*, 200(5):812–829. *cited on page 40, 41, 49, and 54*
- Ohji, T., Ohkubo, A., and Nishiguchi, K. (1992). Mathematical modelling of molten pool in arc welding. In *Mechanical Effects of Welding*, pages 207–214. Springer. *cited on page 88*
- Olmos, F., Chinesta, F., and Torres, R. (1996). Finite element resolution of convection–diffusion equations with interior and boundary layers. *International journal for numerical methods in fluids*, 22(7):643–671. *cited on page 61*

- Patera, A. T. and Rozza, G. (2007). Reduced basis approximation and a posteriori error estimation for parametrized partial differential equations. *cited on page 12*
- Poulhaon, F., Rauch, M., Leygue, A., Hascoet, J. Y., and Chinesta, F. (2013). Toward a real time control of toolpath in milling processes. In *Key Engineering Materials*, volume 554, pages 706–713. Trans Tech Publ. *cited on page 31*
- Prulière, E., Férec, J., Chinesta, F., and Ammar, A. (2010). An efficient reduced simulation of residual stresses in composite forming processes. *International Journal of Material Forming*, 3(2):1339–1350. *cited on page 31*
- Quak, W., van den Boogaard, A., González, D., and Cueto, E. (2011). A comparative study on the performance of meshless approximations and their integration. *Computational Mechanics*, 48(2):121–137. *cited on page 107 and 108*
- Quarteroni, A. and Formaggia, L. (2004). Mathematical modelling and numerical simulation of the cardiovascular system. *Handbook of numerical analysis*, 12:3–127. *cited on page 7*
- Quarteroni, A., Manzoni, A., and Negri, F. (2015). *Reduced basis methods for partial differential equations: an introduction*, volume 92. Springer. *cited on page 12*
- Radaj, D. (2000). Eigenspannungen und verzug beim schweissen, rechen- und messverfahren, fachbuchreihe schweisstechnik. *cited on page 88*
- Radermacher, A., Reese, S., and Hadoush, A. M. H. (2013). Selective proper orthogonal decomposition model reduction for forming simulations. *PAMM*, 13(1):115–116. *cited on page 30*
- Rigopoulos, A., Arkun, Y., and Kayihan, F. (1997). Identification of full profile disturbance models for sheet forming processes. *AIChE journal*, 43(3):727–739. *cited on page 30*
- Rosenthal, D. (1946). The theory of moving sources of heat and its application to metal treatments. ASME. *cited on page 87*

- Ryckelynck, D. (2009). Hyper-reduction of mechanical models involving internal variables. *International Journal for Numerical Methods in Engineering*, 77(1):75–89. *cited on page 30*
- Rykaline, N. (1976). Energy sources for welding. *Revista de Soldadura*, 6(3):125–140. *cited on page 87*
- Seidel, J. and Ernst, O. G. (2014). Model reduction for cold rolling processes. *steel research international*, 85(9):1334–1339. *cited on page 30*
- Shanghvi, J. and Michaleris, P. (2002). Thermo-elasto-plastic finite element analysis of quasi-state processes in eulerian reference frames. *International journal for numerical methods in engineering*, 53(7):1533–1556. *cited on page 88 and 90*
- Sikström, F., Christiansson, A.-K., and Lennartson, B. (2012). Model order reduction methods applied to a welding model. *Proceedings of the Institution of Mechanical Engineers, Part I: Journal of Systems and Control Engineering*, 226(7):972–984. *cited on page 30*
- Simo, J. C. and Hughes, T. J. (2006). *Computational inelasticity*, volume 7. Springer Science & Business Media. *cited on page 92 and 93*
- Smolyak, S. A. (1963). Quadrature and interpolation formulas for tensor products of certain classes of functions. In *Dokl. Akad. Nauk SSSR*, volume 4, page 123. *cited on page 29*
- Souloumiac, B., Boitout, F., and Bergheau, J. (2002). A new local-global approach for the modelling of welded steel component distortions. *Book-Institute Of Materials*, 784:573–590. *cited on page 67*
- Strouboulis, T., Babuška, I., and Copps, K. (2000). The design and analysis of the generalized finite element method. *Computer methods in applied mechanics and engineering*, 181(1):43–69. *cited on page 37*
- Sudnik, W., Radaj, D., Breitschwerdt, S., and Erofeev, W. (2000). Numerical simulation of weld pool geometry in laser beam welding. *Journal of Physics D: Applied Physics*, 33(6):662. *cited on page 88*

- Sudnik, W., Radaj, D., and Erofeev, W. (1998). Computerized simulation of laser beam weld formation comprising joint gaps. *Journal of Physics D: Applied Physics*, 31(24):3475. *cited on page 88*
- Timoshenko, S., Timoshenko, S. P., Timoshenko, S. P., and Timoshenko, S. P. (1956). *Strength of materials*, volume 210. van Nostrand New York. *cited on page 23*
- Tsai, C., Cheng, W., and Lee, H. (1995). Modeling strategy for control of welding-induced distortion. Technical report, Minerals, Metals and Materials Society, Warrendale, PA (United States). *cited on page 66*
- Ueda, Y., Fukuda, K., and Tanigawa, M. (1979). New measuring method of three dimensional residual stresses based on theory of inherent strain (welding mechanics, strength & design). *Transactions of JWRI*, 8(2):249–256. *cited on page 67*
- Weiss, D., Schmidt, J., and Franz, U. (1995). A model of temperature distribution and weld pool deformation during arc welding. *Mathematical Modelling of Weld Phenomena*, 2:22–39. *cited on page 88*
- Yang, Y., Brust, F., and Kennedy, J. (2002). Lump-pass welding simulation technology development for shipbuilding applications. In *ASME 2002 Pressure Vessels and Piping Conference*, pages 47–54. American Society of Mechanical Engineers. *cited on page 66*
- Yang, Y.-P. and Athreya, B. P. (2013). An improved plasticity-based distortion analysis method for large welded structures. *Journal of materials engineering and performance*, 22(5):1233–1241. *cited on page 68*
- Yoo, J. W., Moran, B., and Chen, J.-S. (2004). Stabilized conforming nodal integration in the natural-element method. *International Journal for Numerical Methods in Engineering*, 60(5):861–890. *cited on page 107, 108, and 112*
- Zienkiewicz, O. C. and Taylor, R. L. (2005). *The finite element method for solid and structural mechanics*. Butterworth-heinemann. *cited on page 38*

Thèse de Doctorat

Diego Canales Aguilera

Titre de la thèse : Stratégies numériques avancées pour la simulation efficace de procédés de soudage conventionnels et non conventionnels : Une approche de réduction de modèles.

Title of thesis: Advanced Numerical Simulations for Conventional and Non-Conventional Welding Processes: A Model Order Reduction Approach.

Résumé

Les simulations numériques représentent un outil fondamental pour la conception et l'optimisation de procédés industriels de fabrication tels que le soudage. Malgré le développement impressionnant des méthodes numériques et des moyens de calcul utilisables, la complexité des procédés de fabrication et les nouvelles exigences des industries les plus avancées obligent à repenser les méthodes, les stratégies et les algorithmes de simulation disponibles.

Dans cette thèse, de nouvelles méthodes numériques avec une approche de Réduction des Modèles sont proposées, une discipline consolidée qui a fourni des solutions étonnantes dans différentes applications, comme les procédés de fabrication avancés.

Tout d'abord, différentes stratégies sont proposées pour la simulation efficace des procédés de soudage conventionnel, à cet effet, l'utilisation de *Computational Vademecums* est introduite. L'introduction de ces abaques numériques améliorent des méthodes telles que : les Éléments Finis Généralisés pour le calcul thermique, l'approche *local-global* pour le calcul mécanique et enfin, la construction directe des abaques numériques utiles pour la phase de pré-design.

En second lieu, un solveur PGD efficace est présenté pour les simulations thermo-mécaniques de soudage par friction-malaxage.

Cette thèse montre comment la réduction des modèles, en plus d'être une fin en soi, peut être un excellent ingrédient pour améliorer l'efficacité des méthodes numériques traditionnelles. Cela représente un grand intérêt pour l'industrie.

Mots-clés

Simulation numérique du soudage, Soudage par friction malaxage, Réduction des modèles numériques, Proper Generalized Decomposition, Abaques Numériques, Generalized Finite Element method, Local-global method, Soudage stationnaire.

Abstract

Numerical simulations represent a fundamental tool for the design and optimization of industrial manufacturing processes such as welding. Despite the impressive development of the numerical methods and the means of calculation, the complexity of these processes and the new demands of the more advanced industries make it necessary to rethink the available methods, strategies and simulation algorithms.

In this thesis, we propose new numerical methods with a Model Order Reduction approach, a consolidated discipline that has provided surprising solutions in different applications, such as advanced manufacturing processes.

First, different strategies for the efficient simulation of conventional welding processes are proposed. To this end, the use of *Computational Vademecums* is introduced for the improvement of methods such as the Generalized Finite Element for thermal calculation, the local-global approach for the mechanical calculation or the direct construction of vademecums useful for pre-design phases. Then, an efficient PGD solver for thermo-mechanical simulations for friction stir welding is presented.

This thesis shows how Model Reduction, besides being an end, it can be an excellent ingredient to improve the efficiency of traditional numerical methods, with great interest for the industry.

Key Words

Computational Welding Mechanics, Welding, Friction Stir Welding, Model Order Reduction, Proper Generalized Decomposition, Computational Vademecum, Generalized Finite Elements, Local-Global methods, Steady-state welding.

